ISTANBUL TECHNICAL UNIVERSITY ★ GRADUATE SCHOOL

LANDING DAMPERS FOR AIRCRAFT CARRIER DECKS

M.Sc. THESIS

Mustafa Enes PEKDEMIR

Department of Shipbuilding and Ocean Engineering

Offshore Engineering Programme

JULY 2024

ISTANBUL TECHNICAL UNIVERSITY ★ GRADUATE SCHOOL

LANDING DAMPERS FOR AIRCRAFT CARRIER DECKS

M.Sc. THESIS

Mustafa Enes PEKDEMİR
(508211213)

Department of Shipbuilding and Ocean Engineering

Offshore Engineering Programme

Thesis Advisor: Assist. Prof. Dr. Serdar Aytekin KÖROĞLU

JULY 2024

İSTANBUL TEKNİK ÜNİVERSİTESİ ★ LİSANSÜSTÜ EĞİTİM ENSTİTÜSÜ

UÇAK GEMİSİ GÜVERTELERİ İÇİN İNİŞ SÖNÜMLEYİCİLERİ

YÜKSEK LİSANS TEZİ

Mustafa Enes PEKDEMİR
(508211213)

Gemi ve Deniz Teknolojisi Mühendisliği Anabilim Dalı

Açık Deniz Mühendisliği Programı

Tez Danışmanı: Dr. Öğr. Üyesi. Serdar Aytekin KÖROĞLU

TEMMUZ 2024

Mustafa Enes Pekdemir, a M.Sc. student of İTU Graduate School student ID 508211213 successfully defended the thesis entitled "LANDING DAMPERS FOR AIRCRAFT CARRIER DECKS", which he prepared after fulfilling the requirements specified in the associated legislations, before the jury whose signatures are below.

Thesis Advisor :	**Assist. Prof. Dr. Serdar Aytekin KÖROĞLU** İstanbul Technical University	.....
Jury Members :	**Assoc. Prof. Dr. Bilge Tutak** Istanbul Technical University	.....
	Res. Asst. Dr. Tarık TUFAN Istanbul Medeniyet University	.....

Date of Submission : 22 May 2024
Date of Defense : 09 July 2024

To my family, friends and spouse,

FOREWORD

This thesis represents one of the most significant steps in my academic journey. Achieving this milestone would not have been possible without the support and encouragement of many individuals.

First and foremost, I would like to extend my deepest gratitude to my family, who have always been by my side and supported me unconditionally. Their love, patience, and belief in me have been invaluable throughout this process. Additionally, I want to thank my friends for their moral support and understanding, which have made this journey much more manageable.

I am especially grateful to my advisor, Assist. Prof. Dr. Serdar Aytekin KÖROĞLU, for his guidance and support at every stage of this process. His knowledge and experience have been a guiding light for me, and I am deeply thankful for his interest and dedication.

Finally, I would like to thank everyone who has supported and contributed to this work. It is with your support that I have been able to successfully complete this significant step.

July 2024

Mustafa Enes PEKDEMIR
(Ships and Ocean Engineer)

TABLE OF CONTENTS

Page

ABBREVIATIONS

DNV	**:** Det Norske Veritas
GS	**:** Glide Slope
LR	**:** Lloyd's Register
PID	**:** Proportional-Integral-Derivative
RINA	**:** Registro Italiano Navale

SYMBOLS

$\ddot{U}$	: Second derivative, i.e., acceleration.
$\dot{U}$	: Second derivative, i.e., acceleration.
A	: Coefficient matrix / Amplitude..
$A0$	: Net orifice area.
A_a	: Pneumatic area.
A_h	: Hydraulic area.
A_o	: Area of opening in orifice plate.
A_p	: Cross-sectional area of metering pin or rod in plane of orifice.
C_d	: Orifice discharge coefficient.
d	: Damping coefficient of supporting damper.
F_a	: Pneumatic force in shock strut.
F_C	: Damping force applied on the floating mass.
F_h	: Hydraulic force in shock strut.
F_K	: Spring force applied on the floating mass.
F_S	: Total axial shock-strut force.
F_{Va}	: Vertical force, applied at axle.
F_{Vg}	: Vertical force, applied to tire at ground.
h	: Bulge height (height of upper surface of floating mass over runway)
K	: Stiffness matrix.
K_L	: Lift factor, L/w.
L	: Lift force.
M	: Mass matrix.
m,r	: Constants corresponding to the various regimes of the tire-deflection process.
n	: Polytropic exponent for air-compression process in shock strut.
p_{a0}	: Air pressure in upper chamber of shock strut at zero stroke.
p_h	: Hydraulic pressure in lower chamber of shock strut.
R	: External force vector.
r_d	: Radius of deflected tire.
s	: Shock-strut axial stroke.

U : Displacement vector.

v_0 : Air volume of shock strut at zero stroke.

w : Total dropping weight.

w_1 : Weight of upper mass above strut.

w_2 : Weight of lower mass below strut.

w_3 : Weight of floating mass.

z_1 : Vertical displacement of upper mass from position at initial contact.

z_2 : Vertical displacement of lower mass from position at initial contact.

z_3 : Vertical displacement of floating mass from position at initial contact.

B : Integration constant.

δ : Deflection of the tire / Integration constant.

Δt : Time step.

Δx : Spatial step

ρ : Mass density of hydraulic fluid.

A : Amplitude.

C : Damping matrix

c : Damping coefficient (Ns/m).

g : Acceleration due to gravity (m/s^2).

k : Stiffness (N/m).

m : Mass.

t : Time (s).

x : Displacement (m).

ζ : Damping ratio (dimensionless).

λ : Eigenvalue.

ω: Natural frequency (rad/s).

ϕ : Phase shift.

LIST OF TABLES

Page

LIST OF FIGURES

Page

LANDING DAMPERS FOR AIRCRAFT CARRIER DECKS

SUMMARY

Shock absorbers are integral components in mitigating landing events, especially within the context of aircraft carrier landing gear design, where the formidable impact forces of horizontal or vertical landings are prevalent. Typically crafted from elastomeric materials such as pads or cables, these shock absorbers are meticulously engineered to absorb and dissipate energy upon the abrupt contact of an aircraft with the carrier deck, thus effectively reducing the force of impact.

The primary objective of this study is to undertake a comprehensive analysis and evaluation of the performance exhibited by landing dampers employed during landing operations on aircraft carrier decks. This endeavour involves a multifaceted approach that encompasses various methodologies including data analysis, numerical modelling, simulations, and real-world testing. Through this concerted effort, the efficacy of these dampers is being rigorously assessed to provide a holistic understanding of their functionality.

Moreover, this study endeavours to embark on the development of shock absorber designs tailored specifically for ship decks, based on the insights garnered from the aforementioned analyses. These designs are then subjected to dynamic analysis to ascertain their structural integrity and operational efficiency under realistic conditions. By leveraging advanced analytical techniques, this phase aims to optimize shock absorber designs, thereby enhancing their performance and reliability during landing operations on aircraft carrier decks.

Furthermore, a comparative analysis is being conducted to juxtapose the functionality of shock-absorbing deck designs against their non-shock-absorbing counterparts. This comparative study seeks to elucidate the distinct advantages and efficacy offered by the integration of landing dampers into aircraft carrier deck configurations. By highlighting the inherent benefits of shock-absorbing deck designs, this analysis underscores their pivotal role in bolstering the safety and operational efficiency of aircraft carrier landings.

In conclusion, the findings of this study are poised to make significant contributions to the field of maritime engineering by enhancing our understanding of landing dampers and their impact mitigation capabilities. By optimizing shock absorber designs and elucidating their advantages, this research endeavour not only augments the safety and operational efficiency of aircraft carrier landings but also furnishes invaluable insights for the optimization of shock absorber designs in diverse maritime environments

UÇAK GEMİSİ GÜVERTELERİ İÇİN İNİŞ SÖNÜMLEYİCİLERİ

ÖZET

Bu çalışmada, uçak gemisi güvertelerine iniş yapan uçakların karşılaştığı zorluklar ve bu zorlukların üstesinden gelmek için geliştirilen sönümleyici sistemler kapsamlı bir şekilde ele alınmıştır. Uçak gemileri, ülkelerin hava ve deniz üstünlüğünü sağlamak için geliştirdikleri kritik askeri platformlar olup, bu platformlar sayesinde savaş uçakları, operasyonel bölgelerine daha yakın bir konumda konuşlandırılabilir. Bu stratejik avantaj, bir ülkenin savunma kapasitesini ve küresel etkisini önemli ölçüde artırır. Ancak, bu avantajın tam anlamıyla kullanılabilmesi için, uçakların güvenli ve etkin bir şekilde bu gemilere iniş yapabilmesi gerekmektedir. Bu durum, hem pilotlar hem de uçak gemisi personeli için ciddi bir mühendislik sorunu olarak öne çıkar. Uçakların yüksek hızla hareket eden ve sürekli değişen bir güverteye iniş yapma zorunluluğu, bu sorunun temelini oluşturur ve mühendislik açısından çözülmesi gereken birçok zorluğu beraberinde getirir.

Bu çalışmanın ana amacı, uçak gemisi güvertelerine iniş sırasında kullanılan sönümleyici sistemlerin performansını detaylı bir şekilde incelemek ve bu sistemlerin uçak ve gemi güvertesi üzerindeki etkilerini kapsamlı bir şekilde değerlendirmektir. Sönümleyici sistemler, uçakların inişi sırasında oluşan dinamik yükleri emerek, bu yüklerin gemi güvertesi üzerinde yaratacağı olumsuz etkileri minimize etmek için tasarlanmıştır. Çalışmada kullanılan metodolojiler arasında kapsamlı veri analizi, sayısal modelleme, yüksek doğrulukta simülasyonlar ve gerçek dünya testleri yer almaktadır. Bu çok yönlü yaklaşım, iniş sönümleyicilerin işlevselliğini ve etkinliğini bütünsel bir perspektifle anlamayı ve değerlendirmeyi amaçlamaktadır. Ayrıca, bu çalışmada elde edilen veriler doğrultusunda gemi güvertelerine özel amortisör tasarımları geliştirilmiş ve bu tasarımlar dinamik analizlerle test edilmiştir. Bu testler, amortisörlerin yapısal bütünlüklerini ve operasyonel verimliliklerini gerçekçi koşullar altında değerlendirmeyi amaçlamaktadır. Çalışma, bu sistemlerin optimizasyonu üzerine odaklanarak, iniş operasyonları sırasında performanslarını ve güvenilirliklerini artırmayı hedeflemektedir.

Uçak gemilerine iniş yapmak, havacılığın en zor ve karmaşık görevlerinden biri olarak kabul edilir. Bu durum, uçak gemilerinin altı serbestlik derecesine sahip hareketli platformlar olmalarından kaynaklanmaktadır. İniş sırasında geminin hareket etmesi, güverte üzerindeki engeller, deniz ve hava koşullarındaki sürekli değişiklikler gibi faktörler, iniş sürecini son derece karmaşık hale getirir. Özellikle kötü hava koşulları, yoğun sis, yağmur ve fırtınalar, inişi daha da zorlaştırarak pilotların güvenli bir şekilde gemiye inmelerini engelleyebilir. Bu koşullar altında, pilotların doğru navigasyon tekniklerini kullanmaları ve ani değişikliklere hızla adapte olmaları gerekmektedir. Güverteye doğru yaklaşma sırasında meydana gelebilecek en ufak bir hata, inişin başarısız olmasına veya ciddi kazaların meydana gelmesine neden olabilir.

Uçak gemisi inişlerinde yaşanan diğer bir zorluk ise, uçakların güverteye inerken karşılaştığı yüksek dikey hızdır. Uçakların yüksek hızla güverteye inmesi, iniş

takımları üzerinde büyük yükler oluşturur ve bu durum iniş takımlarının ve uçağın genel tasarımında önemli etkilere yol açar. Uçak gemisi tabanlı uçakların iniş sırasında sahip oldukları yüksek hız, kara tabanlı uçaklara göre çok daha yüksek dinamik yüklere maruz kalmalarına neden olur. Bu yüksek yükler, iniş takımlarının ve uçağın genel tasarımında ciddi etkilere yol açar ve iniş sırasında meydana gelen dinamik yüklerin etkili bir şekilde sönümlenmesini gerektirir. Ayrıca, geminin hareketi, güvertede bulunan diğer uçaklar ve ekipmanlar üzerinde de tehlikeli bir baskı oluşturabilir. Bu nedenle, sönümleyici sistemlerin tasarımı, hem iniş sırasında oluşan yükleri absorbe etmek hem de bu yüklerin güverte üzerindeki diğer elemanlara zarar vermesini engellemek için kritik bir öneme sahiptir.

Bu çalışmada, uçak gemisi inişleri sırasında karşılaşılan dinamik yüklerin etkilerini azaltmak için geliştirilen sönümleme sistemleri detaylı bir şekilde incelenmiştir. Sönümleme sistemleri, titreşimleri azaltmak ve istenmeyen dinamik etkileri hafifletmek için kullanılan mekanik cihazlardır. Yaylar, şok emiciler ve diğer bileşenlerden oluşan bu sistemler, uçak gemisi güverteleri gibi dinamik ortamlarda meydana gelen büyük enerjileri etkili bir şekilde absorbe eder ve dağıtır. Bu sistemler, uçakların güvenli bir şekilde gemiye inmelerini sağlamak için kritik bir rol oynar. Sönümleyici sistemlerin tasarımı, uçağın iniş sırasında karşılaşacağı maksimum yükleri göz önünde bulundurarak yapılır ve bu yüklerin gemi güvertesi üzerinde en az etkiyi yaratacak şekilde dağıtılmasını sağlar.

Wei tarafından geliştirilen iniş takımı yay ve sönümleme sistemi, bu çalışmada detaylı bir şekilde ele alınmıştır. Bu sistem, iniş takımlarının rijit bir kütleye bağlı olduğu ve yalnızca dikey doğrultuda hareket ettiği bir sistem olarak tanımlanmıştır. İniş takımları, iki serbestlik derecesine sahip olarak tasarlanmış ve üst kütlenin dikey yer değiştirmesi ile alt kütlenin dikey yer değiştirmesi bu sistemin temel dinamik parametreleri olarak ele alınmıştır. Ayrıca, tipik bir oleopnömatik şok emici de bu sistem içinde incelenmiştir. Bu tür sistemler, uçakların güverteye inişi sırasında oluşan enerjiyi absorbe ederek, inişin daha yumuşak ve güvenli olmasını sağlar. Bunun yanı sıra, bu tür sönümleme sistemleri, gemi güvertesinde bulunan diğer ekipman ve personelin de güvenliğini sağlamaya yardımcı olur. Çünkü iniş sırasında oluşan aşırı yüklerin etkin bir şekilde absorbe edilmesi, güverte üzerindeki diğer elemanların zarar görmesini engeller.

Explicit analiz, özellikle hızlı dinamik olayların simülasyonu için kullanılan bir yöntemdir. Bu analiz yöntemi, uçakların iniş sırasında karşılaştıkları karmaşık dinamik süreçleri detaylı bir şekilde modellemek için kullanılır. Çarpışmalar, patlamalar ve yüksek hızlı seyahatler gibi dinamik olayların simülasyonu sırasında explicit analiz, sistemin her bir zaman adımındaki davranışını hesaplayarak yüksek hassasiyet ve detay sağlar. Bu çalışmada, LS-DYNA yazılımı kullanılarak explicit analizler gerçekleştirilmiş ve bu analizler sonucunda elde edilen veriler, iniş sönümleyicilerin performansını değerlendirmek için kullanılmıştır.

Explicit analiz yöntemi, mühendislik simülasyonlarında sıklıkla tercih edilen bir yöntem olup, özellikle hızlı ve karmaşık dinamik olayların incelenmesinde büyük avantajlar sunar. Bu yöntemin temel avantajı, sistemin davranışını her zaman adımında hesaplayarak yüksek doğrulukta sonuçlar elde etmesidir. Bu çalışmada, explicit analiz yöntemi kullanılarak uçak gemisi inişlerinde kullanılan sönümleyici sistemlerin performansı detaylı bir şekilde incelenmiş ve bu sistemlerin iniş sırasında oluşan dinamik yükleri nasıl etkili bir şekilde absorbe ettiği değerlendirilmiştir.

Çalışmada, analitik çözümler ile LS-DYNA modeli arasında yapılan karşılaştırmalar, elde edilen sonuçların doğruluğunu ve güvenilirliğini değerlendirmek için gerçekleştirilmiştir. Bu karşılaştırmalar, LS-DYNA modelinin analitik sonuçlarla ne derece uyumlu olduğunu göstermek ve modelin geçerliliğini sağlamak amacıyla yapılmıştır. LS-DYNA modelinin analitik çözümlerle tutarlı sonuçlar vermesi, bu modelin iniş sönümleyicilerin performansını doğru bir şekilde simüle edebildiğini ortaya koymaktadır. Analitik ve simülasyon sonuçları arasındaki uyum, çalışmanın genel doğruluğunu ve güvenilirliğini artırmaktadır.

Bu çalışma, uçak gemisi güvertelerine iniş sırasında kullanılan sönümleyici sistemlerin etkinliğini ve bu sistemlerin yapısal dayanıklılığı nasıl artırabileceğini kapsamlı bir şekilde ele almıştır. İniş bölgesi uygulamasının iniş sırasında oluşan gerilme ve deformasyon değerlerinde önemli düşüşlere yol açtığı, bu çalışmanın en dikkat çekici bulguları arasında yer almaktadır. Ayrıca, iniş bölgesi uygulamasının iniş sırasında oluşan şok yüklerinin daha iyi dağıtılmasını sağladığı ve bu sayede yapısal hasarın en aza indirildiği gözlemlenmiştir.

Bu çalışmanın sonuçları, uçak gemisi güvertelerine iniş yapan uçaklar için geliştirilen sönümleyici sistemlerin etkinliğini net bir şekilde ortaya koymaktadır. İniş bölgesi uygulamasının gerilme ve deformasyon değerlerini düşürmesi, bu sistemlerin gemi güvertesi üzerindeki olumsuz etkileri nasıl azalttığını göstermektedir. Bu bulgular, gelecekteki çalışmalar için önemli bir temel oluşturmaktadır.

Gelecekteki çalışmalar için, aktif sönümleme sistemlerinin geliştirilmesi ve bu sistemlerin iniş sırasında dinamik yükleri anında tespit ederek nasıl tepki verdiği üzerine araştırmalar yapılabilir. Aktif sönümleme sistemleri, iniş sırasında oluşan yüklerin anında tespit edilip etkili bir şekilde dağıtılması konusunda büyük bir potansiyele sahiptir. Bu tür sistemlerin geliştirilmesi ve optimize edilmesi, gelecekteki mühendislik uygulamaları için önemli bir avantaj sağlayabilir. Örneğin, aktif sönümleme sistemleri, gerçek zamanlı sensörler ve kontrol mekanizmaları ile donatılarak, iniş sırasında oluşan yükleri anında tespit edebilir ve bu yükleri etkili bir şekilde dağıtabilir. Bu tür bir sistem, uçak gemisi güvertelerinin güvenliğini ve dayanıklılığını önemli ölçüde artırabilir.

Sonuç olarak, bu çalışma, denizcilik mühendisliği alanına önemli katkılar sağlamaktadır ve iniş güvenliğini artırmak için yeni tasarımlar geliştirilmesine olanak tanımaktadır. Uçak gemisi güvertelerine iniş sırasında kullanılan sönümleyici sistemlerin etkili bir şekilde tasarlanması ve uygulanması, bu yapısal sistemlerin hizmet ömrünü uzatmak ve operasyonel güvenliği artırmak için kritik bir öneme sahiptir. Bu çalışmada elde edilen bulgular, gelecekteki mühendislik uygulamaları için önemli bir temel oluşturmakta ve iniş güvenliğini artırmak için yeni teknolojilerin geliştirilmesine olanak tanımaktadır.

1. INTRODUCTION

Aircraft carriers are an important product for countries to achieve air and sea superiority in their own environment. This product can make the defense lines of the country very strong. It is very advantageous for the country to deploy its own aircraft or move them to a location closer to a certain region. It also provides a strategic alternative for the country.

However, landing and taking off of aircraft carriers is a very sensitive problem. Particularly personnel competence, weather conditions during landing, use of technological systems and operation management are among these problems.

The main difference between carrier-based aircraft and land-based aircraft lies in their takeoff and landing methods [1]. Research has consistently focused on the dynamics of landing gear during these phases [2]. Dynamic issues are a significant cause of takeoff and landing accidents, especially for carrier-based aircraft [3]. Consequently, the buffering load during ship landings for carrier-based aircraft is considerably higher, often double, because their sink speed upon landing is much greater compared to land-based aircraft [4]. Moreover, factors such as ship motion [7], deck obstacles [6], and airflow interference [5] amplify the impact load during the ship landing process.

As illustrated in Figure 1.1 , the substantial buffering overload due to the high sink speed of carrier-based aircraft has led to several adverse effects on the design of landing gear and carrier-based aircraft [8]. Aircraft also have to endure a significant headinglongitudinal overload because of their short deck length, which means they must immobilize in 50 to 70 meters [9]. Modern aircraft carriers all use arresting systems to catch landing aircraft in order to bring them to immobility quickly. Carrier-based aircraft will lower an arresting hook upon landing so that it meshes with the arresting wires that are mounted on the deck [10]. This arresting device uses up a significant portion of the horizontal kinetic energy of the carrier-based aircraft [11]. Since the American aircraft carriers have been using this technology for a long time, it is considered relatively mature [10].

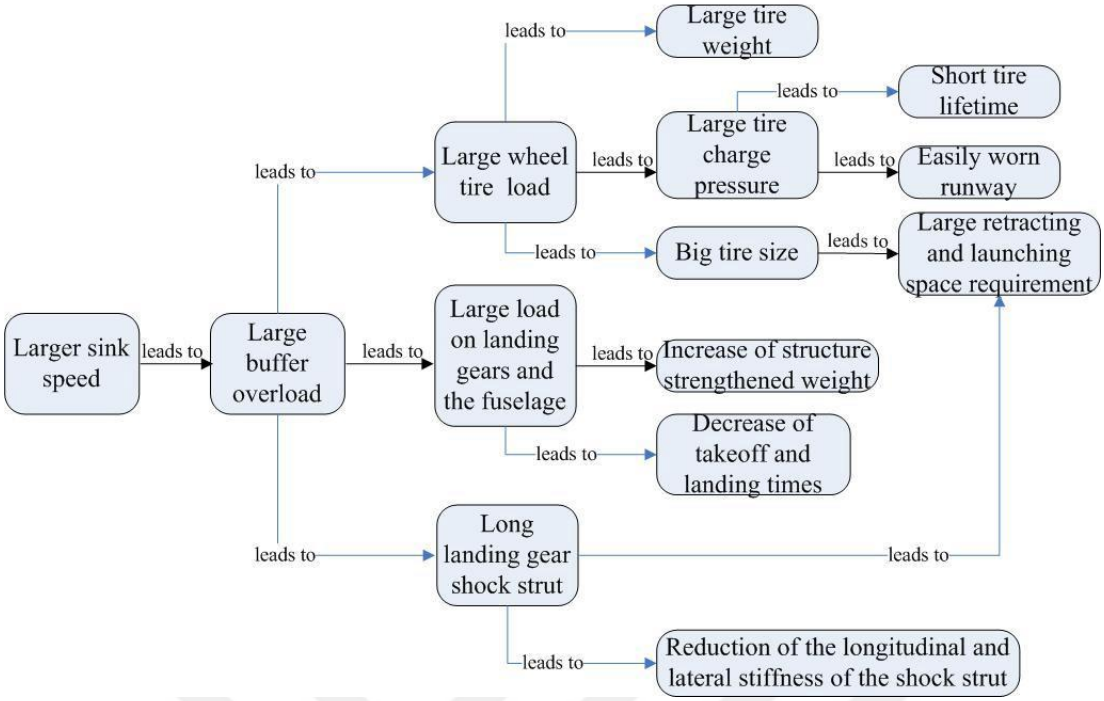

Figure 1.1: Significant buffer overload has a negative impact on the design of landing gear and aircraft built on carriers [10].

However, there are still certain shortcomings with this arresting system: the arresting hook may strike the deck and miss the cable [12,13]; the four arresting cables in this intricate system are installed passively, making them rigid under all circumstances; the arresting cables are costly and valuable, requiring frequent maintenance. Moreover, the new landing zone design is difficult to align with the current arresting system [14].

The main goal of this study is to design a buffer area with a special landing zone to increase the safety of aircraft landing on aircraft carriers. This buffer area will reduce the impact load that may occur under the impact of aircraft landing on the ship, thus ensuring that the aircraft land on the ship more safely. The landing zone to be designed will play a critical role for the safety of both pilots and ship personnel and will contribute to more efficient and reliable ship operations. This project aims to contribute to safer and more effective future aircraft carrier operations by aiming to increase safety standards in the aviation and maritime industry.

2. DECK LANDING

Significant naval air forces that are built for carrier operations—which are crucial to modern navies—are carrier-based aircraft. They have to be able to land on the carrier after a brief launch. When landing, an aircraft should maintain its approaching speed and closely follow the glide slope in order to land at the optimal touchdown site with a relatively small error margin. Accurate landings become very difficult due to unfavorable conditions, such as poor visibility, strong winds, carrier airwake, a limited deck with six degrees of freedom, and a complex and unstable ocean environment [15].

2.1 Definition of Deck Landing

When an aircraft lands successfully in the optimal landing spot with minimal errors, it is said to have made a safe carrier landing. The approach phase, descent phase, and touchdown phase are the three stages that make up a normal landing operation. The airplane must align at a precise height with the runway's centerline during the approach phase. At about constant altitude, this is accomplished at a constant speed. The airplane descends at a constant speed and glide slope angle during this phase. The two main ways that deck motion affects landing during the touchdown stage are as follows: first, longitudinal motion changes the height of the touchdown point, increasing the risk that the aircraft won't land on the ideal spot; second, lateral motion causes the aircraft to veer off the runway's centerline, increasing the chance that it will overshoot the deck runway. Furthermore, the aircraft may be blown off the reference glide slope by the carrier airwake [15].

2.2 Challenges of Deck Landing

It has long been acknowledged that one of the hardest jobs in aviation is landing aircraft at sea on Aircraft Carrier pitching decks. The surroundings are undoubtedly among the most difficult ones that can be found anywhere [16]. Unfavorable weather conditions, such as intense fog, rain, or storms, reduce visibility and make it more challenging for pilots to safely land the ship. When there is fog, it is difficult for

airplanes to see the ship properly during approach and landing, which makes it difficult for pilots to make accurate movements approaching the ship. Rain and storms can intensify the wind impact, altering the landing route and posing control challenges for the aircraft. Pilots must become more vigilant in these difficult weather conditions, employ precise navigation techniques, and quickly adjust to any sudden changes. Furthermore, deteriorating weather could postpone or cancel the landing, which would have an influence on ship operations and make it impossible to finish missions on schedule. As a result, it's imperative to keep a careful eye on the weather throughout deck landing operations and make improvements. However, the landing problem is dominated by a number of engineering constraints, independent of environmental factors [16]. The plane needs to land;

1) in the intended location to activate a Cross Deck Pendant

2) during the run-out, which refers to the distance the aircraft travels along the deck after making contact with the carrier's surface until it comes to a complete stop, without lateral drift to remain inside the landing area

3) with the appropriate mindset to insert the hook into the wires correctly

It is imperative that every aircraft tracks closely to the centerline stripe during either landing rollout or bolter, which is a situation where an aircraft attempting to land on an aircraft carrier fails to catch any of the arresting wires with its tailhook and must immediately take off again for another landing attempt. Merely landing near the landing area's centerline is insufficient. Merely landing near the landing area's centerline is insufficient. Because flight deck space is at a premium, airplanes are parked so close to the landing area's edge about 5-8 centimeters. Any wingtip excursion over the landing area's foul-line, no matter how small, will unavoidably come into touch with and damage another aircraft. The more dangerous of the two is drift during a bolter because pulling the arresting gear does center the aircraft being arrested and lowers the likelihood of impact velocity. Foul-line excursions are the most frequent type of landing accident; they usually only result in Category B or C mishaps and lack the dramatic quality of accidents caused by GS faults. The most common offenders are undoubtedly airplanes with a large wingspan; this is especially true of the F-14, which had extremely poor lateral-directional flight quality prior to the installation of a digital flight control system During the rollout, the pilot has no control

over direction; they must accept the trajectory that momentum and the forces of the arresting gear establish. Therefore, a safe landing necessitates a touchdown that is both precisely located lateral and free of considerable lateral drift [16].

A hook touchdown in the middle of the wires does not ensure an effective arrest. Despite its weight, the hook may bounce off the deck and over any cables due to the force of the hit at such high speeds. Actuators or dampers that are pneumatic or hydraulic may be able to withstand this occurrence, but in order for them to work, the aircraft still needs to be near the proper touchdown attitude. The most typical cause of "hook-skip bolters" is a last-minute nose-down adjustment made to avoid being "over-powered at the ramp". Although the aircraft is successfully guided into the wires by this "play" for the deck, the attitude is lowered to the point where insufficient pressure is provided to keep the hook-point low to the deck [16].

2.3 Landing Dynamics

Ongoing research and development in the aviation sector have led to significant advancements in landing dynamics, enhancing the safety, effectiveness, and efficiency of aircraft landings. These advancements stem from a deeper understanding of aerodynamic principles and the application of novel materials and technologies, which contribute to the durability of aircraft and reduce landing stresses. Consequently, safety standards in the aviation industry have strengthened, and pilot performance during landings has improved.

Landing Gear Enhancements

Researchers have focused on improving landing gear performance and design to address the significant impact overload from rapid sink speeds during carrier-based aircraft landings [2]. Control mechanisms have been added to landing gear systems to mitigate landing buffer overload [10]. Nie Hong has studied shock strut design and dynamic behavior analysis for landing gear [17]. Berg proposed a control plan for using electrorheological fluid-based smart landing gear oleos [18]. Ringleb's 1956 monograph on cable dynamics provided a methodical analysis of cable dynamics [19]. Gibson and colleagues developed a comprehensive theory of cable design, improving cable construction and design practices [20, 21]. Billec tested the performance of the Mark 7 Mod 1 arresting-gear dynamics with various pitch-diameter fairlead sheaves

and deck spans [22, 23]. Gao Zejiong discussed the performance of wire rope or nylon systems in arresting-gear dynamics and their effect on different arresting cable lengths [24].

Modeling and Analysis

Models of landing gear falling vibration dynamics and ship landing dynamics have been developed to study carrier-based aircraft's dynamic landing performance [25, 26]. Airflow interference during deck landings, deck obstacles, and ship motion interference are integrated into fundamental modeling techniques [5, 6, 7, 27]. Research includes high sink speed effects, nonlinear landing characteristics, and dual-chamber shock absorbers with variable orifices [28, 29, 30, 31]. Leask developed a mathematical model to predict dynamic performance of shore-based rotary-hydraulic aircraft arresting gears, advancing arrested landing dynamics modeling and analysis [32].

Dynamic Equations and Numerical Solutions

Hsin created a second-order partial differential equation for short-distance takeoff and landing aircraft and determined dynamic reactions during deck landings [33]. Jone developed comprehensive dynamic equations for arrested landings using the Lagrange equation, considering the airplane as a rigid model with six degrees of freedom [34, 35].

Research (1990s)

Jin Changjiang and Wang Menghui provided concise explanations of carrier-based aircraft takeoff and landing dynamics [36, 37]. Hu Guoquan devised a method to compute the arresting force for asymmetric and eccentric deck landings considering the arresting hook's sliding ability [9]. Cao Shuhua used simulation techniques to examine fluctuating parameters during the arresting process, such as aircraft overload and arresting cable tension [38]. Wu Juan constructed an arresting model, analyzing system stability and the uniqueness of the arresting differential equation's solution [39]. Li Daye redesigned the hydraulic system by replacing the throttle valve with an electro-hydraulic proportional overflow valve control system [40]. Zhang Xin studied the dynamic reaction of the arresting cable, focusing on the bent wave during landing [41]. Xu Sheng examined arrested landing dynamics using six-degree-of-freedom aircraft models in MATLAB/Simulink [42].

Luo Qin researched the varying hook loads and working strokes during landings with different landing weights and meshing speeds [43]. Zhang Shusen optimized deceleration trajectories and used feedback linearization in a nonlinear dynamics model of the arresting system [44]. Zhou Jianbin proposed a combined pulley mechanism and hydraulic energy absorption arresting system [45]. Zhang Ping developed a dynamics model for optimal arrestment using the discrete kink-wave model [46]. Li Qiming studied the stress wave produced when an arresting hook strikes an arresting cable [47]. Tao Yang established dynamic equations to evaluate the safe range of carrier-based aircraft bump cables [58]. Zhang Minghui developed a mathematical model of an aircraft arrester including a pulley buffer system and a hydraulic arresting system [59].

New Landing Zone Design

Wei's research focuses on designing a new landing zone to address shortcomings in current designs, aiming to make aircraft carrier landings safer and more effective [10]. This novel design is expected to significantly advance aircraft carrier operations.

The ongoing research and development in landing dynamics have led to substantial improvements in aircraft landing safety and efficiency. These advancements result from enhanced landing gear designs, better understanding of cable dynamics, advanced modeling and analysis techniques, and innovative new designs for landing zones. These efforts continue to elevate safety standards and improve the operational effectiveness of aircraft carriers.

3. SPRING AND DAMPING SYSTEM

Mechanical devices like spring and damping systems are used to reduce vibration and mitigate undesired effects. These systems, which have several uses, are made up of springs, shock absorbers, and other parts. Springs are materials with the ability to stretch and rebound in response to outside stimuli [50]. Their ability to collect and release energy makes them perfect for mitigating vibration. Devices known as shock absorbers work by changing kinetic energy into thermal energy in order to reduce vibration.

Vibration across a broad frequency range can be efficiently controlled by combining dampening and spring systems. These systems have a wide range of uses, including earthquake isolators in buildings, vibration isolators in machinery, and suspensions in cars. Depending on the intended use and performance, spring and damping system designs differ. There are various kinds of springs and shock absorbers available, and each has special qualities and benefits of its own. Selecting the appropriate dampening system and springs guarantees that vibration is efficiently reduced and the system functions safely and effectively.

3.1 Spring-Mass-Damping System

In the spring-mass system, *x(t)* represents the displacement (m) of the mass *m* (kg) from its equilibrium position as a function of time *t* (s), the equation of motion for this system is after summing forces in Figure 3.1(b) [51].

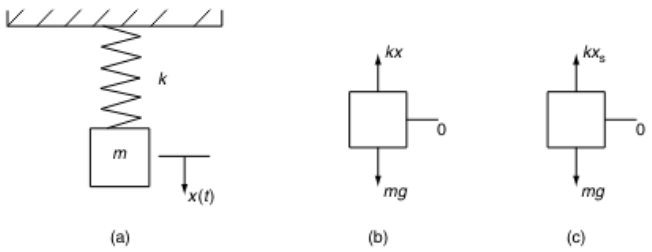

Figure 3.1 : Spring-mass system(a), free body diagram(b), static spring-mass system free body diagram (c) [51].

$$m\ddot{x} + k(x + x_s) - mg = 0 \tag{3.1}$$

where the overdots indicate differentiation with respect to time, g is the acceleration due to gravity (m/s2), x_s is the static displacement (m) of the spring under gravity load, and k is the stiffness of the spring (N/m). $mg = kx_s$ is the result of adding up the forces in the free body diagram for the spring's static deflection [Figure 3.1(c)], which gives rise to the equation of motion above.

$$m\ddot{x}(t) + kx(t) = 0 \tag{3.2}$$

Equation 3.2 can be solved to obtain the time history of the mass *(m)* position given its initial position and velocity after m and k have been established by static experimentation.

$$x(t) = A\sin(\omega_n t + \phi) \tag{3.3}$$

where the natural frequency (rad/s) is denoted by $\omega_n = \sqrt{(k / m)}$. Here, the initial conditions dictate the integration constants for the amplitude, A, and phase shift, ϕ.

To continue, the constants A and ϕ can be computed by simple substitution if x_0 is the given initial displacement from mass m's equilibrium and v_0 is its defined initial velocity.

$$x(t) = \sqrt{\frac{\omega_n^2 x_0^2 + v_0^2}{\omega_n^2}}\sin\left[\omega_n t + \tan^{-1}\left(\frac{\omega_n x_0}{v_0}\right)\right] \tag{3.4}$$

Also it could be;

$$x(t) = \frac{v_0}{\omega_n}\sin\omega_n\, t + x_0\cos\omega_n\, t \tag{3.5}$$

after implementing a basic trigonometric formula.

To solve equation 3.2 strictly mathematically, one can suppose that the solution takes the form $x(t) = Ae^{\lambda t}$ and solve for λ, i.e.,

$$m\lambda^2 e^{\lambda t} + ke^{\lambda t} = 0 \tag{3.6}$$

Due to $e^{\lambda t} \neq 0$, and $A \neq 0$, it suggests that

$$\lambda^2 + \left(\frac{k}{m}\right) = 0 \tag{3.7}$$

or

$$\lambda = \pm j\left(\frac{k}{m}\right)^{1/2} = \pm\omega_n j \tag{3.8}$$

In the case where $j = (-1)^{1/2}$, the conventional answer is

$$x(t) = A_1 e^{-\omega_n jt} + A_2 e^{\omega_n jt} \tag{3.9}$$

where the initial conditions establish the arbitrary complex conjugate constants of integration, A_1 and A_2. Equations 3.3 and 3.5 are then obtained by applying Euler's formulas. The exponential technique is frequently more appropriate for more complex systems than attempting to infer the solution's form (sinusoid) from the motion alone.

When perturbed, most systems do not oscillate endlessly, as equation 3.4's solution suggests. The periodic motion usually stops after a while. The simplest method to approach this mathematically is to add a force term depending on velocity, $c\dot{x}$, to equation 3.2 and analyze the equation [51].

$$m\ddot{x} + c\dot{x} + kx = 0 \tag{3.10}$$

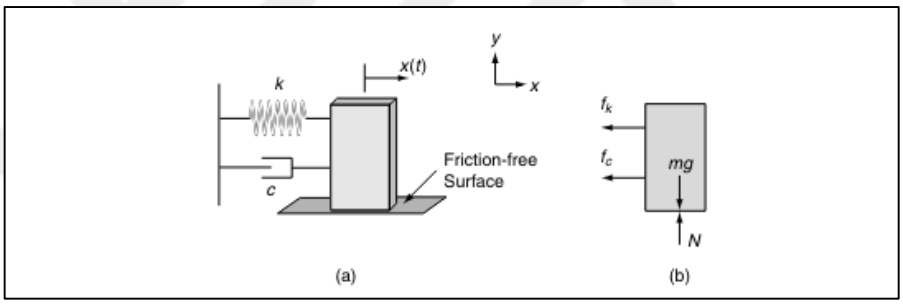

Figure 3.2 : Spring-mass-damping system(a) and it's free body diagram (b) [51].

As seen in Figure 3.2, this also occurs physically when a *dashpot* or *damper* is added to dissipate energy.

Assuming that the dashpot applies a dissipative force on the mass *m* that is proportional to its velocity, equation 3.10 accords with the summing forces in Figure 3.2 . Regretfully, unlike *m* and *k*, the constant of proportionality, *c*, cannot be determined using static techniques. Furthermore, a lot of structures release energy in ways that aren't related to velocity. In terms of fundamental units, the constant of proportionality *c* is expressed as N s/m or kg/s [51].

Once more, under certain beginning conditions, the unique solution of equation 3.10 can be determined by assuming that $x(t)$ is of the form

$$x(t) = Ae^{\lambda t} \tag{3.11}$$

and using this in place of equation (3.6) to produce

$$A\left(\lambda^2 + \frac{c}{m}\lambda + \frac{k}{m}\right)e^{\lambda x} = 0 \tag{3.12}$$

Since it is not desired to have a trivial solution, A ≠ 0, and since $e^{\lambda t}$ is never zero, equation 3.12 produces

$$\lambda^2 + \frac{c}{m}\lambda + \frac{k}{m} = 0 \tag{3.13}$$

Equation 3.13 is referred to as equation 3.10's characteristic equation. With basic algebra, the two answers to are

$$\lambda_{1,2} = -\frac{c}{2m} \pm \frac{1}{2}\sqrt{\frac{c^2}{m^2} - \frac{4k}{m}} \tag{3.14}$$

The *discriminant*, which is the number under the radical, decides whether the roots are real or complex along with the sign of *m*, *c* and *k*. Since *m*, *c*, *k*, and the other physical variables are all positive in this instance, the type of roots of equation 3.13 depends on the discriminant's value.

The dimensionless *damping ratio*, ζ, is conveniently defined as

$$\zeta = \frac{c}{2\sqrt{km}} \tag{3.15}$$

Furthermore, for $0 < \zeta < 1$, let ω_d, the *damped natural frequency*, be defined as

$$\omega_d = \omega_n\sqrt{1 - \zeta^2} \tag{3.16}$$

equation 3.10 then turns into

$$\ddot{x} + 2\zeta\omega_n\dot{x} + \omega_n^2 x = 0 \tag{3.17}$$

hence equation 3.14 becomes into

$$\lambda_{1,2} = -\zeta\omega_n \pm \omega_n\sqrt{\zeta^2 - 1} = -\zeta\omega_n \pm \omega_d j \tag{3.18}$$

It is evident that the type of solution to equation 3.10 depends on the damping ratio, ζ. Three noteworthy cases exist; underdamped, overdamped and critically damped.

An underdamped scenario arises when the system's parameters are set in a way that

$$0 < \zeta < 1$$

in such a way that the roots create a complex conjugate pair of values and the discriminant in equation 3.12 is negative. After that, the answer to equation 3.11 is

$$x(t) = e^{-\zeta\omega_n t}(A\cos(\omega_d t) + B\sin(\omega_d t)) \tag{3.19}$$

or

$$x(t) = Ce^{-\zeta\omega_n t}\sin(\omega_d t + \phi) \tag{3.20}$$

where the given starting position, x_0, and velocity, v_0 , define the constants *A*, *B*, *C*, and ϕ:

$$A = x_0, \quad C = \frac{\sqrt{(v_0 + \zeta\omega_n x_0)^2 + (x_0\omega_d)^2}}{\omega_d}$$

$$B = \frac{v_0 + \zeta\omega_n x_0}{\omega_d}, \quad \phi = \tan^{-1}\left(\frac{x_0\omega_d}{v_0 + \zeta\omega_n x_0}\right) \tag{3.21}$$

A lowering frequency oscillation of ω_d′s characterizes the underdamped response, which takes the shape seen in Figure 3.3.

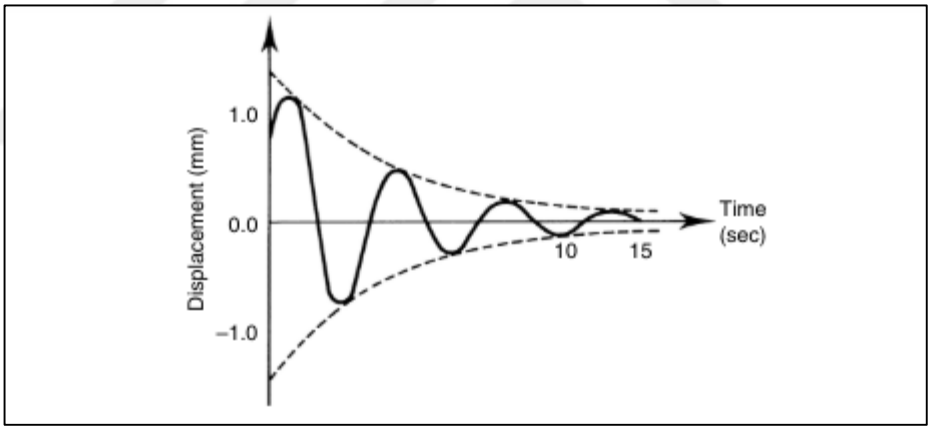

Figure 3.3 : Underdamped system response [51].

An overdamped scenario arises when the system's parameters are set in a way that

$$\zeta > 1$$

in order for equation 3.18 to have a positive discriminant and for the roots to be two negative real integers. After that, the answer to equation 3.17 is

$$x(t) = Ae^{\left(-\zeta+\sqrt{\zeta^2-1}\right)\omega_n t} + Be^{\left(-\zeta-\sqrt{\zeta^2-1}\right)\omega_n t} \tag{3.22}$$

where *A* and *B* are once more constants that are established by x_0, and v_0,. They're

$$A = \frac{v_0 + \left(\zeta + \sqrt{\zeta^2 - 1}\right)\omega_n x_0}{2\omega_n\sqrt{\zeta^2 - 1}}$$

$$B = -\frac{v_0 + \left(\zeta - \sqrt{\zeta^2 - 1}\right)\omega_n x_0}{2\omega_n\sqrt{\zeta^2 - 1}} \tag{3.23}$$

Figure 3.4 shows the form of the overdamped response. An overdamped system returns exponentially to its rest position rather than oscillating.

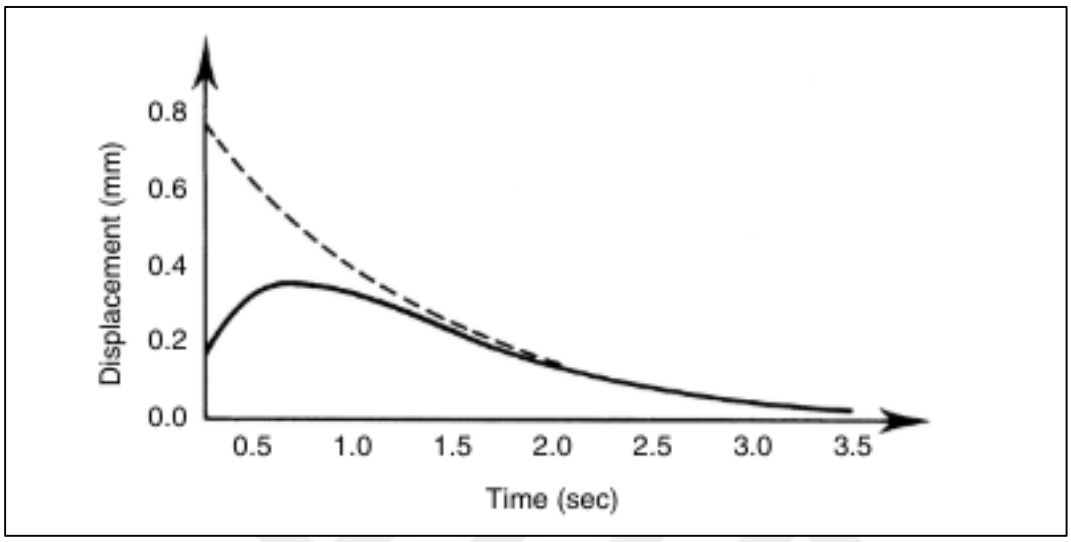

Figure 3.4 : Overdamped system response [51].

A critically damped instance arises when the system's parameters are set in a way that

$$\zeta = 1$$

in order for equation 3.18 to have zero discriminant and for the roots to be two negative real repeating integers. After that, the answer to equation 3.17 is

$$x(t) = e^{-\omega_n t}[(v_0 + \omega_n x_0)t + x_0] \tag{3.24}$$

Figure 3.5 shows the critically damped response for x_0 = 0.2 and a range of initial condition values v_0.

It is noteworthy that there are multiple methods to conceptualize critically damped systems. Initially, they depict systems that have the lowest damping rate possible, resulting in a system that is nonoscillating. Another way to conceptualize critical damping is as the condition that distinguishes oscillation from nonoscillation [51].

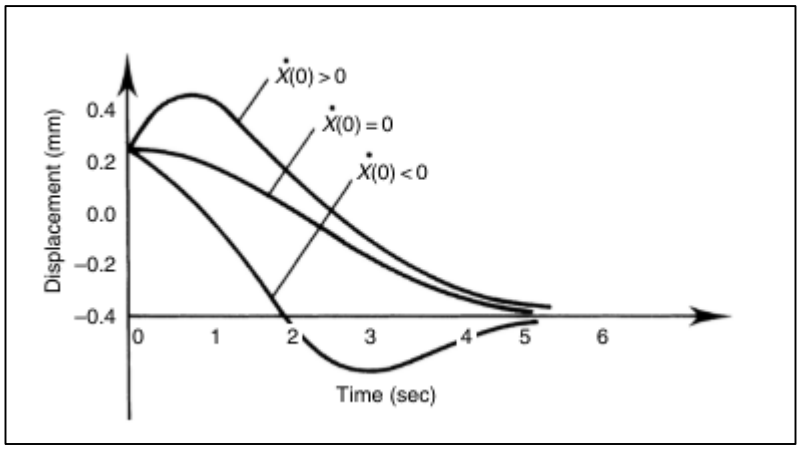

Figure 3.5 : Critically damped system response [51].

3.2 Wei's Landing Gear Spring and Damping System

The study is based on the concept that the landing gear is attached to a rigid mass with only vertical translational movement. It is assumed that the gear remains infinitely rigid when bent. As depicted in Figure 3.6, the system comprising the airplane and landing gear has two degrees of freedom defined by the vertical displacement of the upper mass and the vertical displacement of the lower, or unsprung, mass. Figure 3.6 also illustrates a typical oleopneumatic shock strut. Considering the forces and pressures acting within the shock strut, it is clear from Figure 3.6 [52] that the total axial force due to hydraulic resistance and air compression can be expressed as

$$F_S = F_h + F_a \tag{3.25}$$

where

$$F_h = \frac{\dot{s}\rho A_h^3}{|\dot{s}|2(C_d A_0)^2}\dot{s^2}$$

$$F_a = p_{a0}A_a\left(\frac{v_0}{v_0 - A_a s}\right)^n \tag{3.26}$$

Tire force can be calculated using the exponential properties of the tire without hysteresis as follows (p_{a0} = air pressure in upper chamber of shock strut at zero stroke, A_a = pneumatic area, s = shock-strut axial stroke, A_h = hydraulic area, C_d = orifice discharge coefficient, v_0 = air volume of shock strut at zero stroke):

$$F_{vg} = m\delta^r \tag{3.27}$$

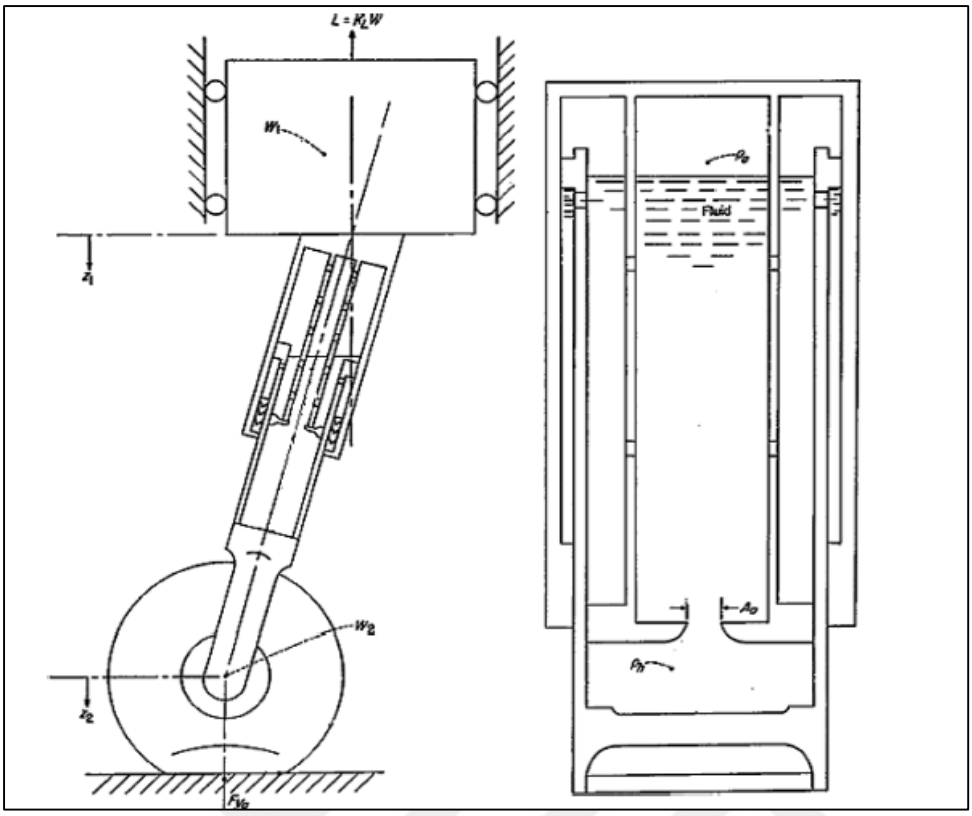

Figure 3.6 : Landing gear system representation with two degree of freedom sytem and demonstration of shock strut [52].

To account for tire bottoming in strong impacts, the tire-bottoming regime utilizes revised values for *m* and *r* .

The mechanical system established on a runway is referred to as the landing region. It consists of three main components: a supporting spring, a supporting damper, and a floating mass. In the first approximation, the floating mass is locked when its upper surface descends to the runway surface. The rigid mass is considered to have only vertical translational freedom, while the supporting spring and damper are linear and viscous, respectively. The balance of forces and reactions within this system is schematically illustrated in Figure 3.7.

Based on the previously stated hypotheses, spring force and damping force are determined by

$$F_K = kz_3, \quad F_C = d\dot{z}_3 \tag{3.28}$$

The landing impact can be divided into three distinct phases. The first phase starts from the moment of contact until the start of the shock strut deflection. The second phase covers the period from the beginning of the shock strut deflection to the point where

the floating mass locks. The third phase extends from the locking of the floating mass to the completion of the impact.

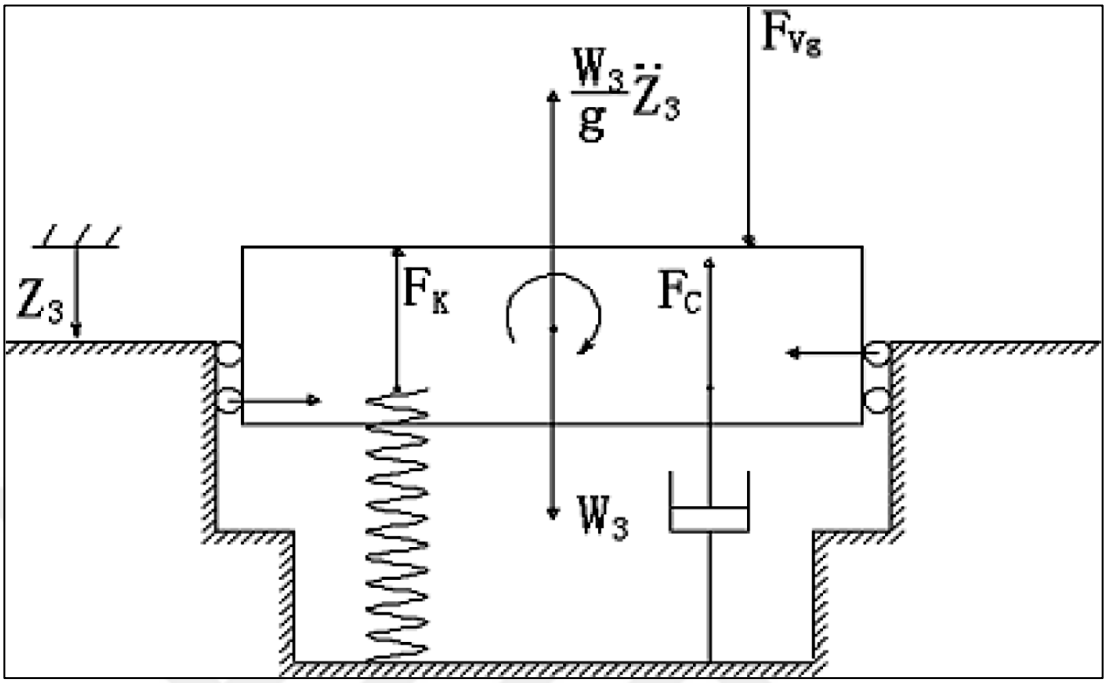

Figure 3.7 : Landing region spring-damping system [52].

Since $\ddot{z_1} = \ddot{z_2} = \ddot{z}$ during the first phase of the impact, the system can be regarded as having two degrees of freedom: z and z_3. Therefore, the overall dynamic equilibrium of the landing gear can be expressed as follows (z_1 = vertical displacement of upper mass from position at initial contact, z_2 = ertical displacement of lower mass from position at initial contact, z_3 = vertical displacement of floating mass from position at initial contact):

$$F_{vg}(z - z_3) = -\left(\frac{w}{g}\right)\ddot{z} - w(K_L - 1) \tag{3.29}$$

The governing equation for the floating mass is expressed as follows:

$$w_3 + F_{\mathrm{Vg}}(z - z_3) - F_K - F_C = \left(\frac{w_3}{g}\right)\ddot{z_3} \tag{3.30}$$

As the shock strut starts to deflect in the second phase of the impact, the system can be viewed as having three degrees of freedom: z_1, z_2 and z_3 [52].The equation of motion for the upper mass is given by

$$F_S + L - w_1 = -\left(\frac{w_1}{g}\right)\ddot{z_1} \tag{3.31}$$

The lower mass's equation of motion is

$$F_S + w_2 - F_{\mathrm{Vg}}(z_2 - z_3) = \left(\frac{w_2}{g}\right)\ddot{z}_2 \tag{3.32}$$

The floating mass's equation of motion is

$$w_3 + F_{\mathrm{Vg}}(z_2 - z_3) - F_K - F_C = \left(\frac{w_3}{g}\right)\ddot{z}_3 \tag{3.33}$$

Since the floating mass is locked during the third phase of impact, the system can be considered to have two degrees of freedom : z_1 and z_2 . The equation of motion for the upper mass remains the same as in equation 3.29. The equation of motion for the lower mass is given by:

$$F_S + w_2 - F_{\mathrm{Vg}}(z_2 - h) = \left(\frac{w_2}{g}\right)\ddot{z}_2 \tag{3.34}$$

4. OVERVIEW OF EXPLICIY ANALYSIS

In engineering and simulation, explicit analysis is a technique used to study complex and dynamic events by calculating the behavior of the system at each time step to achieve high precision and detail. This method is particularly effective for simulating fast-moving dynamic events such as collisions, explosions, metal forming, and high-speed travel. By breaking down the event into time steps, explicit analysis allows for an in-depth understanding of the intricate physical processes involved, making it an essential tool for accurately modeling and resolving engineering challenges. This approach is widely used in various industries, including automotive, aerospace, and defense, due to its ability to realistically simulate rapid and intricate physical phenomena.

4.1 Definition of Explicit Analysis

Explicit analysis is used for transient dynamic analysis of highly nonlinear problems through an explicit time integration scheme, a variant of the central difference method. In this approach, equilibrium is evaluated at the current time step, while the next time step remains unknown. According to Newton's laws, any imbalance in forces results in accelerations, which are integrated to derive velocities and displacements. These values are then used to compute forces that guide the system towards equilibrium, although exact equilibrium is not achieved in a single time step due to constant changes in forces.

To maintain stability and avoid errors, the time step size must not exceed a critical value determined by the Courant-Friedrichs-Levy (CFL) criterion. The critical time step is calculated conservatively, considering the sound speed and the finite element dimensions. Typically, these time steps are very small for a reasonable finite element discretization. Nonlinear systems of equations are solved using this integration scheme by inverting the mass matrix at each time step. With a lumped mass matrix, which is diagonal, each equation simplifies to a division by a scalar.

The main computational effort involves forming internal forces through the elements and contact surfaces. This process can be optimized for various computer architectures, including vector and parallel computers. Addressing geometrically nonlinear problems, including those with large strains and contacts, is straightforward with explicit analysis. The explicit time integration scheme eliminates the need for iteration or convergence control of nonlinear systems, avoiding convergence issues.

Explicit analysis is used in applications such as crash and occupant simulations, metal forming, drop tests, and other contact-related scenarios. LS-DYNA is one of the primary tools used in these analyses [53]. In many industrial applications, the finite element discretizations mainly consist of thin shell elements, supplemented with some beam and solid elements. Various shell element formulations, based on Mindlin theory, are available, allowing users to balance computational efficiency and accuracy. Reduced integration is often chosen for large deformation analyses due to its efficiency and robustness against element distortions. Several methods and formulations are available to prevent hourglassing issues.

Explicit analysis provides various material models to represent different types of nonlinear material behavior, including rate-dependent, viscoelastic, viscoplastic, and foam material laws, many of which account for material failure. Rigid body kinematics are incorporated, simplifying the description of body motion into six master degrees of freedom. Other nodes in the finite element part are coupled to a master node through geometric relationships that accommodate large rotations. Nodes and surface segments of rigid bodies can define contact surfaces.

Contact algorithms in explicit analysis are advanced and efficient. Shell thicknesses are considered, and contact zones can be defined with precision. Additionally, general contact algorithms are available, which can be activated for the entire model or selected parts.

4.2 Dynamic Analysis in LS-Dyna

LS-DYNA is highly capable of performing transient dynamic analysis, producing results that closely match previous simulations. Figure 4.1 illustrates the crushing force, global deformation, and absorbed energy of the deformed FE model, all of which are generated by LS-DYNA [54].

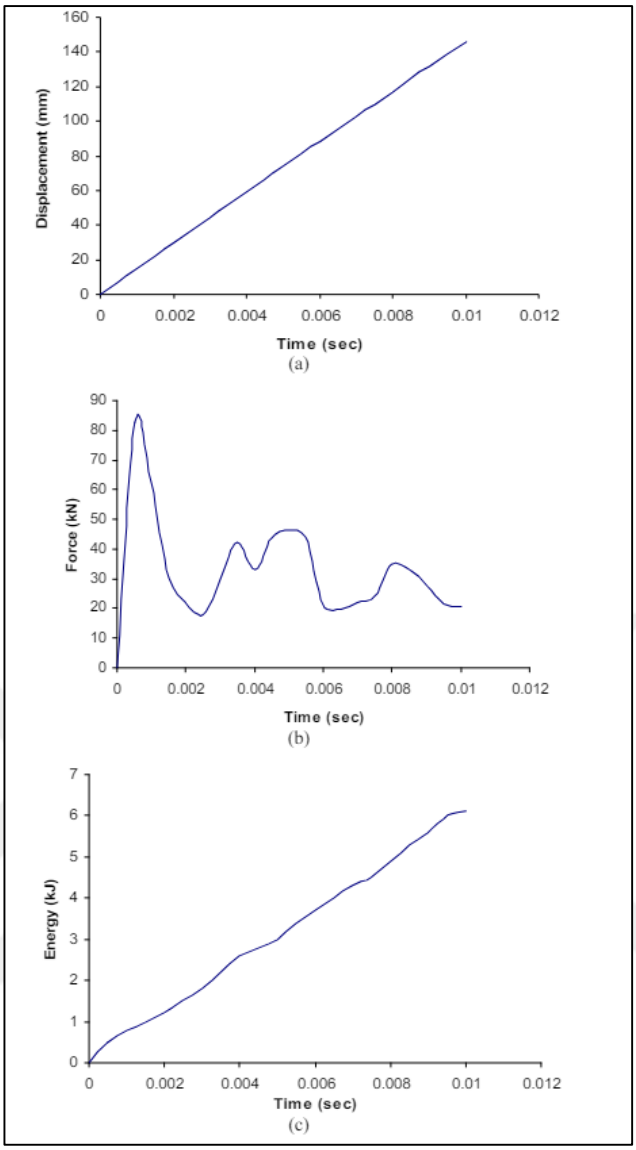

Figure 4.1: LS-Dyna analysis results; displacement(a), impact forces(b) and energy absorption (c) [54].

4.3 Central Difference Method

In this study, the Central Difference Method, which is the most commonly used numerical method in simulations that progress over time, especially in explicit analysis, is employed.

The Center Difference Method is especially effective in the analysis of systems that oscillate at high frequencies and in the simulation of short-term dynamic events (such as collisions, explosions). The advantage of this method is that it is quite fast because the calculation steps are direct and simple. However, choosing a small time step is important to preserve the accuracy and stability of the solution.

The central difference approach operates under the approach that [54]:

$$\ddot{U}_\iota = \frac{1}{\Delta x^2}(U_{i-1} - 2U_i + U_{i+1}) \tag{4.1}$$

$$\dot{U}_\iota = \frac{1}{2\Delta t}(U_{i+1} - U_{i-1}) \tag{4.2}$$

consist of the following states: t – Δt, t + Δt, and t at time t. At time t, the governing equilibrium equation.

$$M\ddot{U}_\iota + C\dot{U}_\iota + KU_i = R_i \tag{4.3}$$

If we substitute 4.1 and 4.2 in 4.3, we obtain :

$$\left(\frac{1}{\Delta t^2}M + \frac{1}{2\Delta t}C\right)U_{i+1} = R_i - \left(K - \frac{2}{\Delta t^2}M\right)U_i - \left(\frac{1}{\Delta t^2}M - \frac{1}{2\Delta t}C\right)U_{i-1} \tag{4.4}$$

As can be shown from 4.3, U_i (displacement at t) and U_{i-1} (displacement at t – Δt) both influence U_{i+1} (displacement at t + Δt). Thus, in order to compute the displacement at time t = –1, U_{-1}before beginning the operation, use equations 4.1 and 4.2, where i = 0 .

$$U_{i-1} = U_0 - \Delta t\dot{U}_0 + \frac{\Delta t^2}{2}\ddot{U}_0 \tag{4.5}$$

The states of motion , $\ddot{U}_{i+1}$, and $\dot{U}_{i+1}$ can then be fully solved after solving U_{-1}.

An implicit solution procedure using the Newmark method, which is an implicit time integration scheme, requires matrix inversion to calculate U_{i+1}. In contrast, the explicit central difference method does not require matrix inversion.- Consequently, the explicit integration method is more computationally efficient and can handle dynamic problems more quickly than the implicit method. Unlike the implicit integration method, which maintains stability even with large time steps, the explicit integration method requires a time step size that is smaller than the critical threshold specific to the finite element system being simulated to ensure stability. The undamped critical time step size is $2/\omega_n$ (where ω_n is the largest natural circular frequency and varies during the response calculation), which is typically very small [54].

To clearly demonstrate the stability of both implicit and explicit schemes, a simple undamped structure with the equilibrium equation $\ddot{x_\iota} + \omega^2 x_i = r_i$ is solved for stability analysis, with each integration method applied separately.

$$\ddot{x}_{i+1} + \omega^2 x_{i+1} = r_{i+1} \tag{4.6}$$

$$\dot{x}_{i+1} = \dot{x}_i + [(1-\delta)\ddot{x}_i + \delta\ddot{x}_{i+1}]\Delta t \tag{4.7}$$

$$x_{i+1} = x_i + \dot{x}_i \Delta t + \left[\left(\frac{1}{2} - \alpha\right)\ddot{x}_i + \alpha\ddot{x}_{i+1}\right]\Delta t^2 \tag{4.8}$$

Equations 4.7 and 4.8 can be substituted into 4.6 to produce the following relation with $\alpha = 1/4$ and $\delta = 1/2$:

$$\begin{bmatrix} \ddot{x}_{i+1} \\ \dot{x}_{i+1} \\ x_{i+1} \end{bmatrix} = A \begin{bmatrix} \ddot{x}_i \\ \dot{x}_i \\ x_i \end{bmatrix} + L_{r_{i+1}} \tag{4.9}$$

where

$$A = \begin{bmatrix} -0.25\beta & \frac{\beta}{\Delta t} & \frac{\beta}{\Delta t^2} \\ \Delta t[0.5 - 0.125\beta] & 1 - 0.5\beta & -\frac{\beta}{2\Delta t} \\ \Delta t^2[0.25 - 0.0625\beta] & \Delta t[1 - 0.25\beta] & 1 - 0.25\beta \end{bmatrix} \tag{4.10}$$

and

$$\beta = \left(\frac{1}{\omega^2 \Delta t^2} + \frac{1}{4}\right)^{-1} \tag{4.11}$$

this will be employed in the stability analysis.

By substituting A into the eigenvalue equation $A\mathrm{u} = \lambda\mathrm{u}$, the eigenvalue

λ can be determined. For stability, it is required that $\lambda \leq 1$. Upon solving the equation, it is found that for any Δt, the inequality $\lambda \leq 1$ is satisfied. Therefore, the implicit analysis is unconditionally stable.

Using the explicit analysis and the central difference approach, we may obtain:

$$\ddot{x}_i + \omega^2 x_i = r_i \tag{4.12}$$

$$\ddot{x}_i = \frac{1}{\Delta t^2}(x_{i-1} - 2x_i + x_{i+1}) \tag{4.13}$$

$$\dot{x}_i = \frac{1}{2\Delta t}(x_{i+1} - x_{i-1}) \tag{4.14}$$

After entering 4.13 and 4.14 as substitutes into 4.12 and solving for x_{i+1}, we get that:

$$x_{i+1} = (2 - \omega^2 \Delta t^2)x_i - x_{i-1} + \Delta t^2 r_i \tag{4.15}$$

The following can be used to rewrite solution 4.15 in form 4.9 :

$$\begin{bmatrix} x_{i+1} \\ x_i \end{bmatrix} = A \begin{bmatrix} x_{i+1} \\ x_i \end{bmatrix} + L_{r_i} \tag{4.16}$$

where

$$A = \begin{bmatrix} 2 & -1 \\ 1 & 0 \end{bmatrix} \tag{4.17}$$

By substituting A into the eigenvalue equation $A\mathrm{u} = \lambda\mathrm{u}$ and solving for the inequality $\lambda \leq 1$, it is found that the inequality is satisfied only when $\Delta t \leq 2/\omega_n$ (where ω_n is the largest natural circular frequency) This indicates that the explicit analysis is conditionally stable. One of the primary drawbacks of the explicit integration method is the severe time step restriction [54].

.

5. ANALSYS MODEL, LOADS AND BOUNDARY CONDITIONS

In this section, the setup of studies for the analysis of new landing areas for deck landings will be discussed in detail. First, the basic principles used in the design of landing areas and the technical details of the structural installation will be examined. The geometric features and sizing criteria to be taken into account during the installation phase of the structure will be evaluated in accordance with different landing scenarios.

In addition, the forces to which the landing areas will be exposed and the boundary conditions that determine the behavior of the structure under the influence of these forces will also be detailed. These analyzes are critical for the safe and efficient use of landing areas. In particular, the effects of dynamic loads and environmental factors that may occur during landing will be examined comprehensively. As a result, the analyzes carried out in this section aim to provide important data in terms of the design and feasibility of new landing areas.

5.1 Structure and Geometry

Various references were used for the geometric model and structural structure prepared to be used in deck landing analyses. The main reason for choosing these references is to ensure that the structure responds to the forces it will be exposed to as realistically as possible.

First of all, the general topology and geometric dimensions of the structure are designed based on reference [56], also it is shown in Figure 5.1. The purpose of choosing this reference is that the model has the structural features of the deck structure there and the calculated natural frequency values are compatible with each other. Thus, the accuracy and reliability of landing analyzes are increased. The model prepared in this way exhibits realistic behavior and enables a more accurate evaluation of the dynamic loads and environmental effects that may occur during landing.

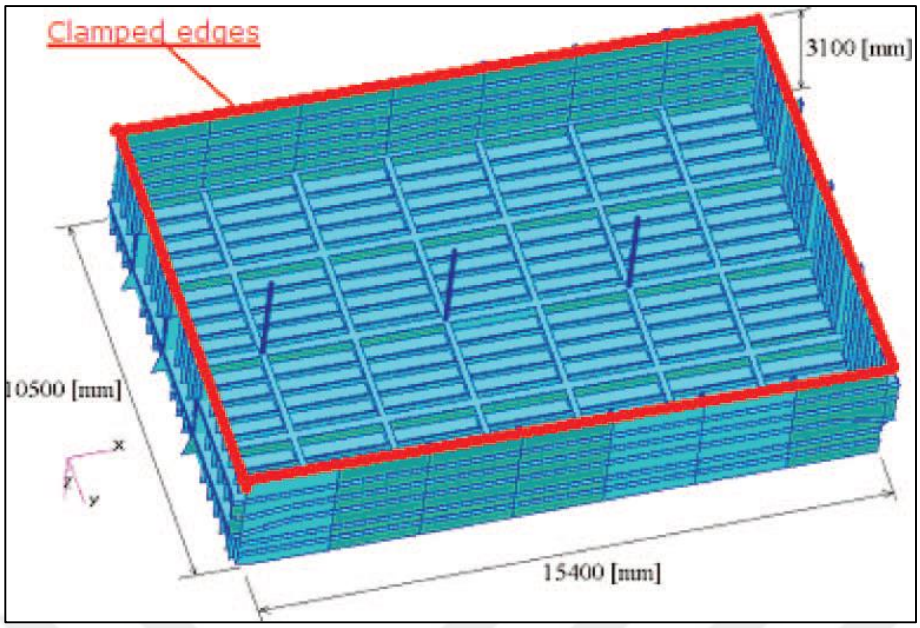

Figure 5.1 : Inspired deck model according to reference [56].

Following geometric and structural topology adaptations, the structural scantling of the structure was adjusted to the standards of classification societies such as DNV, LR and RINA rules. This scantling process was performed using reference [56]. After the dimensioning was completed, a natural frequency was calculated to ensure that the structure behaves realistically and to increase the accuracy of landing analyses. The natural frequencies of the model can be seen at Table 5.1. Also, first mode and third mode deflection can be seen at Figures 5.2 and 5.3.

Table 5.1 : Natural frequencies of the model.

Mode Number	Natura Freqeuncies
1	38.395
2	45.209
3	47.216
4	48.754
5	50.438

5.2 Mesh Adjustment on the Model

We examined the structure using a mesh model created with 100 mm element size. Using a 100 mm element size in explicit analysis provides a balanced approach, ensuring sufficient accuracy in capturing dynamic responses and stress distributions while maintaining computational efficiency. This approach ensures that the structure reaches sufficient degrees of freedom and a detailed analysis is performed. In this way,

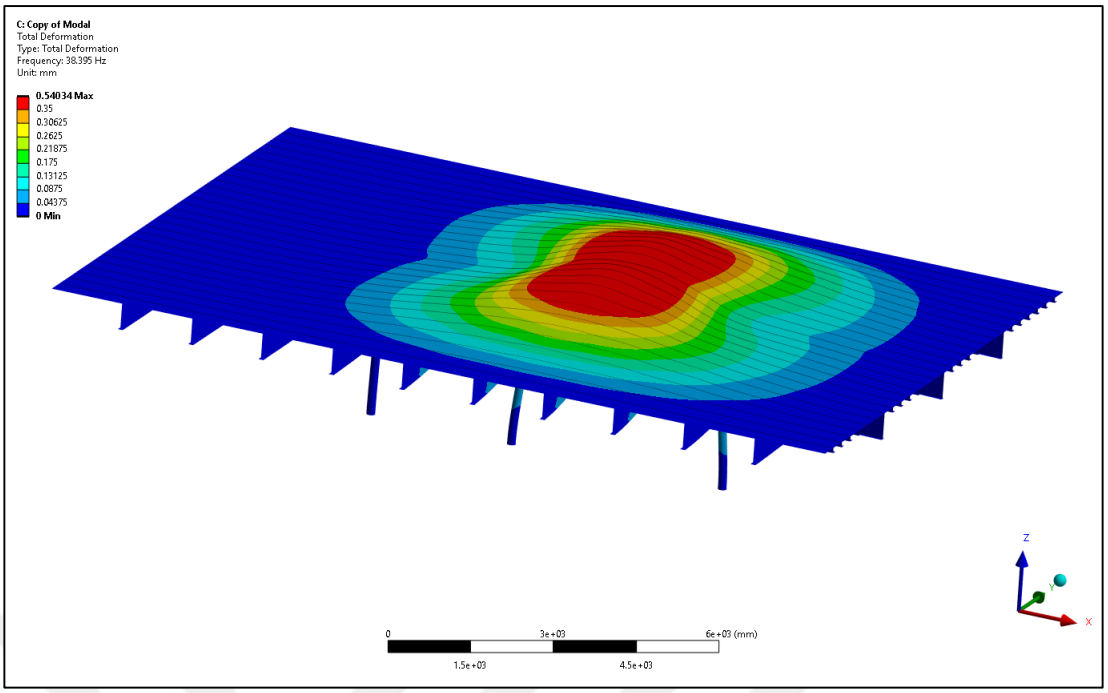

Figure 5.2 : First mode of the structure (1 node vertical bending).

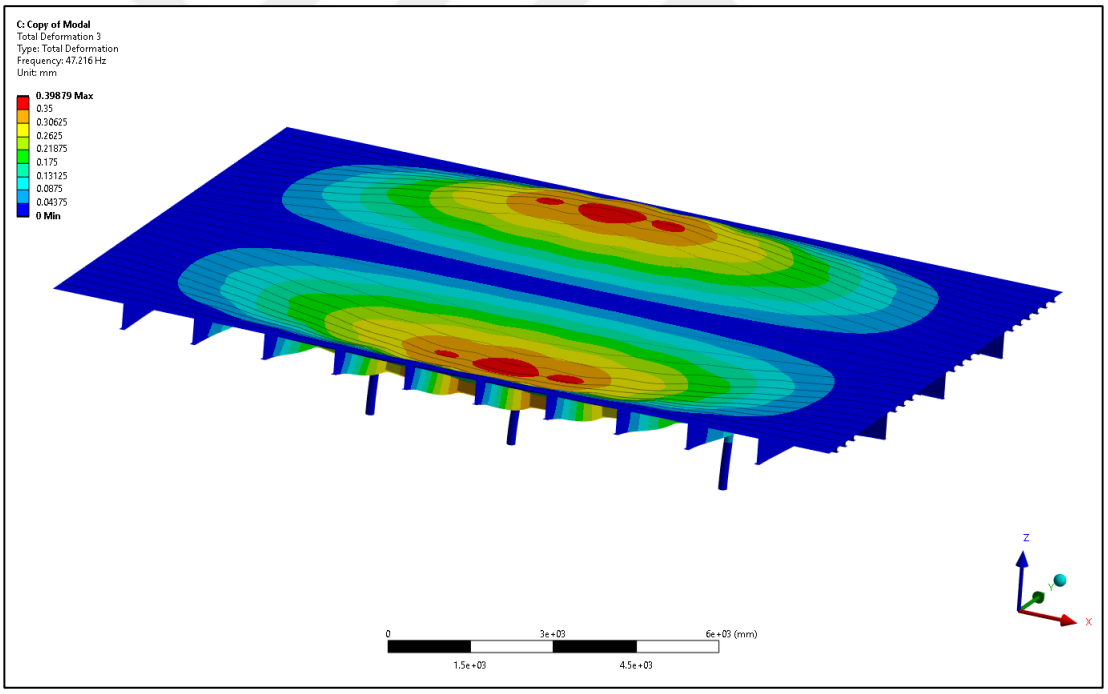

Figure 5.3 : Third mode of the structure (2 node vertical bending).

we can evaluate the mechanical behavior of the structure more precisely and identify possible weak points or areas for improvement. The 100 mm element size applied as shown in Figures 5.4 and 5.5 was the ideal choice to achieve the required accuracy and precision in the analysis.

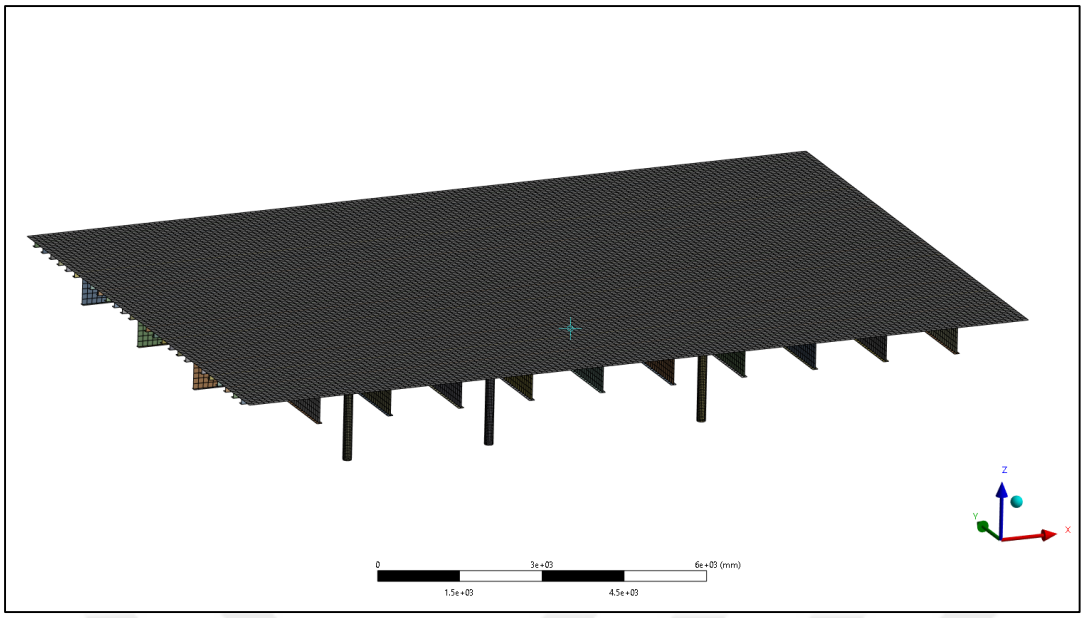

Figure 5.4 : Mesh model of the deck structure.

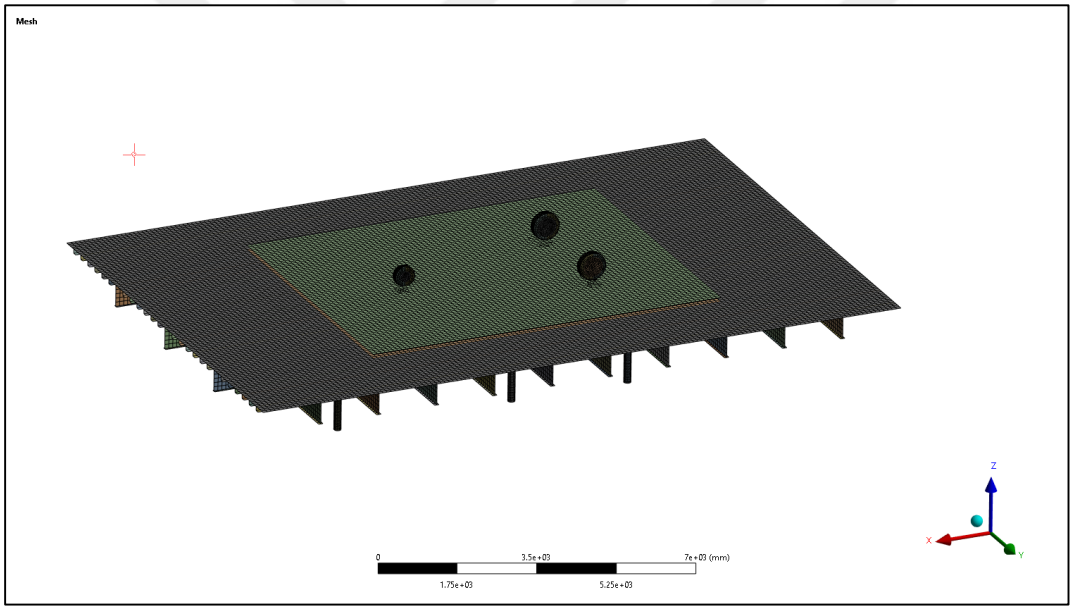

Figure 5.5 : Mesh model of the deck structure with landing zone and dummy landing gear wheels.

5.3 Material Properties

The material selection for the analyses was conducted with great precision, utilizing the standard steel material available in the Ansys library. This choice was made due to the well-documented mechanical properties and durability of steel. The extensive material library in Ansys provides high-quality material data essential for achieving reliable and accurate results in engineering analyses. Standard steel was selected

because it is a commonly used and dependable material in structural analyses. The properties of this standard steel material are presented in the Table 5.2 below:

Table 5.2 : Structural steel properties.

PROPERTY	VALUE
Density	7850 KG/M³
Young's Modulus	210 GPA
Poisson's Ratio	0.3
Yield Strength	250 MPA
Tensile Strength	460 MPA
Thermal Expansion Coefficient	12E-6 /°C
Specific Heat Capacity	486 J/KG·K
Thermal Conductivity	60.5 W/M·K

5.4 Applied Loads and Boundary Conditions

According to reference [56], a free fall analysis of an air fighter dropped from a height of 1.07 meters was conducted, resulting in an approximate impact velocity of 4.6 m/s. In alignment with the methodology presented in reference [57], my study conducted a free fall simulation based on the structural configuration and center of gravity of an F16 aircraft. Additionally, for the purpose of comparative evaluation of the analyses, analyzes were carried out according to the normal impact speed of 2.7 m/s and the severe impact speed of 3.54 m/s specified in reference [52]. These simulations were executed utilizing the LS-Dyna module within the Ansys software suite.

For the simulation, boundary conditions included the application of fixed supports along the perimeter of the deck structure. Additionally, fixed supports were implemented at the bases of the stanchions connected to the deck structure. These boundary conditions were meticulously chosen to facilitate a precise analysis of potential deformations and stresses within the structure. The LS-Dyna module is particularly suited for such dynamic analyses, enabling a detailed examination of the structural behavior and identification of potential vulnerabilities during free fall. The comprehensive nature of this analysis yielded critical insights necessary for optimizing the safety and performance of the structure.

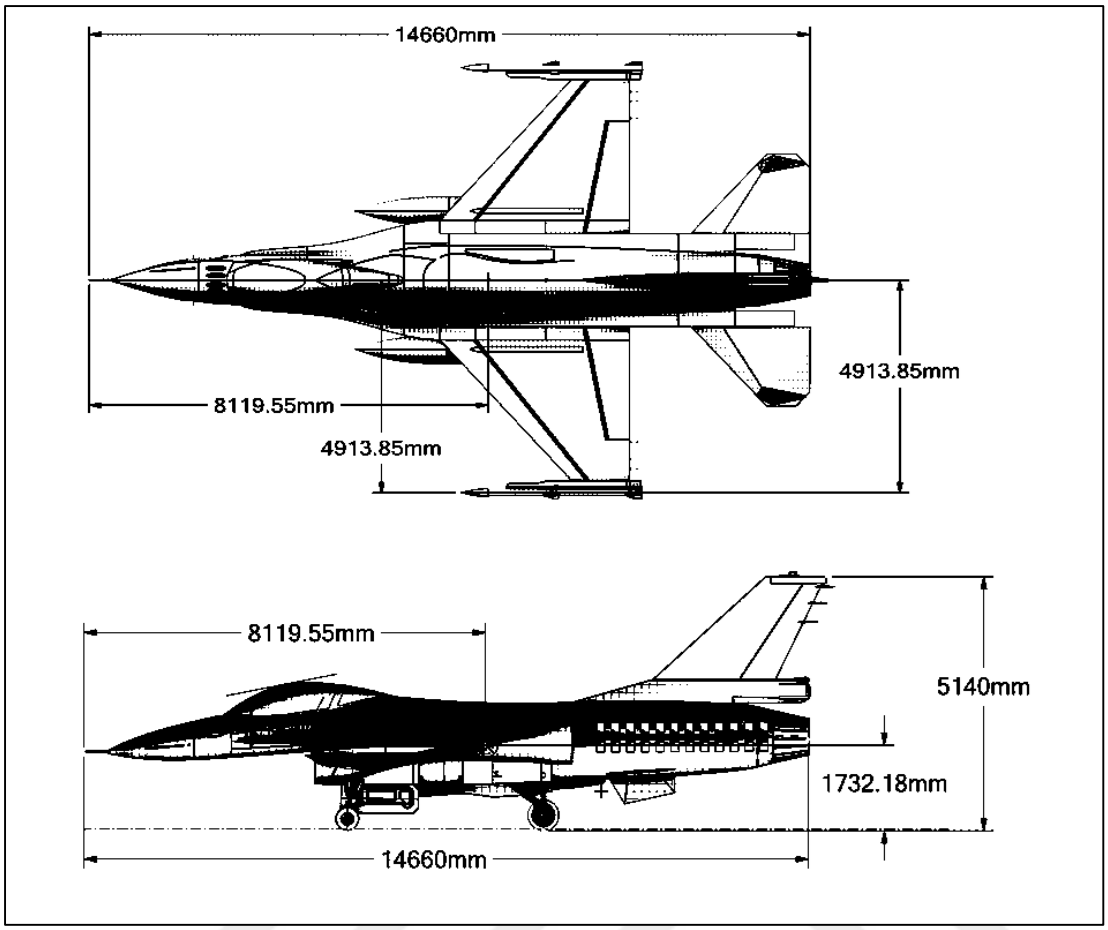

Figure 5.6 : F16 general plan according to Lockheed Martin manual [58].

In the analysis made on the finite element model of the F-16 aircraft, a dummy implementation was carried out on the aircraft model. The weight of the aircraft is 9207 kg and its center of gravity can be examined on Figure 5.6. The purpose of this study is to ensure that the energy of the load created by the F-16 is effectively transferred to the deck.

For the landing zone, a spring-damping system has been added in addition to the crash zone of the dummy F-16 as shown in the Figures 5.7 and 5.8. In addition, the landing zone size was considered to be the size of an aircraft and was designed accordingly and weight of landing zone is 8902 kg. This system was designed inspired by references [52] and [10].

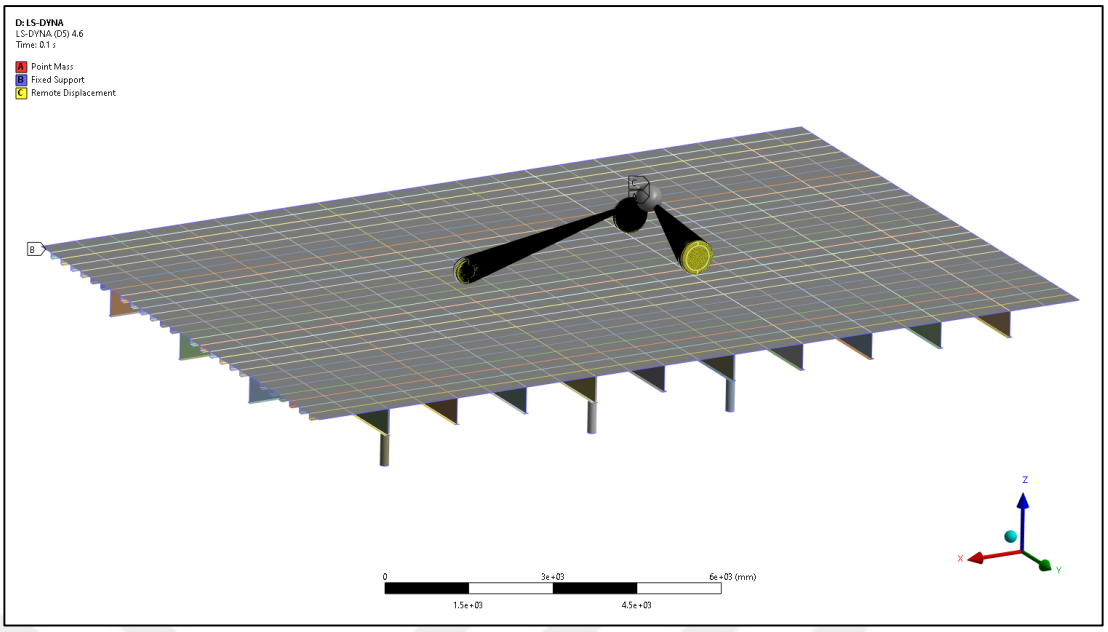

Figure 5.7 : Explicit model preparation without landing zone.

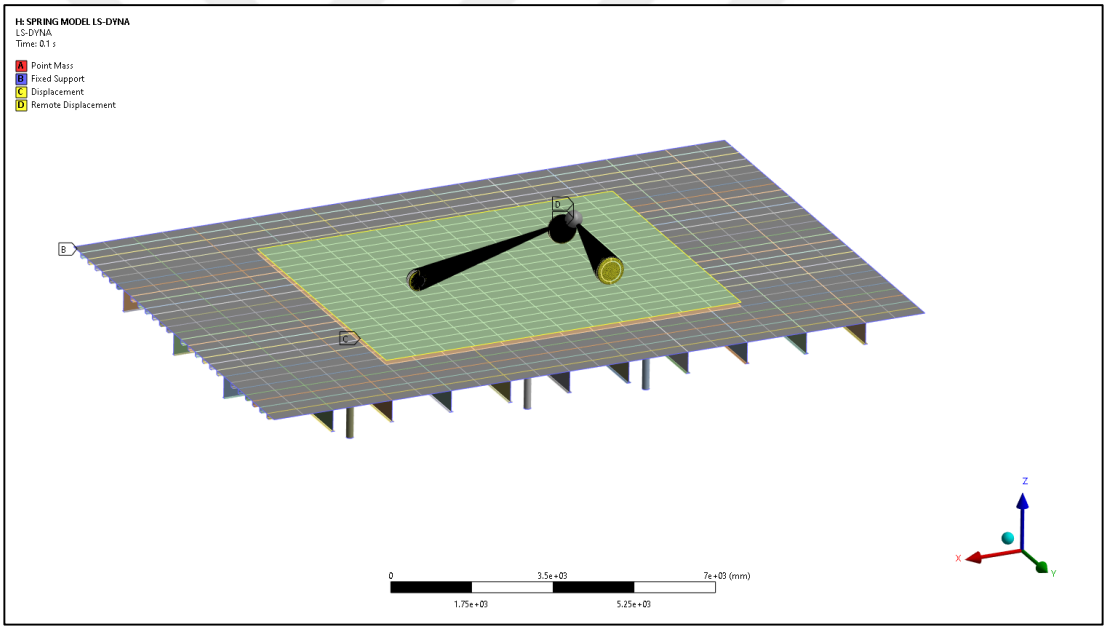

Figure 5.8 : Explicit model preparation with landing zone.

6. RESULTS

6.1 Analytic Solution

This study examines an inelastic collision followed by the motion of a system involving a spring and a damper. The given data are at Table 6.1:

Table 6.1 : Analysis Data.

DATA	VALUE
Aircraft Weight (m_1)	9207 kg
Aircraft Weight (m_2)	8902 kg
Initial velocity of m_1 before the collision	4.6 m/s
Spring Constant (k)	1000000 N/m
Damping coefficient (c)	500000 Ns/m

The total momentum before the collision is calculated as:

$$P_{\text{before}} = m_1 \cdot v_0 = 9207 \cdot 4.6 = 42352.2 \text{ kg} \cdot \text{m/s} \quad (6.1)$$

The total momentum after the collision is:

$$P_{\text{after}} = (m_1 + m_2) \cdot v_{\text{after}} = 18109 \cdot v_{\text{after}} \quad (6.2)$$

According to the principle of conservation of momentum:

$$P_{\text{before}} = P_{\text{after}} \backslash implies 42352.2 = 18109 \cdot v_{\text{after}} \quad (6.3)$$

From this, we can find the post-collision velocity v_{after} :

$$v_{\text{after}} = \frac{42352.2}{18109} \approx 2.34 \text{ m/s} \quad (6.4)$$

The total momentum before the collision is calculated as:

$$P_{\text{before}} = m_1 \cdot v_0 = 9207 \cdot 4.6 = 42352.2 \text{ kg} \cdot \text{m/s} \quad (6.1)$$

The total momentum after the collision is:

$$P_{\text{after}} = (m_1 + m_2) \cdot v_{\text{after}} = 18109 \cdot v_{\text{after}} \quad (6.2)$$

According to the principle of conservation of momentum:

$$P_{\text{before}} = P_{\text{after}} \backslash implies 42352.2 = 18109 \cdot v_{\text{after}} \quad (6.3)$$

From this, we can find the post-collision velocity v_{after} :

$$v_{\text{after}} = \frac{42352.2}{18109} \approx 2.34 \text{ m/s} \tag{6.4}$$

The equation of motion for the system after the collision, taking into account the spring and damping forces, is written as follows:

$$m_{\text{total}}\ddot{x} + c\dot{x} + kx = 0 \tag{6.5}$$

Here:

$$m_{\text{total}} = 18109 \text{ kg}, \quad c = 500000 \text{ Ns/m}, \quad k = 1000000 \text{ N/m}$$

The equation becomes:

$$18109\ddot{x} + 500000\dot{x} + 1000000x = 0 \tag{6.6}$$

The roots are found by:

$$18109r^2 + 500000r + 1000000 = 0 \tag{6.7}$$

The discriminant is calculated as follows:

$$\Delta = 500000^2 - 4 \cdot 18109 \cdot 1000000 = 250000000000 - 72436000000 = 177564000000$$

$$\Delta = 250000000000 - 72436000000 = 177564000000$$

$$r = \frac{-500000 \pm \sqrt{177564000000}}{2 \cdot 18109}$$

$$\sqrt{177564000000} \approx 421351.78$$

$$r_1 = \frac{-500000 + 421351.78}{36218} \approx -2.18$$

$$r_2 = \frac{-500000 - 421351.78}{36218} \approx -25.45$$

The general solution of the equation is:

$$x(t) = Ae^{-2.18t} + Be^{-25.45t} \tag{6.8}$$

Given the initial conditions $x(0) = 0$ and $\dot{x}(0) = 2.34\ m/s$:

$$x(0) = A + B = 0, \ B = -A$$

$$\dot{x}(0) = A(-2.18) + B(-25.45) = 2.34$$

$$A(-2.18) + (-A)(-25.45) = 2.34$$

$$A(-2.18 + 25.45) = 2.34$$

$$A \cdot 23.27 = 2.34$$

$$A = \frac{2.34}{23.27} \approx 0.1006$$

$$B = -A = -0.1006$$

The general solution is:

$$x(t) = 0.1006e^{-2.18t} - 0.1006e^{-25.45t} \tag{6.9}$$

The damping ratio $\boldsymbol{\zeta}$ is calculated as follows:

$$\zeta = \frac{c}{2\sqrt{km}} \tag{6.10}$$

$$\zeta = \frac{500000}{2\sqrt{1000000 \cdot 18109}} \approx 1.857$$

The system is overdamped because the damping ratio is greater than 1. In this case, the system returns to its equilibrium position very slowly without oscillating.

6.2 Analytic Solution and Ls-Dyna Comparison

In this study, a comprehensive comparative analysis was conducted between the analytical solution and the LS-DYNA model. The purpose of this comparison was to evaluate the accuracy and reliability of the LS-DYNA model in replicating the analytical results. Following this comparison, model validation was performed to further ensure the robustness of the LS-DYNA simulations. The results of this comparative analysis, including a detailed comparison of key parameters and performance metrics, are illustrated in Figure 6.1 below.

6.3 Wei's Analytic Model Results

According to Wei, when there is ground contact, a vertical velocity of 2.70 meters per second (8.86 feet per second) is referred to as normal impact. The computed outcomes of this new model are contrasted with those of a model lacking a landing region in Figure 6.2. In the new model, the maximum values are, accordingly, lowered by 45% [52].

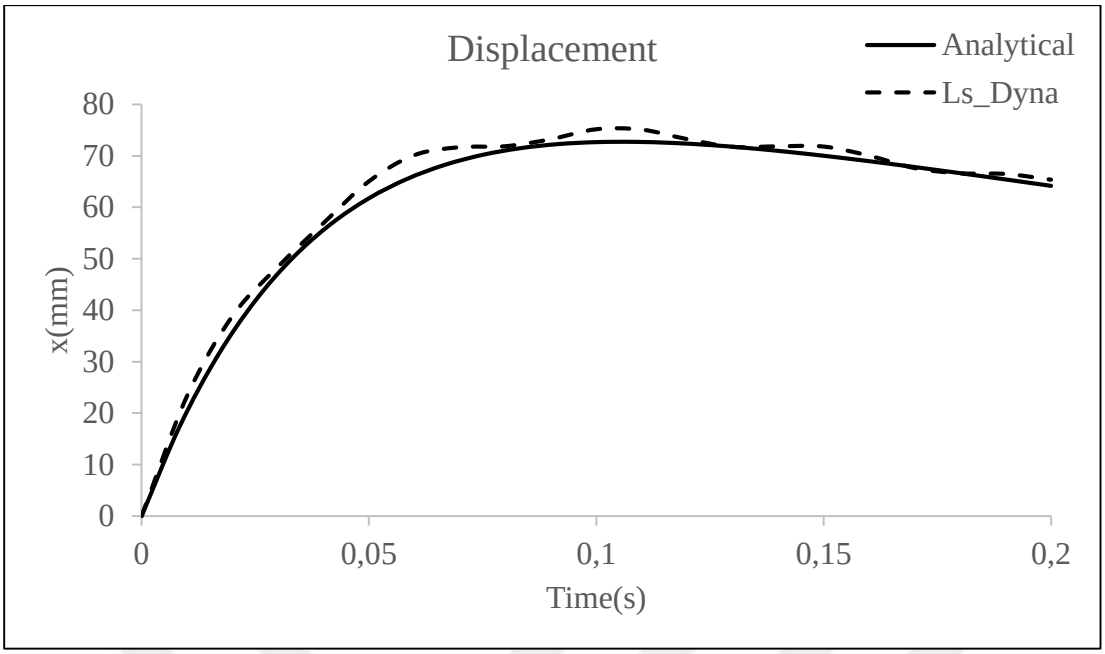

Figure 6.1 : Displacement of Ls-Dyna model and analytical solution equation.

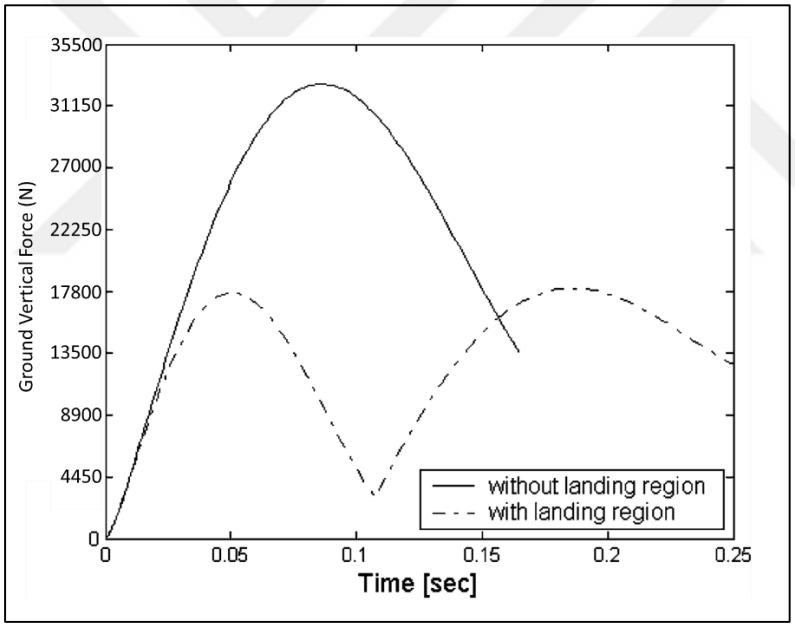

Figure 6.2 : Normal impact results for ground vertical force graph [52].

At the moment of ground contact, a vertical velocity of 3.54 meters per second (11.63 feet per second) is considered a severe impact. In this situation, tire bottoming happens for the model without a landing zone. A comparison between the estimated results using this new model and the calculated results using the model without a landing region is shown in Figure 6.3.

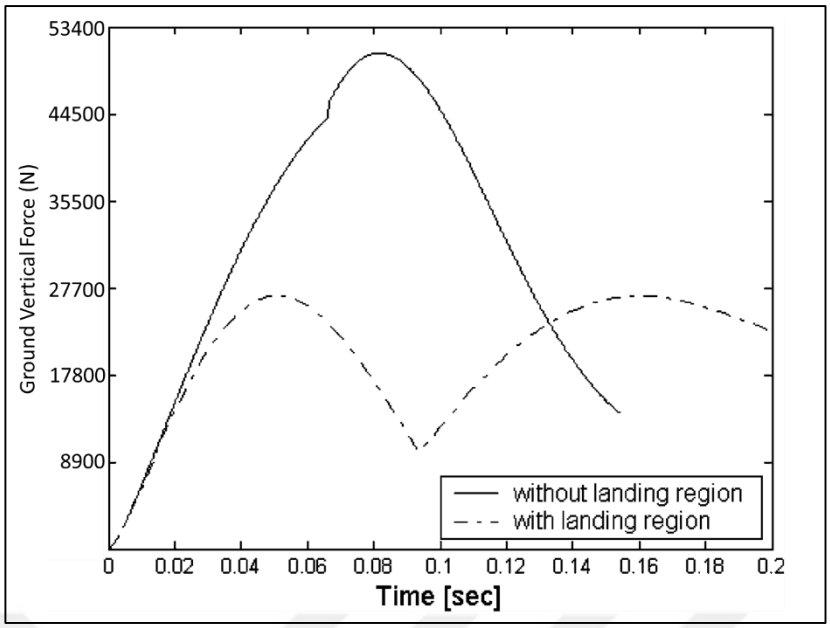

Figure 6.3 : Severe impact results for ground vertical force graph [52].

Figure 6.3 shows that there is a 49.0% reduction in the maximum force on upper mass.

It is discovered that when a normal impact speed of 2.70 meters per second (8.86 fps) and a severe impact speed of 2.70 meters per second (11.63 fps) are taken into consideration, respectively, the force on the ground mass is reduced by 44.7% and 49.0% [52].

6.4 Ls-Dyna Explicit Analysis Results

The results of the explicit analysis performed by providing similar experimental conditions with the mathematical solution can be examined in detail in the figure below. These analyzes aim to evaluate the performance and durability of the structure in the most accurate way by creating scenarios close to real-world conditions. This figure, in which the analysis results are presented, allows us to observe in detail the stress, deformation and other mechanical effects that may occur on the structure. Figures 6.4, 6.5, and 6.6 shows the forces results of model and Figures 6.7, 6.8, and 6.9 shows the von-mises stress results of model.

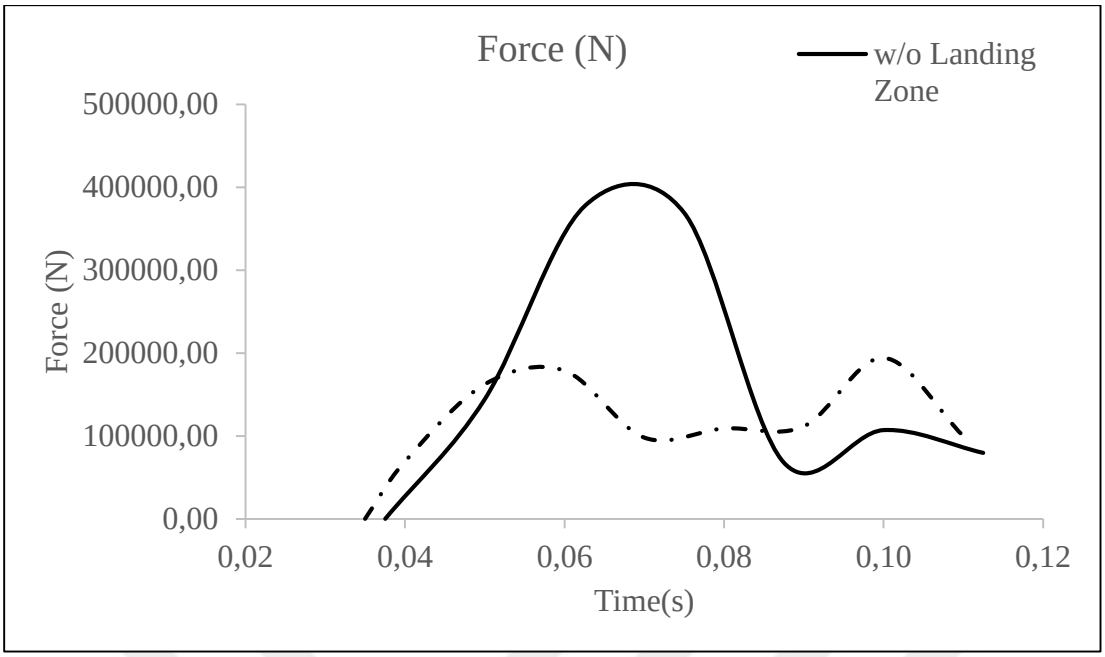

Figure 6.4 : Free Fall Drop from 1.07m simulation force results, velocity = 4.6 m/s.

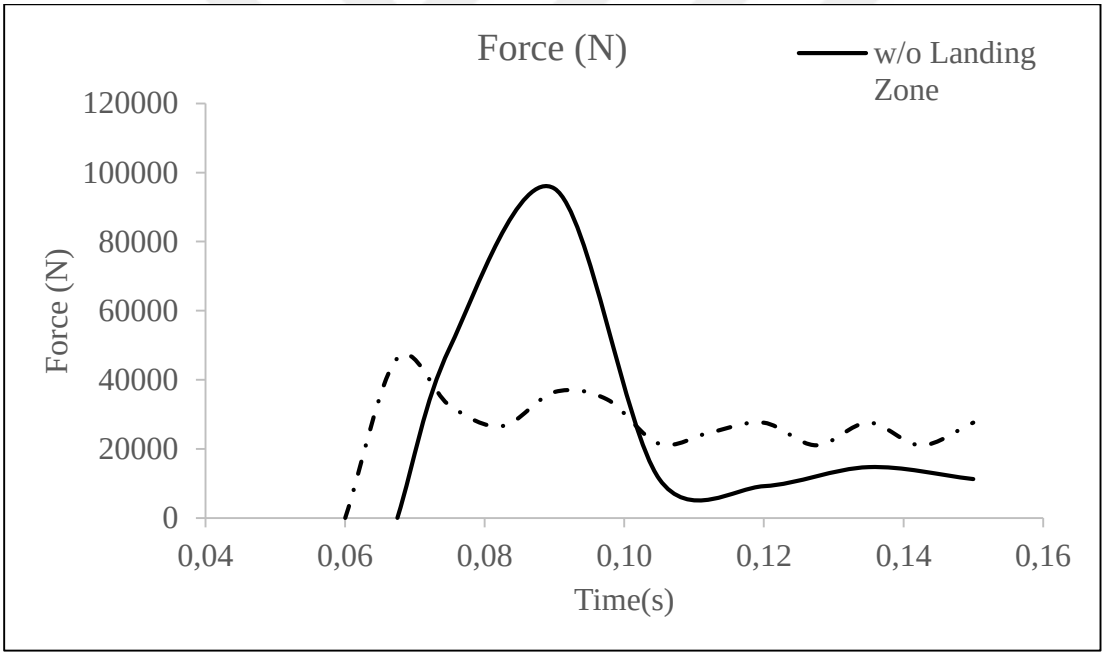

Figure 6.5 : Normal impact simulation force results, velocity = 2.7 m/s.

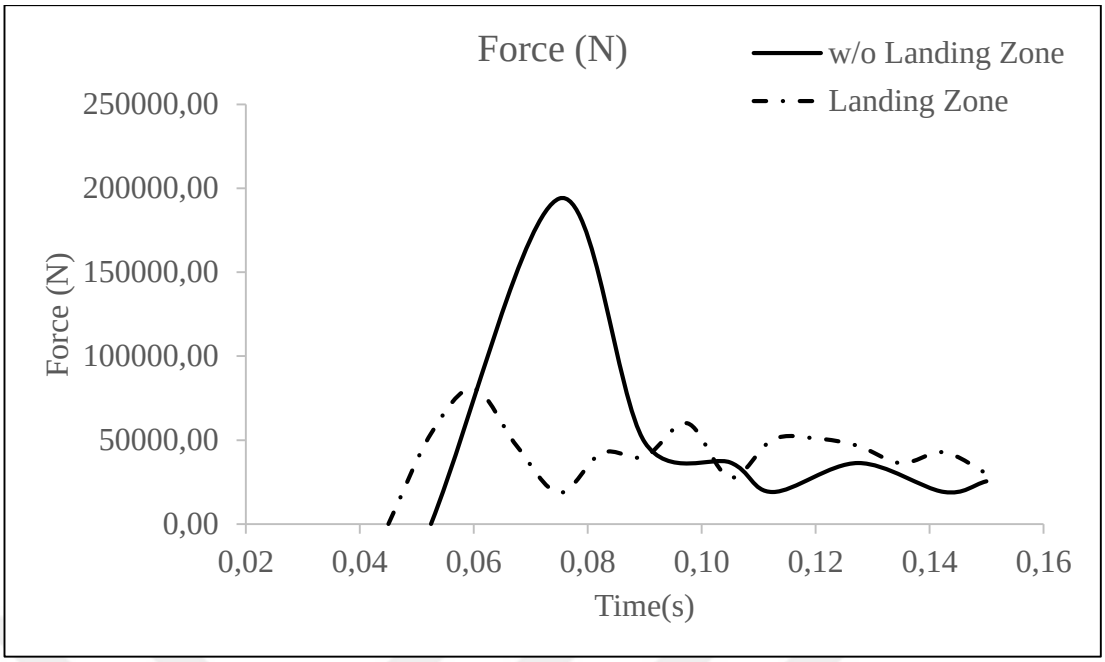

Figure 6.6 : Severe impact simulation force results, velocity = 3.54 m/s.

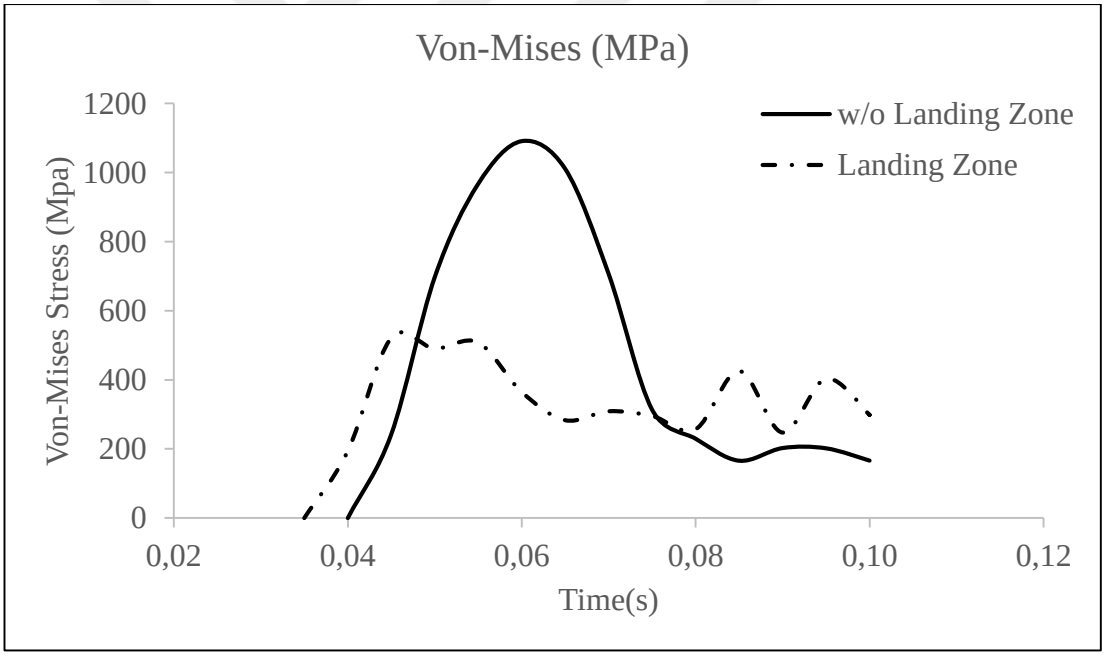

Figure 6.7 : Severe impact simulation von-mises stress results, velocity = 3.54 m/s.

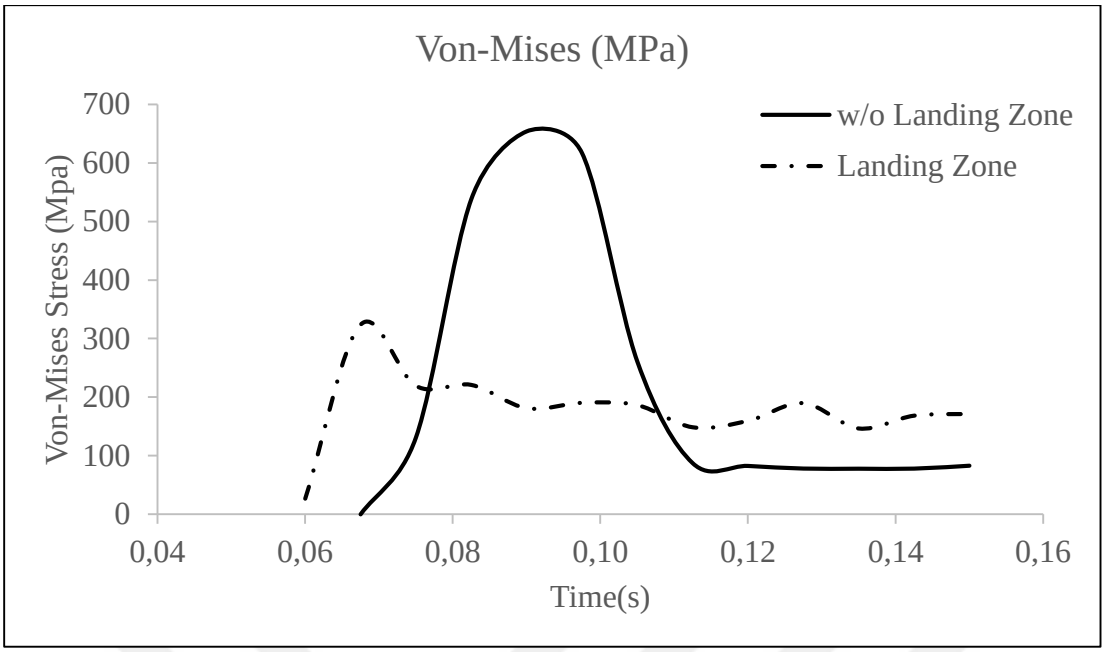

Figure 6.8 : Normal impact simulation von-mises stress results, velocity = 2.7 m/s.

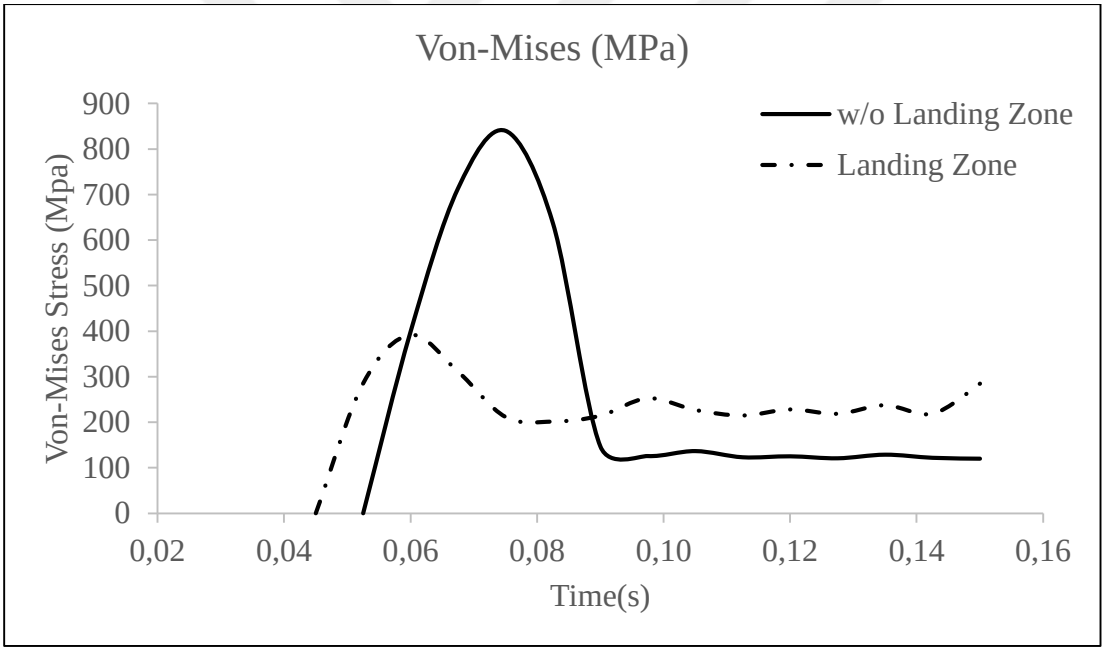

Figure 6.9 : Severe impact simulation von-mises stress results, velocity = 3.54 m/s.

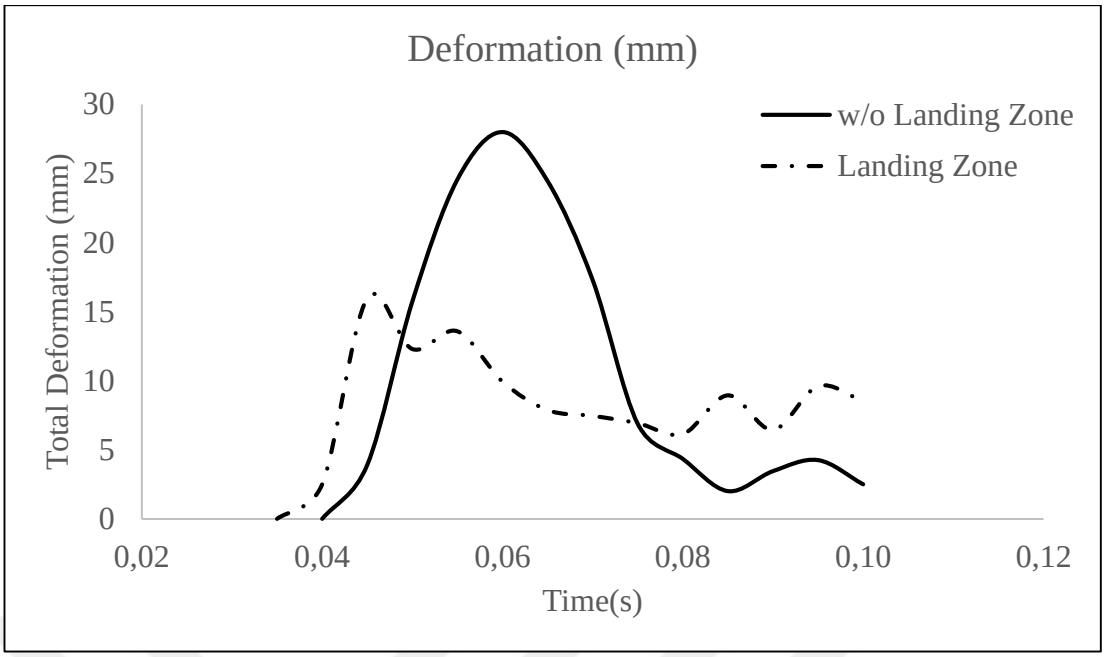

Figure 6.10 : Free Fall Drop from 1.07m simulation deformation results, velocity = 4.6 m/s.

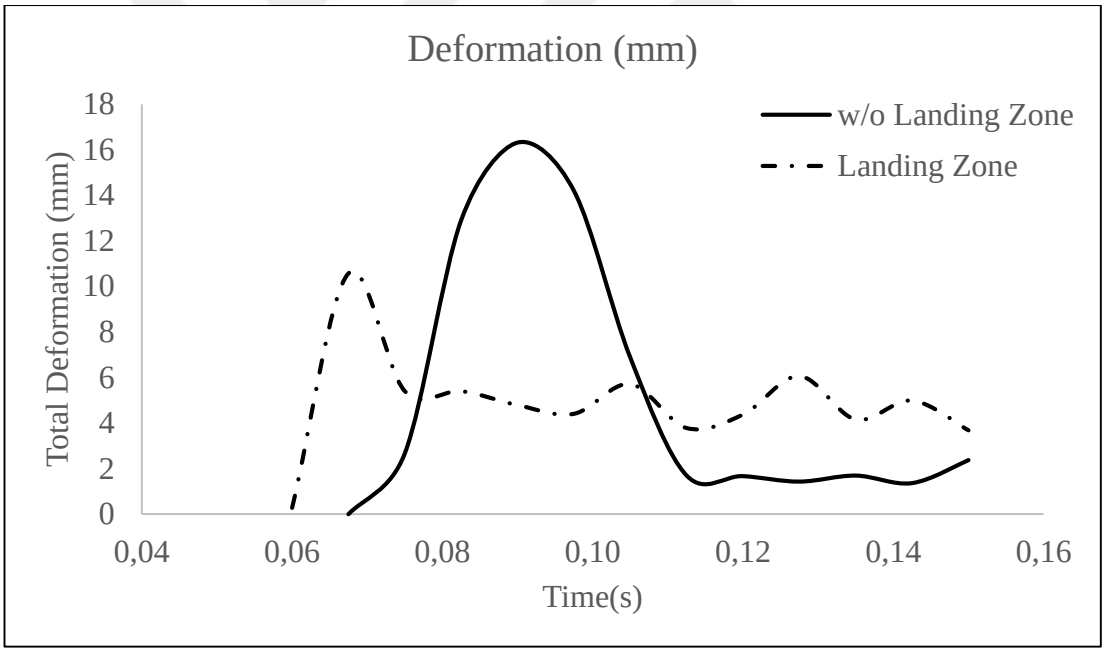

Figure 6.11 : Normal impact simulation deformation results, velocity = 2.7 m/s.

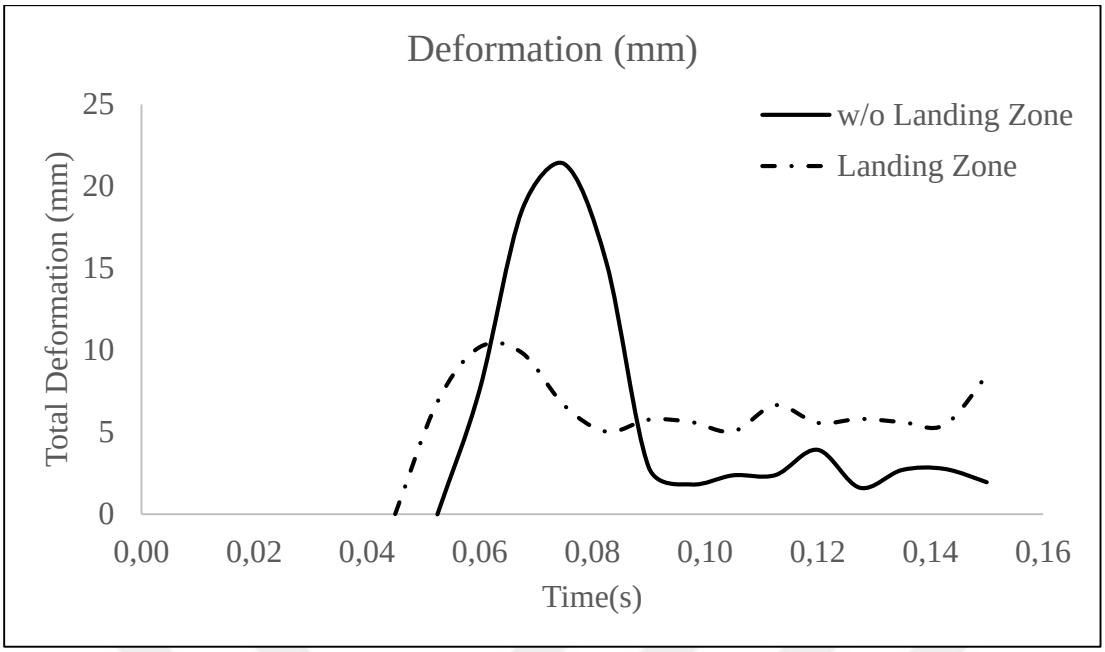

Figure 6.12 : Severe impact simulation deformation results, velocity = 3.54 m/s.

Upon examining the results obtained from explicit analysis, it is observed that the stress values significantly decreased following the implementation of the landing zone. hen we look at the results obtained after explicit analysis; we observe that stress values decreased significantly after landing zone implementation. In particular, according to the force data in Figures 6.4, 6.5 and 6.6, and the von mises stress data in Figures 6.7, 6.8 and 6.9, peak forces and stress values decreased by 53.41%, 50.53% and 53.38%, respectively. This decrease clearly demonstrates the positive effect of landing zone implementation on stress distribution.

Likewise, when we look at the deformation values, a similar improvement is observed. According to the results in Figures 6.10, 6.11 and 6.12, deformation values decreased by 43.04%, 35.23% and 52.31%, respectively. These data show that landing zone implementation significantly improves not only stress values but also deformation levels.

In summary, explicit analyzes prove that landing zone implementation has largely positive effects on both stress and deformation.

7. CONCLUSION

Landing aircraft on aircraft carrier decks presents a significant challenge in terms of engineering, safety, and operational applicability. The dynamic nature of the carrier's movement, coupled with the high precision required for successful landings, underscores the complexity of this problem. Consequently, continuous improvements and innovations in landing systems are essential to enhance safety and efficiency. In this study, a novel landing zone design incorporating an advanced damping system was investigated. The primary objective was to assess the effectiveness of this system in mitigating the impact forces during landing and to determine its potential for integration into future aircraft carrier designs. The results of this investigation provide valuable insights into the performance of the damping system, highlighting its capability to enhance landing safety and overall system reliability.

The research findings indicate that the impact load can be distributed to the area referred to as the "landing zone" at rates ranging from 44 to 49 percent based on analytical results, and between 45 and 50 percent according to explicit analysis. This makes a significant contribution to structural durability. This shock load acting on the structure is also transmitted in a better distributed manner, so that the structure is not damaged more than necessary.

The main purpose of this study is to examine the capacity of the structure to manipulate the impact load it will be exposed to as much as possible. The results obtained show that having a damping system on the air carrier deck can provide the necessary benefit to the deck structure. This is critical for air carriers and similar structural systems because effective distribution of shock loads increases the service life and safety of these structures.

This study on the effects of impact loads on the structure fills an important gap in the engineering literature. In particular, analyzes on the effect of damping systems provide valuable information on how such systems can increase structural durability. The decrease in the peak value of impact loads causes the load to act on the structure for a longer period of time. This can have significant effects on the fatigue life of the

structure. Therefore, it is necessary to accurately estimate the fatigue life of the structure and take necessary precautions against these effects.

In addition, how damping systems will perform if they have active rather than passive operating principles is also an important issue for further research. Active damping systems have great potential for instantaneous detection of impact loads and dynamic response to these loads. Developing and optimizing such systems could provide a great advantage for future engineering applications.

However, it is also imperative to consider the real-life costs associated with implementing this landing zone design. While the proposed system appears beneficial in terms of analysis, its practical applicability and economic feasibility must be thoroughly evaluated. The question remains whether manufacturing such a structure would be more ergonomic and cost-effective compared to current solutions. Additionally, the potential financial implications of not implementing this system—whether it would lead to increased or decreased expenses—need careful consideration. Ultimately, determining the economic and operational viability of this advanced damping system is essential for its successful adoption in future aircraft carrier designs.

In this context, the results of the study emphasize the importance of damping systems used in structural engineering. Effective distribution of impact loads on structures not only reduces structural damage but also improves the overall performance and safety of structures. Especially for critical structures such as air carriers, optimizing and correctly implementing such systems is vital.

In conclusion, this study makes a significant contribution to structural engineering by comprehensively addressing the effects of impact loads on the structure and how these effects can be manipulated. In this context, optimizing and effectively applying damping systems can play a critical role in increasing the durability of structures. Further research in the field of structural engineering will contribute to the further development of such systems and their use in a wider range of applications.

REFERENCES

[1] **Wang, Q. S.** (2005). Critical Technologies in Carrier-Based Aircraft Design and Development. Aircraft Design, 2, 6-10.

[2] **Gao, Z. J., Huang, Z. W., & Yu, J. H.** (2002). Airplane Design Manual Part 14-Takeoff Landing System Design. Beijing: Aviation Industry Press.

[3] **Tao, Y., Jia, Z. H., & Hou, Z. Q.** (2010). Research on the Dynamics of Carrier Aircraft Arrested Deck-Landing. Journal of Naval Aeronautical and Astronautical University, 25(2), 133-136.

[4] **Daughetee, C. C.** (1974). Drop testing naval aircraft and the VSD landing gear dynamic test facility. AIAA Paper No. 74-343.

[5] **Hu, G. C., Wang, Q., Liu, X. Y., & Guo, W. G.** (2009). Influence of Carrier Air Wake on Carrier-Based Aircraft Landing Trajectory and Dynamic Response. Flight Dynamics, 27(6), 18-21.

[6] **Zhao, B. B., Wu, B., & Huang, D. D.** (2008). The Effects of Deck Obstruction on Carrier Plane Landing Performance. Computer Simulation, 25(12), 84-87.

[7] **Qu, Z. Q., & Fu, Z. F.** (1997). Effects of Ship Movements and Deformation on Impact Loads of Aircraft in Landing. Journal of Shanghai Jiaotong University, 31(9), 6-9.

[8] **Curry, N. S.** (1988). Aircraft landing gear design: principles and practice. Washington: AIAA Education Series.

[9] **Hu, M. Q., & Lin, G. H.** (2000). Carrier-based Aircraft Arrested Landing Dynamics Analysis. Journal of Air Force Engineering University (JCR-SCI), 1(5), 8-11.

[10] **Wei, X. (2013).** An overview of researches on deck-landing of carrier-based aircrafts. 2013 International Powered Lift Conference. https://doi.org/10.2514/6.2013-4268

[11] **Liu, G. (2010).** Study on Arresting Hook Impact with Deck and Arresting Dynamics of Carrier-based Aircraft. PhD Thesis, Nanjing University of Aeronautics and Astronautics.

[12] **Liu, G., & Nie, H.** (2009). Dynamics of Arresting Hook Bounce After Initial Touchdown and Impacting with Deck. Acta Aeronautica Et Astronautica Sinica, 30(9), 1672-1677.

[13] **Liu, G., & Nie, H.** (2009). Dynamics of Bounce of Aircraft Arresting Hook Impacting with Deck and Performance of Arresting Hook Longitudinal Damper. Acta Aeronautica Et Astronautica Sinica, 30(9), 2093-2099.

[14] **Wei, X. H., & Nie, H.** (2005). Analysis of Landing Impact Force of Aircraft Landing Gears Based on the Conception of Landing Area. Acta Aeronautica Et Astronautica Sinica, 26(1), 8-12.

[15] **Duan, H., Chen, L., & Zeng, Z.** (2022). Automatic Landing for Carrier-Based Aircraft Under the Conditions of Deck Motion and Carrier Airwake Disturbances. IEEE Transactions on Aerospace and Electronic Systems, 58(6), 5276-5291. doi: 10.1109/TAES.2022.3168247.

[16] **Rudowsky, T., Hynes, M., Luter, M., Niewoehner, R., & Senn, P.** (2002). Review of the Carrier Approach Criteria for Carrier-Based Aircraft - Phase I: Final Report. https://doi.org/10.21236/ada411068

[17] **Nie, H., Qiao, X., Gao, Z. J., et al.** (1991). Dynamic behavior analysis for landing gear with different types of dual-chamber shock struts. Chinese Journal of Aeronautics, 4(2), 235-244.

[18] **Berg, C. D., & Wellstead, P. E.** (1998). The Application of a Smart Landing Gear Oleo Incorporating Electrothelogical Fluid. Journal of Intelligent Material Systems and Structures, 9(8), 592-600.

[19] **Ringleb, F. O.** (1956). Cable Dynamics. Naval Air Engineering Facility Engineering Department, USA.

[20] **Gibson, P. T., & Cress, H. A.** (1965). Analytical Study of Aircraft Arresting Gear Cable Design. Battelle Memorial Institute, Columbus Laboratories, Ohio.

[21] **Godson, M., Clark, G. C., Gibson, P. T., et al**. (1965). Investigation of the influence of hook abrasion and wire materials on the useful service life of deck pendants. Battelle Memorial Institute, Columbus Laboratories, Ohio.

[22] **Billec, W. B.** (1966). Dynamic performance of a mark 7 mod 1 arresting system using 24-inch and 28-inch PD fairlead sheaves. U.S. Naval Air Test Facility, U.S. Naval Air Station Lakehurst, New Jersey.

[23] **Billec, W.** (1967). The effect of deck span upon arresting-gear performance. U.S. Naval Air Test Facility, U.S. Naval Air Station Lakehurst, New Jersey.

[24] **Gao, Z. J. (1990).** A Discussion of bounce kinematics of aircraft arresting hook and cable dynamics. Acta Aeronautica et Astronautica Sinica, 11(12), B543-B548.

[25] **Wei, X. H., & Nie, H.** (2007). Study on Landing Impact Force of Carrier-based Aircraft Landing Gears. China Mechanical Engineering, 18(5), 520-523.

[26] **Zhang, W., Zhang, Z., & Zhu, Q. D., et al.** (2009). Dynamics Model of Carrier-based Aircraft Landing Gears Landed on Dynamic Deck. Chinese Journal of Aeronautics, 22(4), 371-379.

[27] **Milwitzky, B., & Cook, F. E.** (1953). Analysis of Landing-Gear Behavior. NACA Report 1154.

[28] **Deakins, R. R., & Blackburn, C. L.** (1965). Simulation of High Sink Speed Landing Gear. SAE Paper 650845. Society of Automotive Engineering.

[29] **Yadov, D., & Ramamoorthy, R. P**. (1991). Nonlinear Landing Gear Behavior at Touchdown. Journal of Dynamic Systems, Measurement, and Control, 113(4), 677-683.

[30] **Williams, W. W., Williams, G. K., & Garrard, W. C. J.** (1965). Soft and Rough Field Landing Gears. SAE Paper 650844. Society of Automotive Engineering.

[31] **Nie, H., Qiao, X., & Gao, Z. J., et al**. (1991). Dynamic Behavior Analysis for Landing Gear with Different Types of Dual-Chamber Shock Struts. Chinese Journal of Aeronautics (English Edition), 4(2), 235-244.

[32] **George, M. L.** (1972). Development of a mathematical performance prediction model for rotary-hydraulic-type arresting gears. U.S. Naval Air Test Facility.

[33] **Hsin, C. C.** (1974). Arrested Landing Studies for STOL Aircraft. Journal of Aircraft, 11(3), 159-165.

[34] **Jone, W. L.** (1987). Aircraft Landing Dynamic Analysis Volume 1 Equations of motion. Structures Division, Directorate of Flight Systems Engineering.

[35] **Jone, W. L.** (1988). Aircraft Landing Dynamic Analysis Volume 2 computer program. Structures Division, Directorate of Flight Systems Engineering.

[36] **Jin, C. J., & Hong, G. X.** (1990). Dynamic Problems of Aircraft Carrier Catapult Launching and Arrest Landing. Acta Aeronautica Et Astronautica Sinica, 11(12), B535-B542.

[37] **Wang, M. H., & Zhao, B.** (1997). Takeoff Landing Dynamics Studies of Carrier-based Aircraft. Aircraft Design, 1, 21-33.

[38] **Cao, S. H., Song, J. C., Zhang, Z. W., & Zhou, S. H.** (2002). Arresting Performances Simulation Research on Aircraft Arresting System. Aeronautical Computer Technique, 32(3), 34-37.

[39] **Wu, J.** (2003). Airplane arresting system analysis and control study. PhD Thesis, Northwestern Polytechnical University.

[40] **Li, D. Y.** (2004). Study of electro-hydraulic proportional control of aircraft arresting system. Master Thesis, Northeastern University.

[41] **Zhang, X., Li, Y. L., Liu, Y. Y., & Dai, C.** (2008). Arresting Hook and Cable Dynamics of Aircraft Arrest Landing on or Off Center. Journal of Mechanical Strength, 30(4), 549-554.

[42] **Xu, S., Xu, Y. M., & Wang, Y. Q.** (2009). Modeling Studies for Carrier-based Aircraft Arrest Landing. Aircraft Design, 29(5), 5-8.

[43] **Luo, Q., Feng, Y. W., & Feng, Y. S.** (2009). Dynamic Analysis and Simulation of Carrier Aircraft Arrested Deck-Landing Based on Kink-Wave. Journal of Mechanical Strength, 31(4), 543-547.

[44] **Zhang, S. S.** (2008). Nonlinear optimal control of aircraft arresting process. Master Thesis, Nanjing University of Aeronautics and Astronautics.

[45] **Zhou, J. B., Jing, D. P., & Zhang, S. S.** (2009). Dynamic Modeling and Control of Carrier-Based Aircraft Arresting System. Journal of Dynamics and Control, 7(4), 352-357.

[46] **Zhang, P.** (2013). Control of arresting process for carrier aircraft considering kink-wave. Master Thesis, Nanjing University of Aeronautics and Astronautics.

[47] **Li, Q. M., Feng, Y. W., & Yu, L. M.** (2010). Kinetics Analysis and Simulation of Aircraft Arrested Shorelanding. Computer Simulation, 27(1), 27-31.

[48] **Tao, Y., Jia, Z. H., & Hou, Z. Q.** (2010). Research on the Dynamics of Carrier Aircraft Arrested Deck-Landing. Journal of Naval Aeronautical and Astronautical University, 25(2), 133-136.

[49] **Zhang, M. H., Yuan, L., & Hong, G. X.** (2010). Aircraft carrier hydraulic arresting gear arresting force modeling and simulation. Journal of Beijing University of Aeronautics and Astronautics, 36(1), 100-103.

[50] **Liu, T., Bargteil, A. W., O'Brien, J. F., & Kavan, L.** (2013). Fast simulation of mass-spring systems. ACM Transactions on Graphics, 32(6), 1–7. https://doi.org/10.1145/2508363.2508406

[51] **Inman, D. J.** (2008). Engineering Vibration (3rd ed.). Upper Saddle River, NJ: Pearson Education, Inc.

[52] **Wei, X., & Nie, H.** (2005). Dynamic Analysis of Aircraft Landing Impact using Landing-Region-Based Model. Journal of Aircraft, 42(6), 1631–1637. https://doi.org/10.2514/1.6801

[52] **Ansys Inc.** (2023). ANSYS LS-DYNA User's Guide. Retrieved from https://www.ansys.com/products/structures/ansys-ls-dyna

[54] **Rust, W., & Schweizerhof, K.** (2003). Finite element limit load analysis of thin-walled structures by ANSYS (implicit), LS-DYNA (explicit) and in combination. Thin-Walled Structures, 41(2–3), 227–244. https://doi.org/10.1016/s0263-8231(02)00089-7

[55] **Liu, Y.** (2008). ANSYS and LS-DYNA used for structural analysis. International Journal of Computer Aided Engineering and Technology, 1(1), 31–44.

[56] **Mascia, D.** (2010). Structural behaviour of landing deck marine vessel under dynamic actions of aircraft landing. Ships and Offshore Structures, 5(3), 267-282. https://doi.org/10.1080/17445300903566173

[57] **Carter, V. G., & Rizvi, J.** (2021). Computational Analysis of Flight Deck Structural Behaviour under Variable Loadings. Journal of Marine Science and Engineering, 9(11), 1262. https://doi.org/10.3390/jmse9111262

[58] **General Dynamics.** (2002) / Lockheed F-16 C / D Aircraft Flight Manual Block 50 and 52 +.

APPENDICES

APPENDIX A

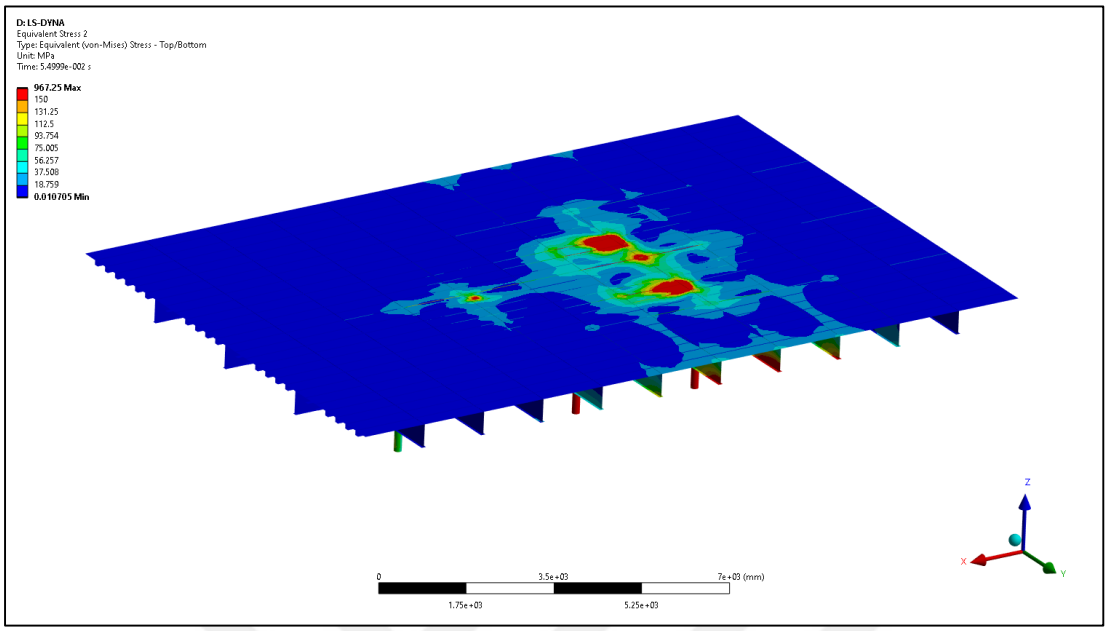

Figure A.1 : Von misses stress (velocity = 4.6 m/s) at time 0.05.

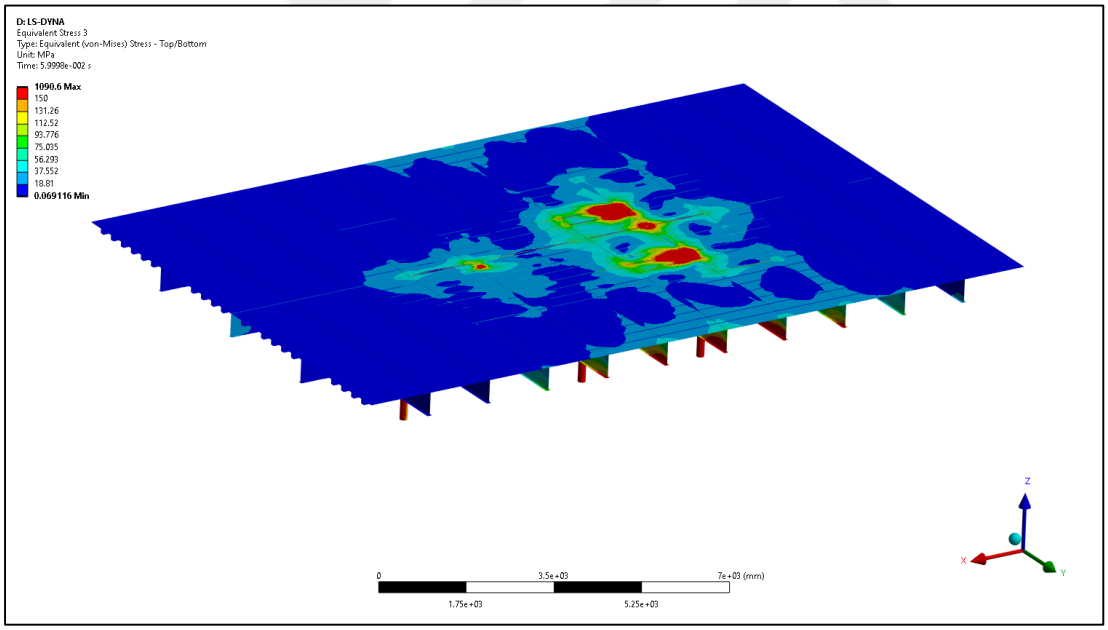

Figure A.2 : Von misses stress (velocity = 4.6 m/s) at time 0.06.

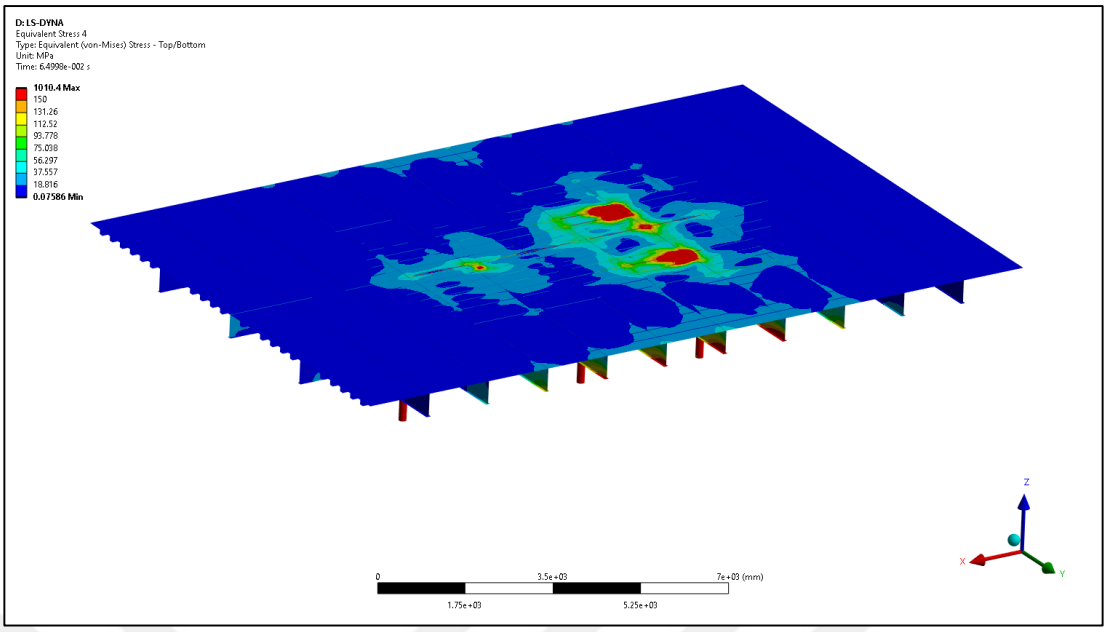

Figure A.3 : Von misses stress (velocity = 4.6 m/s) at time 0.065.

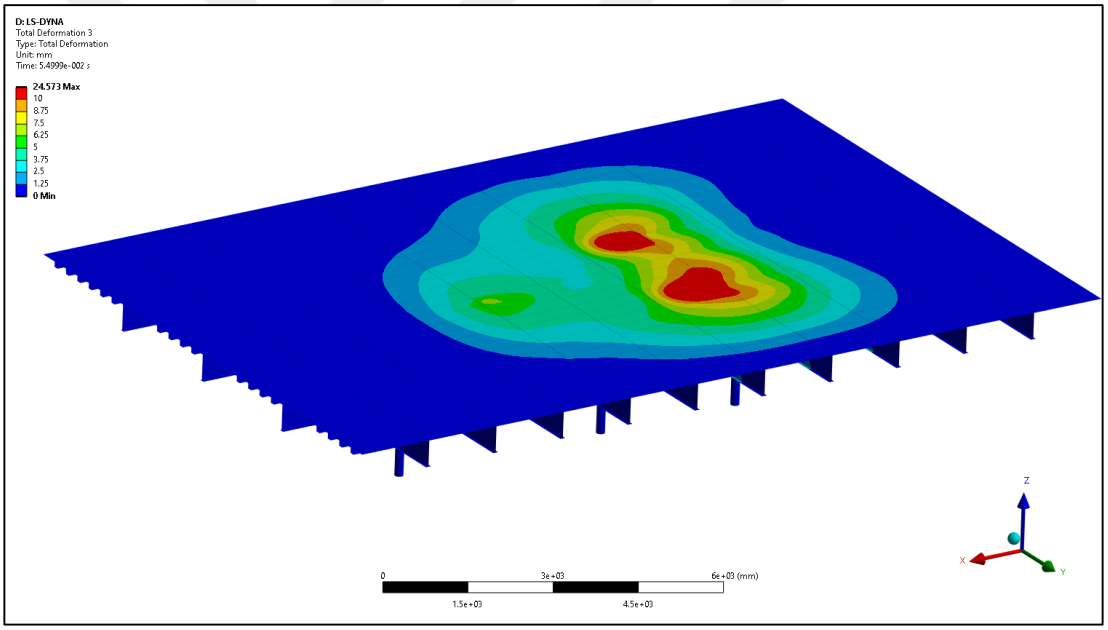

Figure A.4 : Deformation (velocity = 4.6 m/s) at time 0.05.

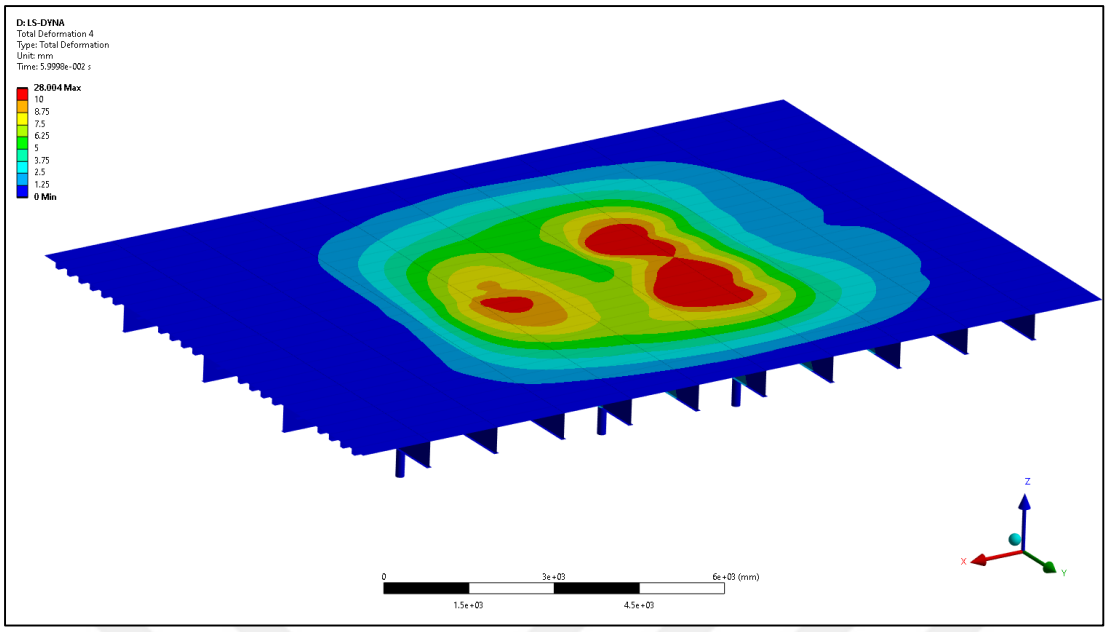

Figure A.5 : Deformation (velocity = 4.6 m/s) at time 0.06.

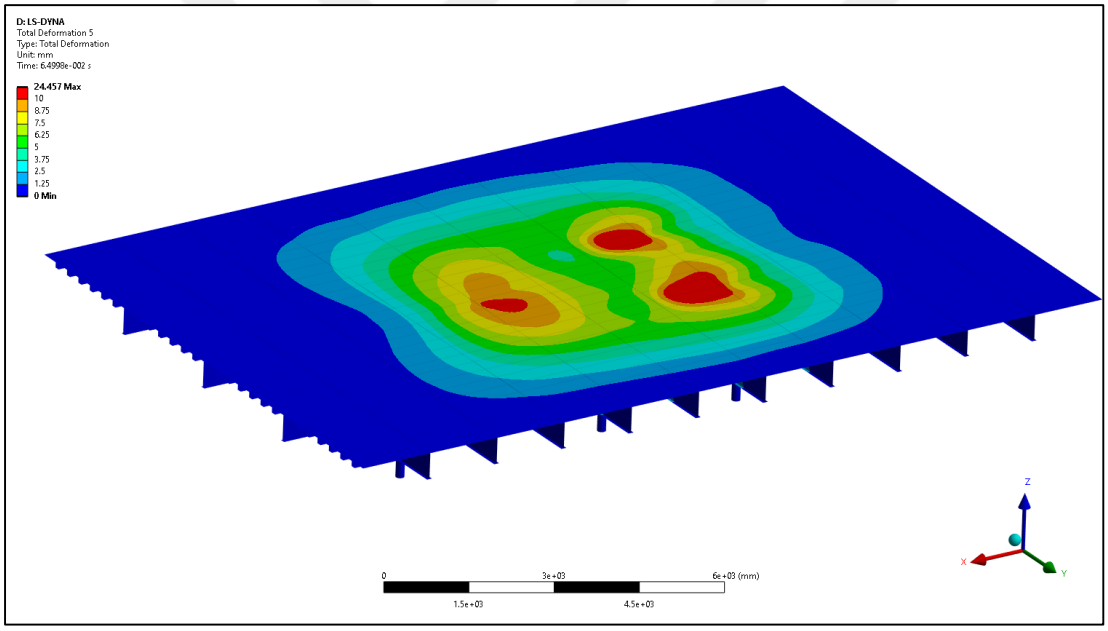

Figure A.6 : Deformation (velocity = 4.6 m/s) at time 0.065.

APPENDIX B

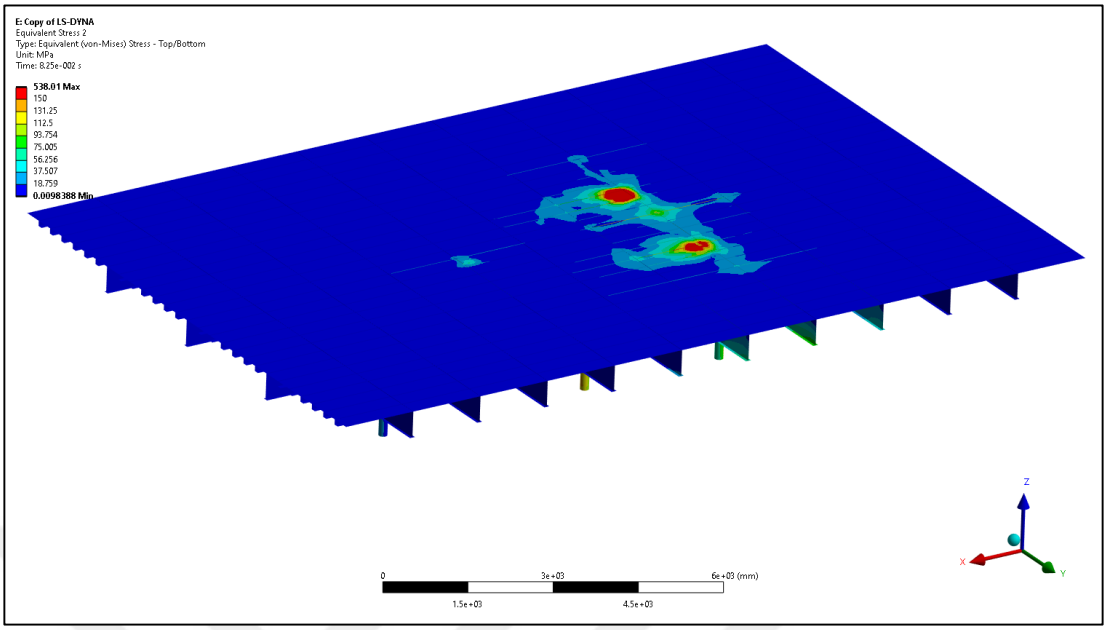

Figure B.1 : Von misses stress (velocity = 2.7 m/s) at time 0.0825.

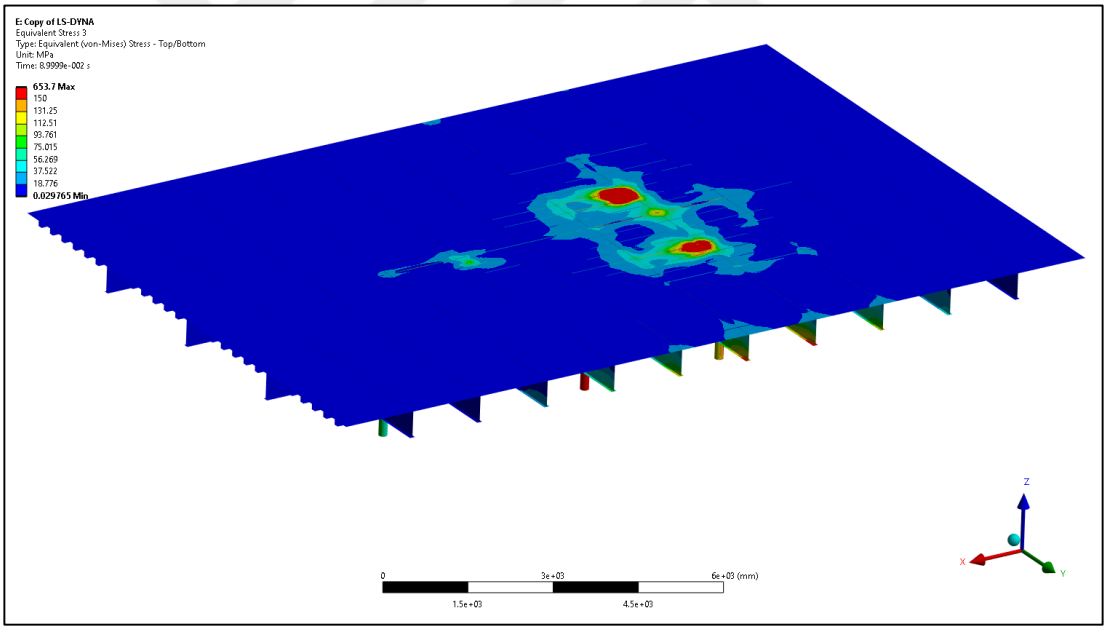

Figure B.2 : Von misses stress (velocity = 2.7 m/s) at time 0.09.

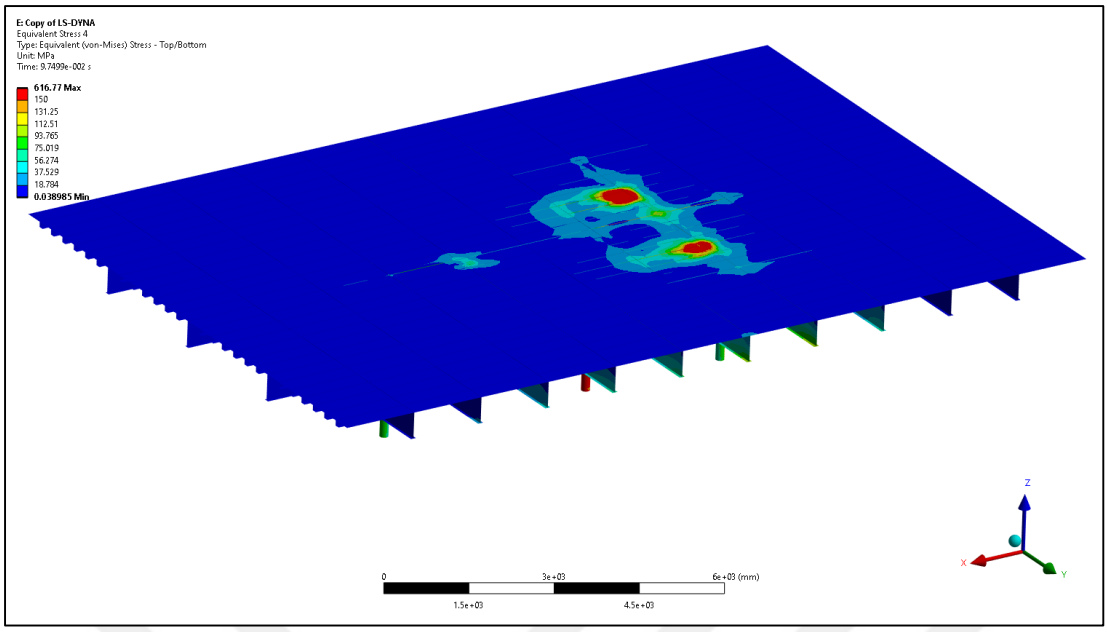

Figure B.3 : Von misses stress (velocity = 2.7 m/s) at time 0.0975.

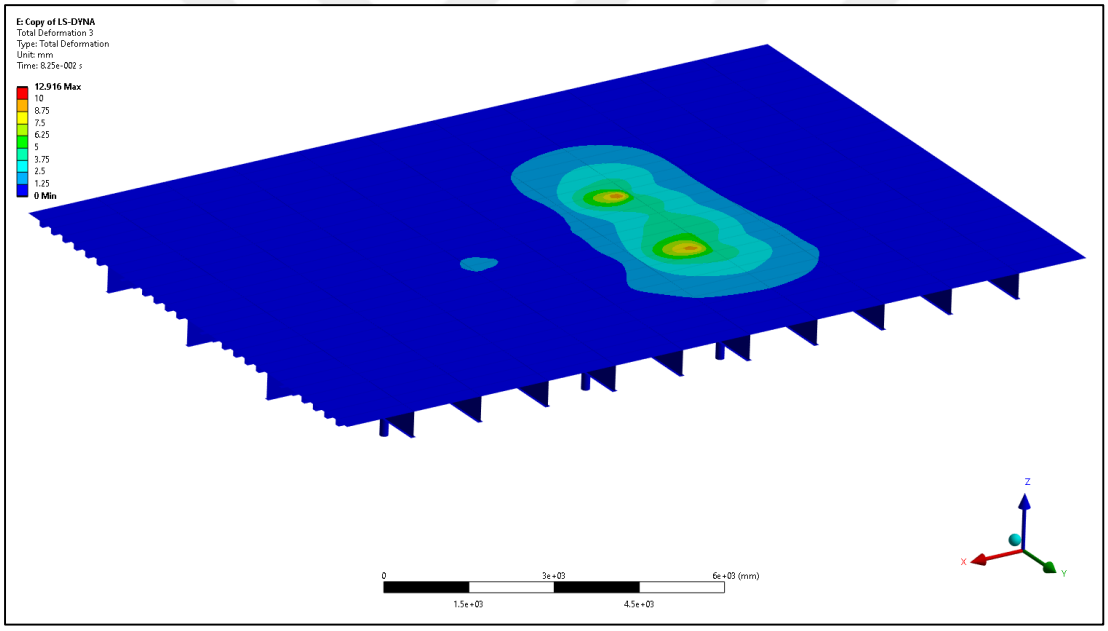

Figure B.4 : Deformation (velocity = 2.7 m/s) at time 0.0825.

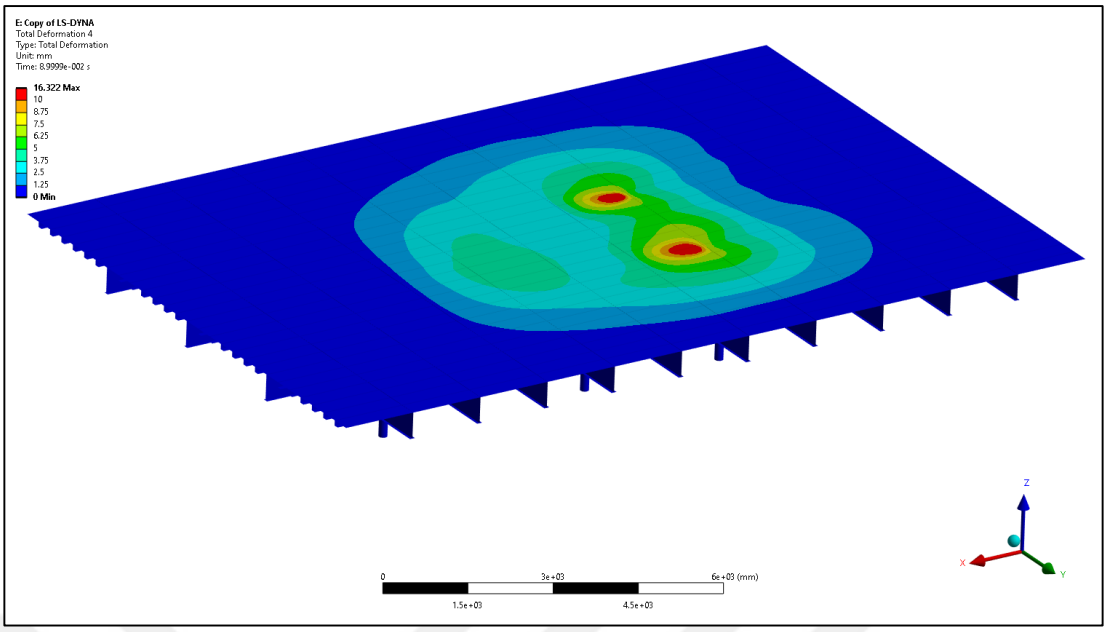

Figure B.5 : Deformation (velocity = 2.7 m/s) at time 0.09.

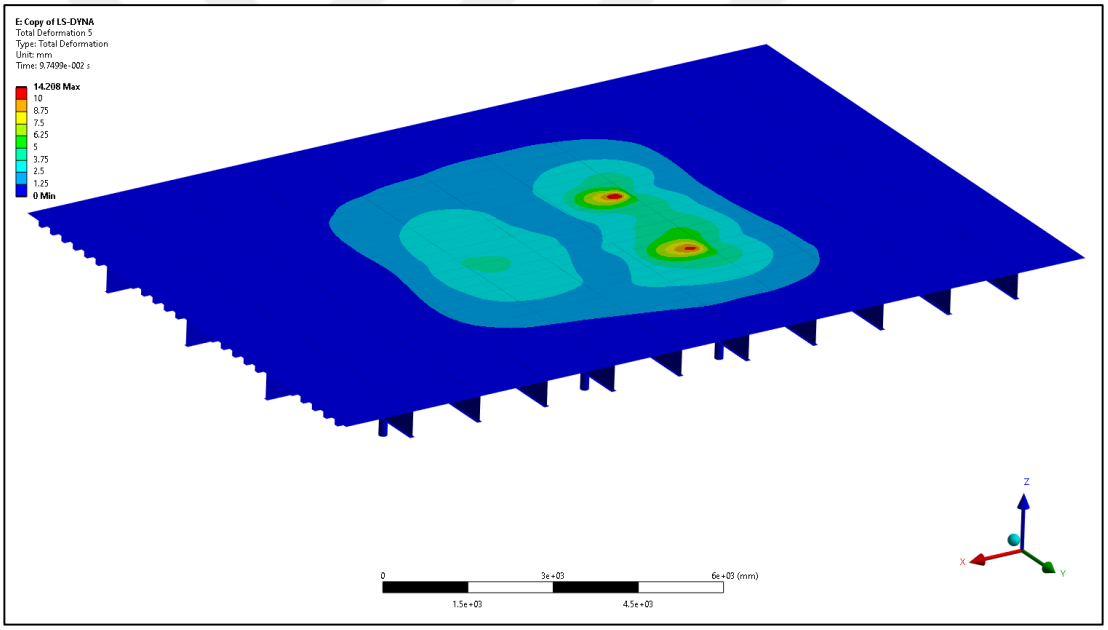

Figure B.6 : Deformation (velocity = 2.7 m/s) at time 0.0975.

APPENDIX C

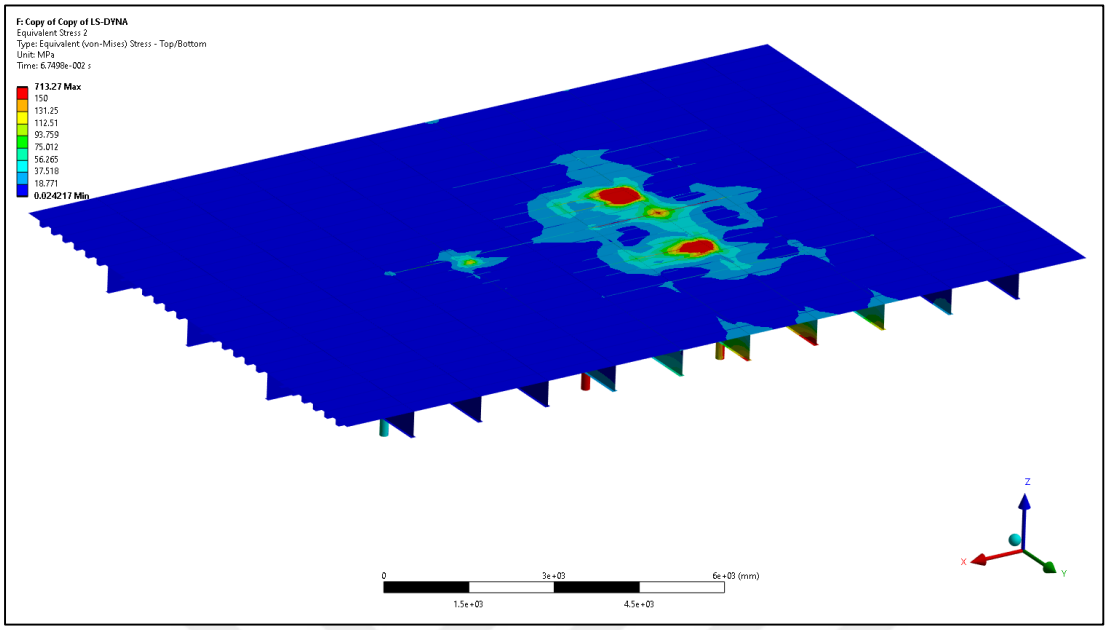

Figure C.1 : Von misses stress (velocity = 3.54 m/s) at time 0.0675.

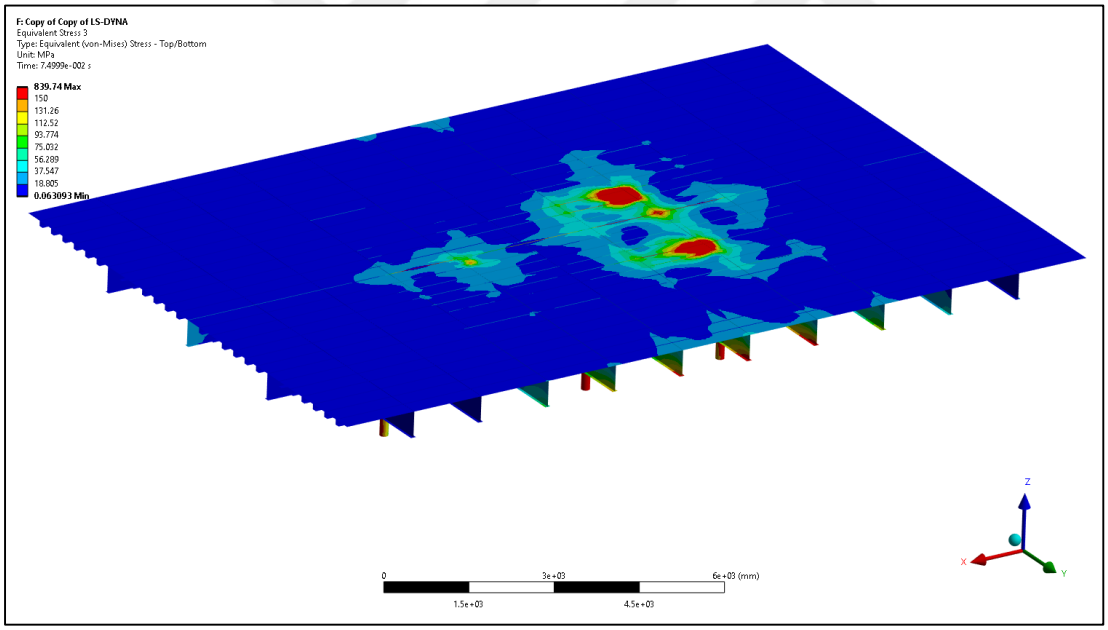

Figure C.2 : Von misses stress (velocity = 3.54 m/s) at time 0.075.

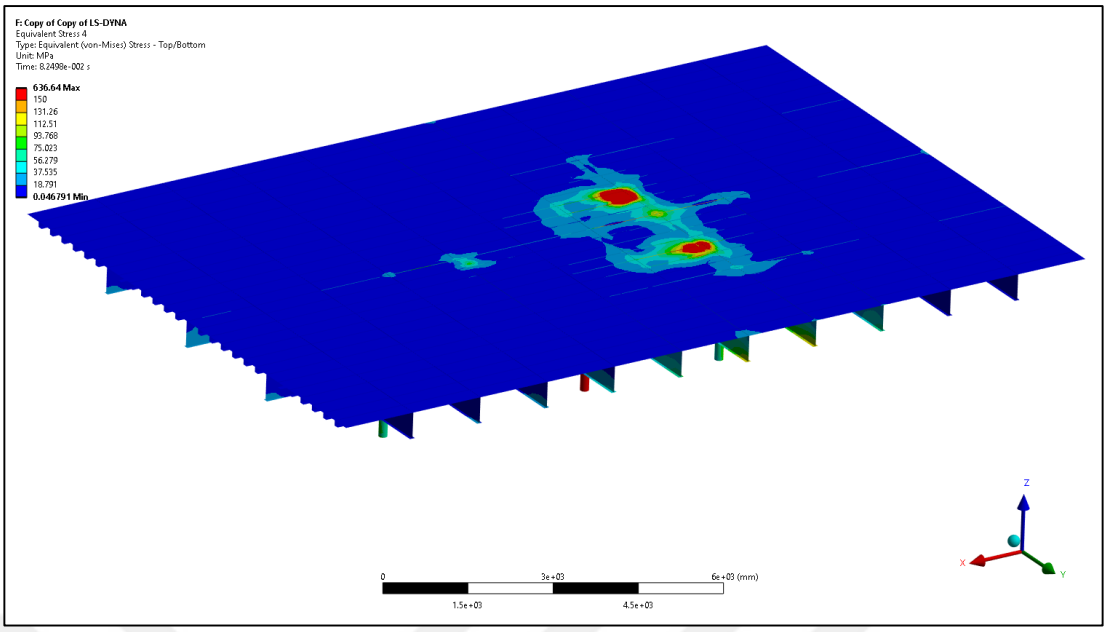

Figure C.3 : Von misses stress (velocity = 3.54 m/s) at time 0.0825.

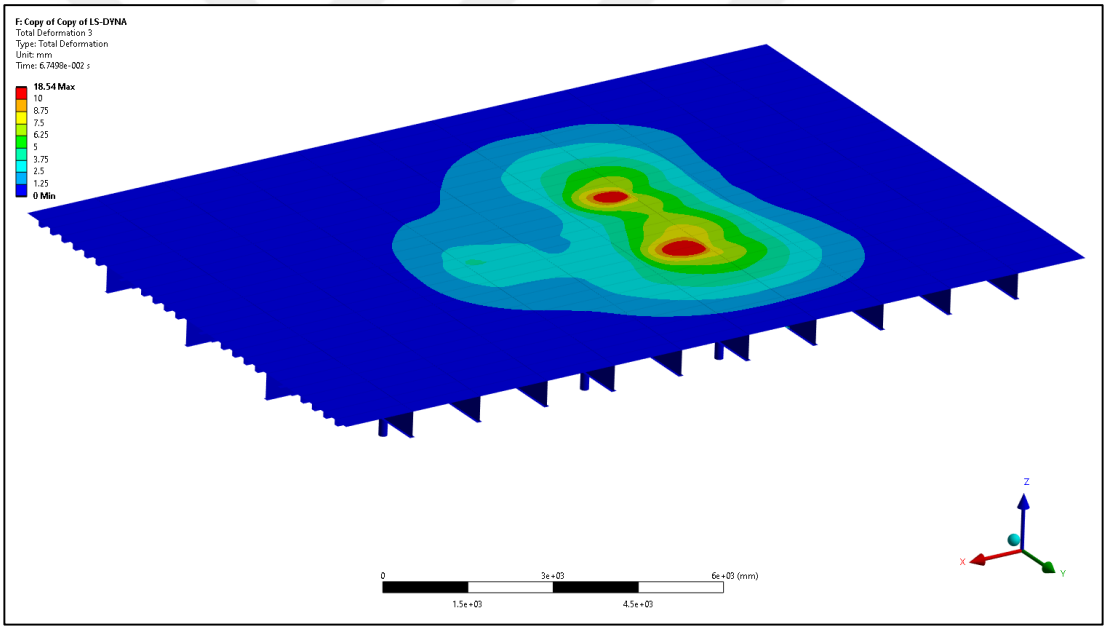

Figure C.4 : Deformation (velocity = 3.54 m/s) at time 0.0675.

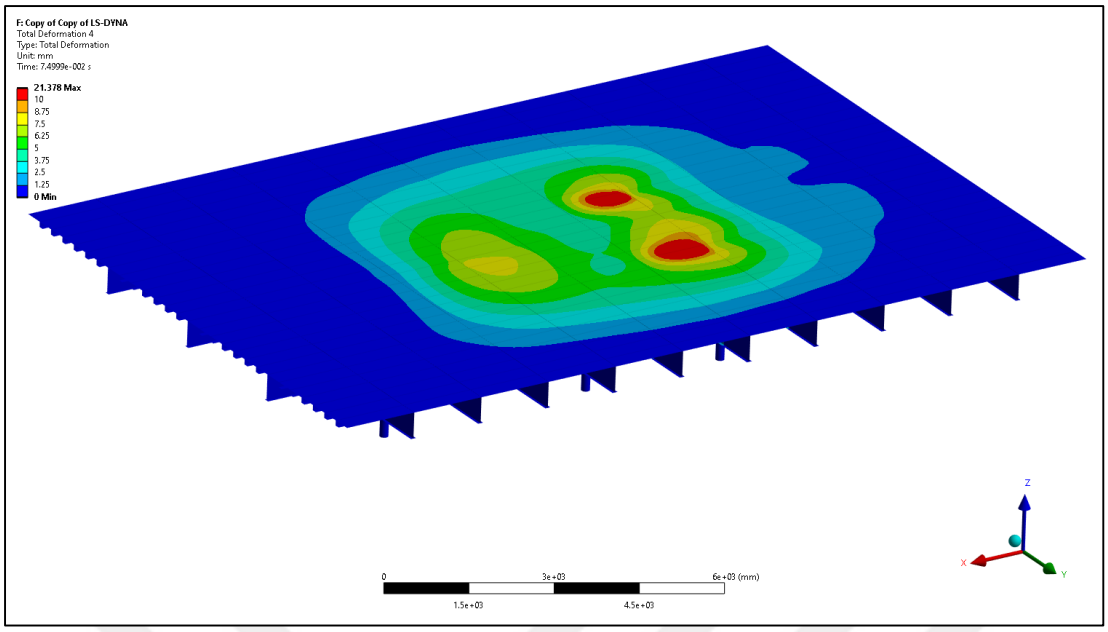

Figure C.5 : Deformation (velocity = 3.54 m/s) at time 0.075.

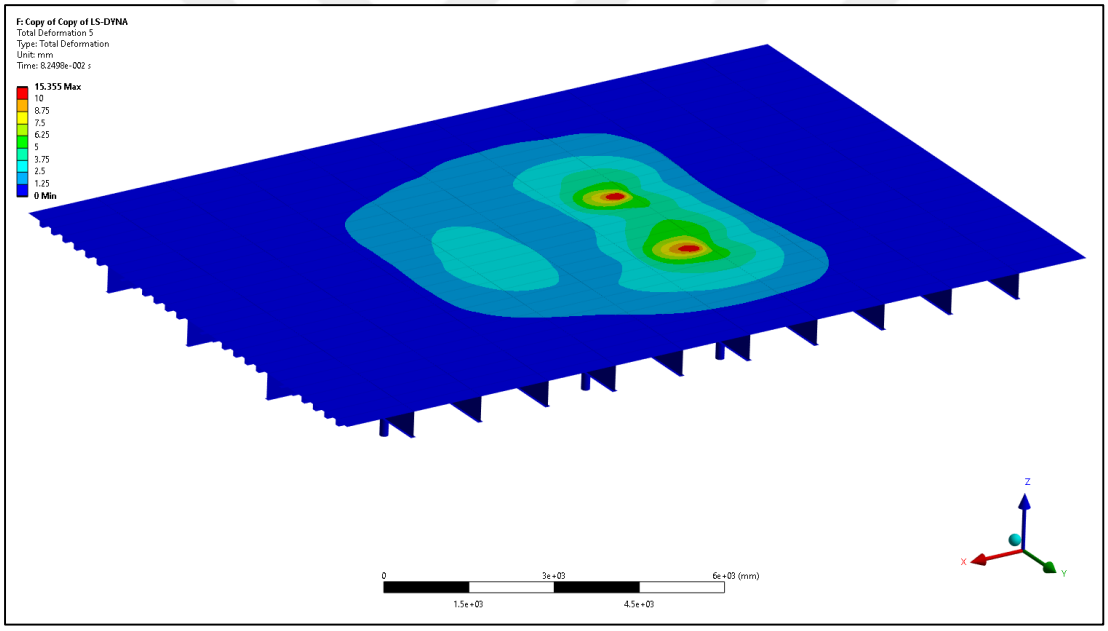

Figure C.6 : Deformation (velocity = 3.54 m/s) at time 0.0825.

APPENDIX D

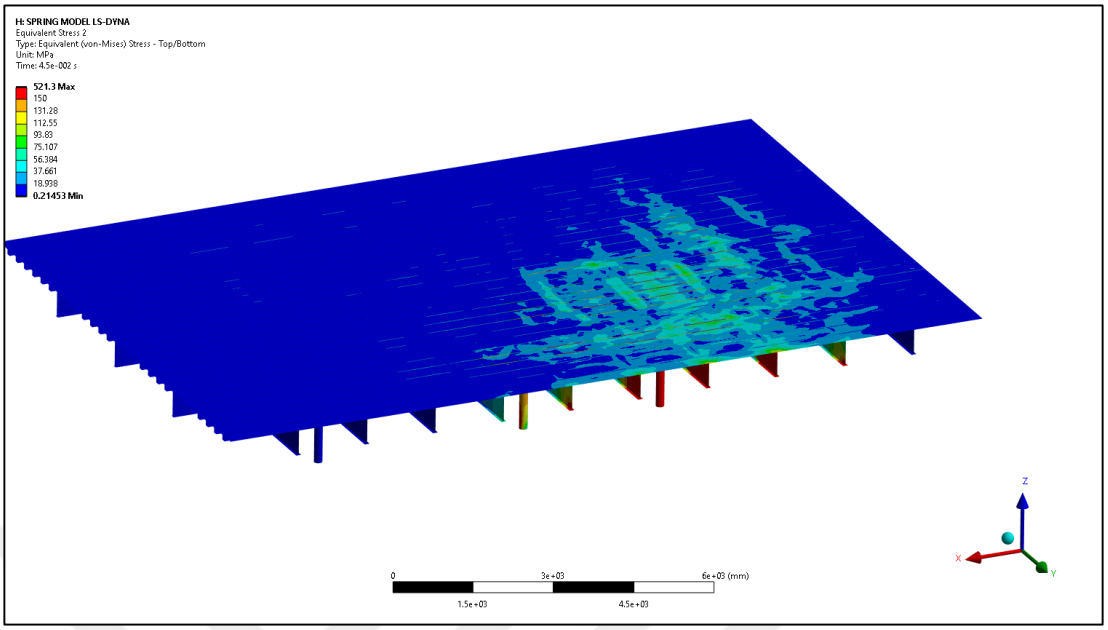

Figure D.1 : Von misses stress (velocity = 4.6 m/s) at time 0.045.

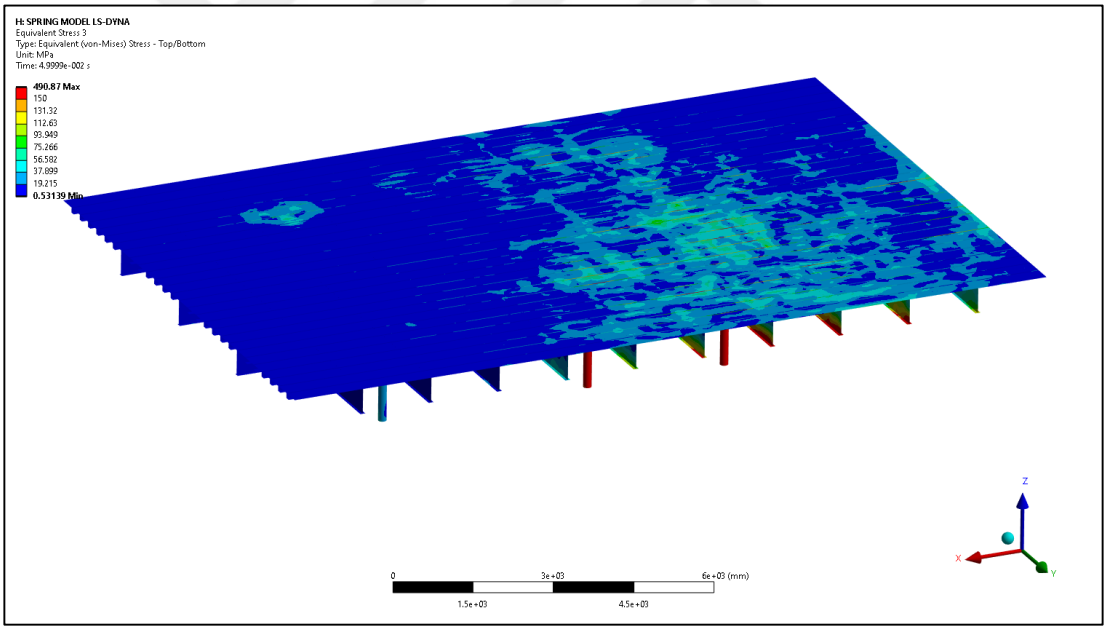

Figure D.2 : Von misses stress (velocity = 4.6 m/s) at time 0.05.

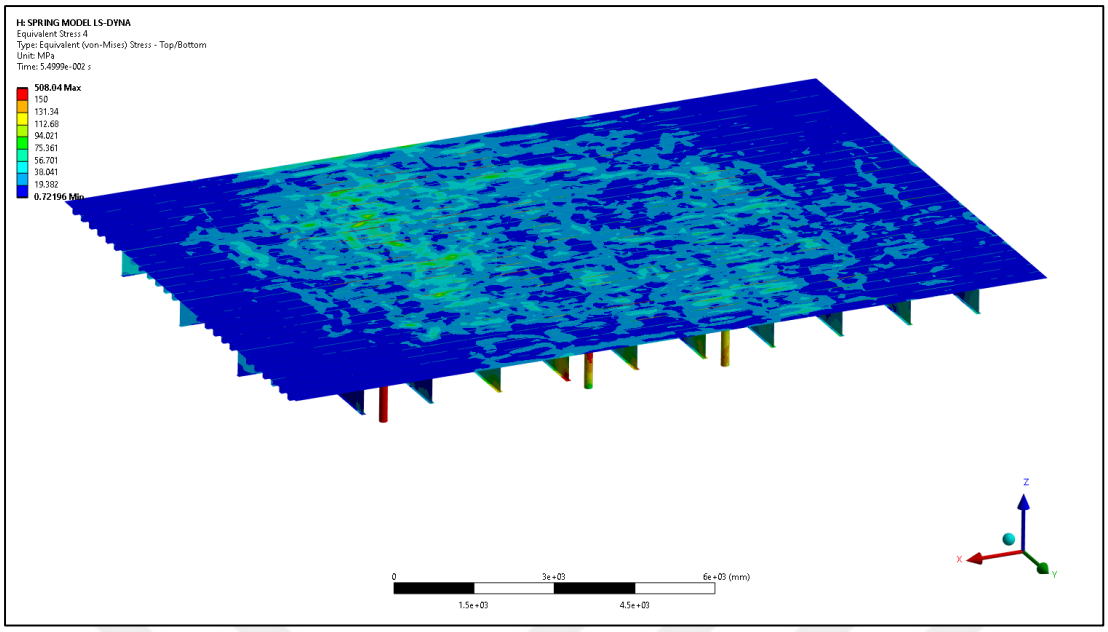

Figure D.3 : Von misses stress (velocity = 4.6 m/s) at time 0.055.

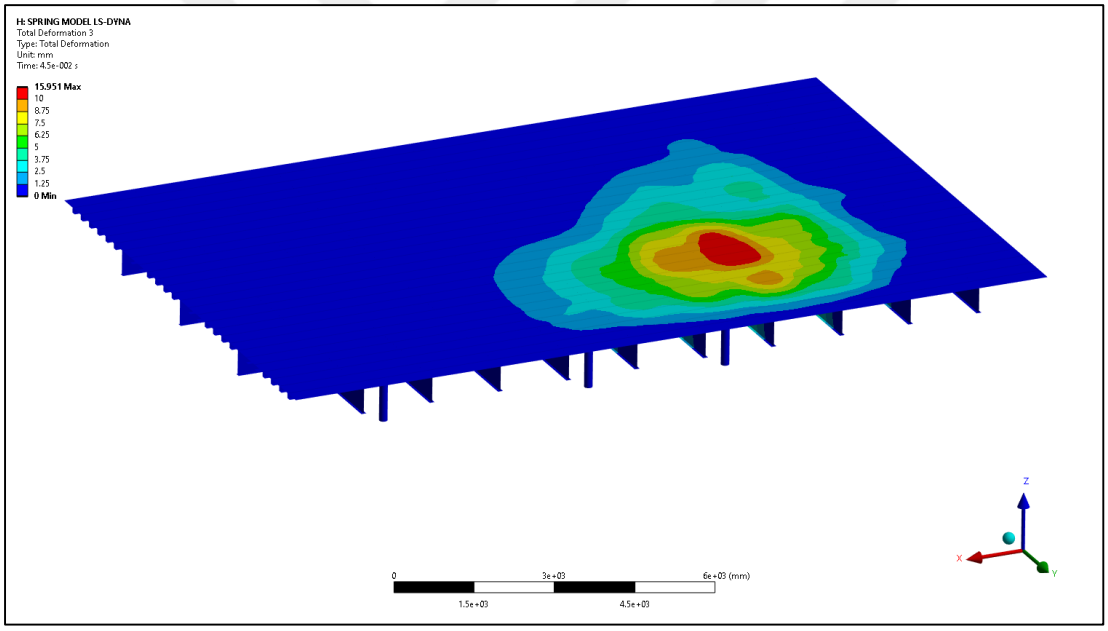

Figure D.4 : Deformation (velocity = 4.6 m/s) at time 0.045.

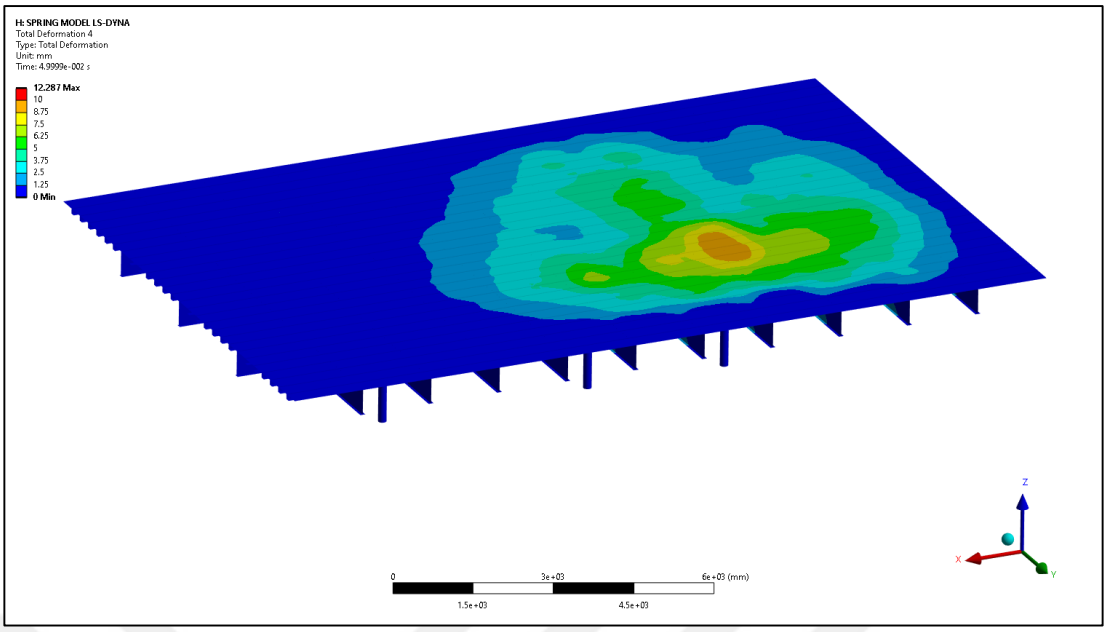

Figure D.5 : Deformation (velocity = 4.6 m/s) at time 0.05.

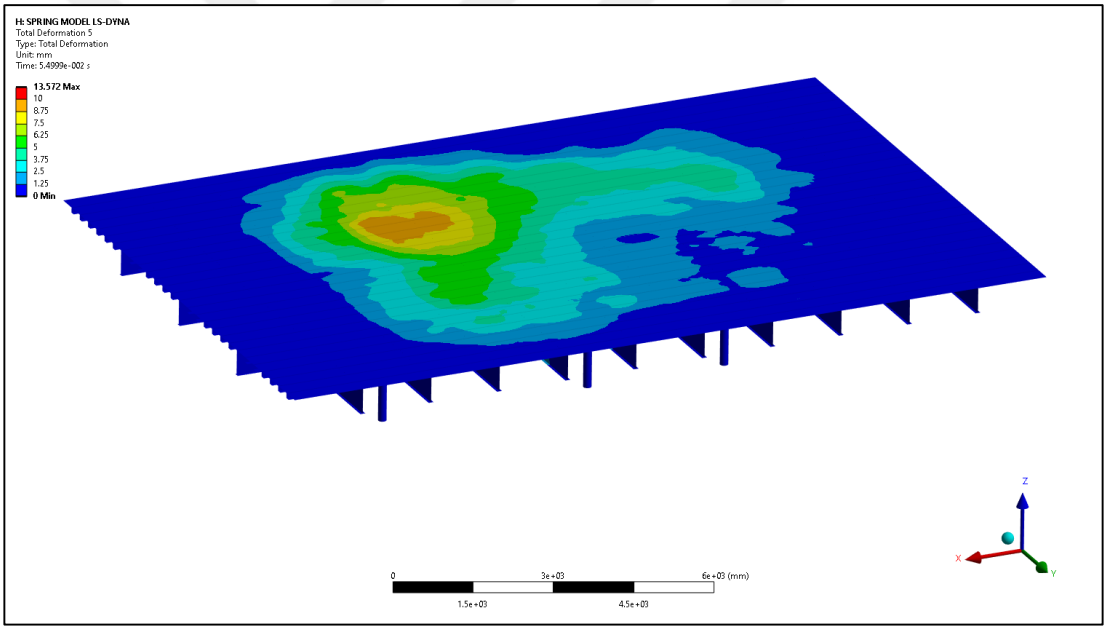

Figure D.6 : Deformation (velocity = 4.6 m/s) at time 0.055.

APPENDIX E

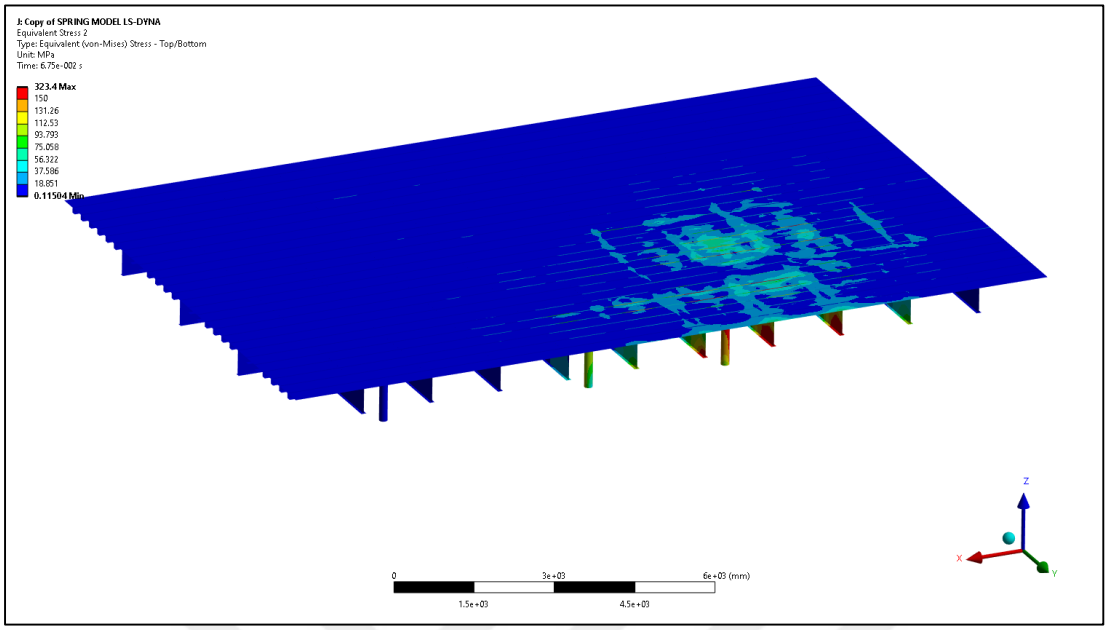

Figure E.1 : Von misses stress (velocity = 2.7 m/s) at time 0.0675.

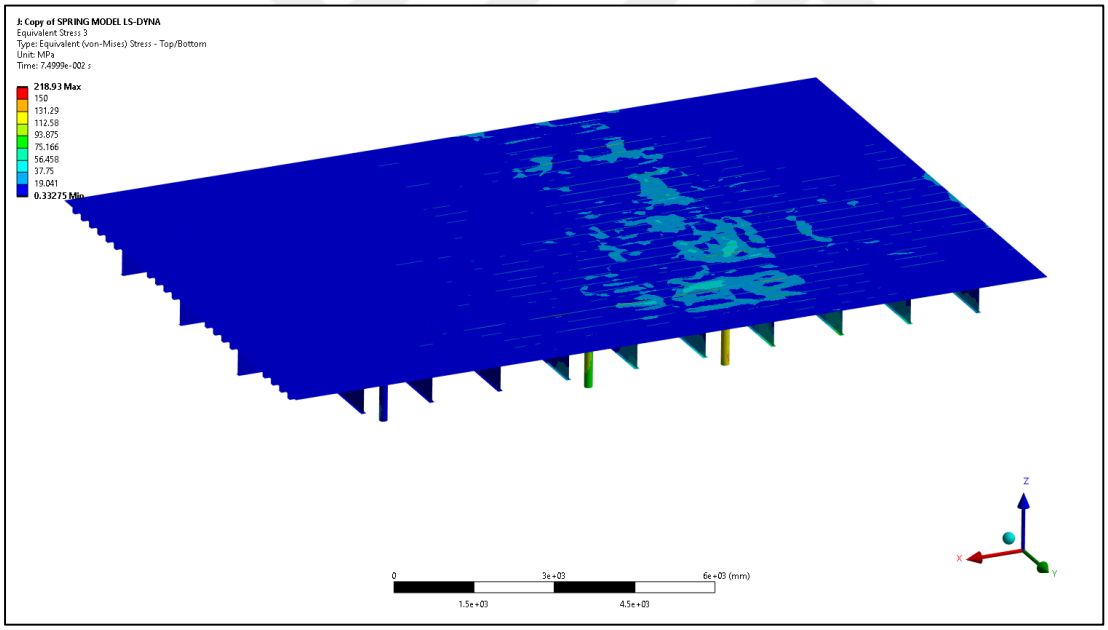

Figure E.2 : Von misses stress (velocity = 2.7 m/s) at time 0.075.

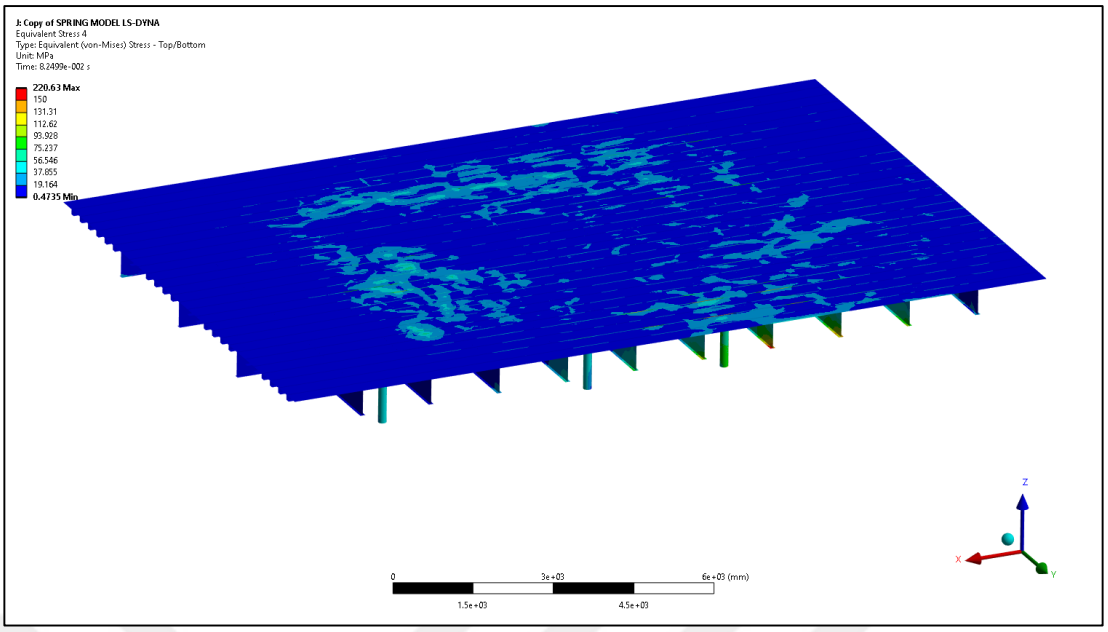

Figure E.3 : Von misses stress (velocity = 2.7 m/s) at time 0.0825.

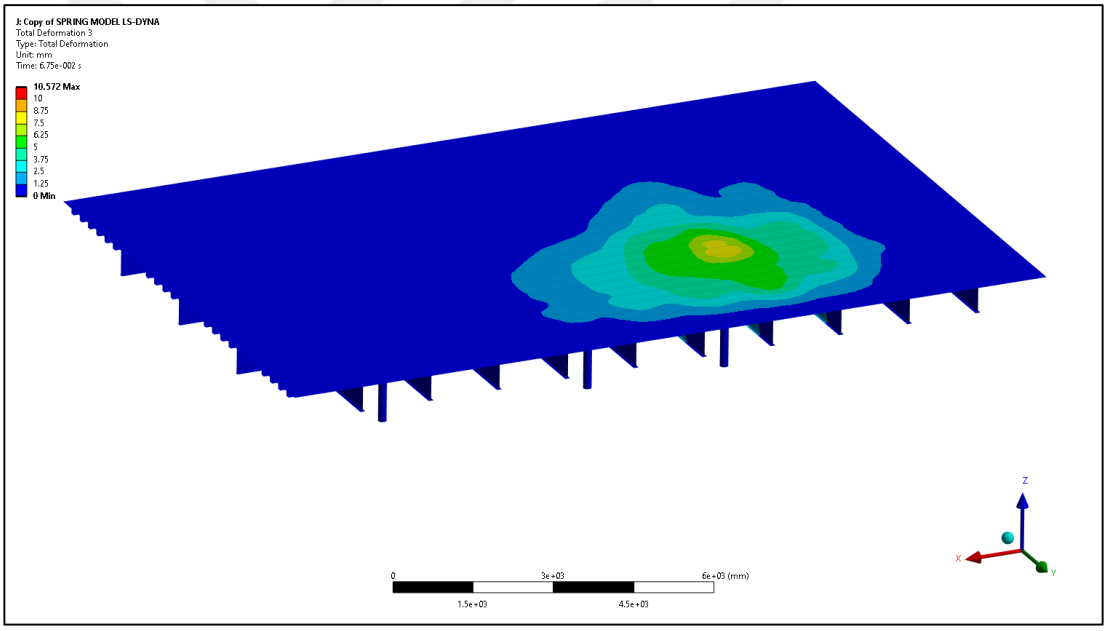

Figure E.4 : Deformation (velocity = 2.7 m/s) at time 0.0675.

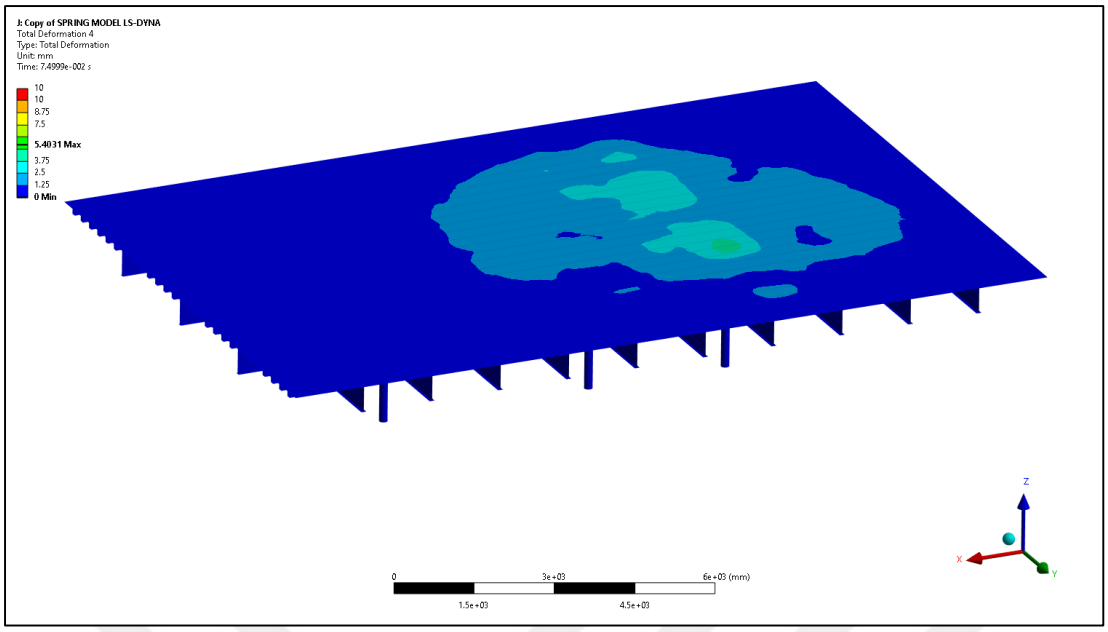

Figure E.5 : Deformation (velocity = 2.7 m/s) at time 0.075.

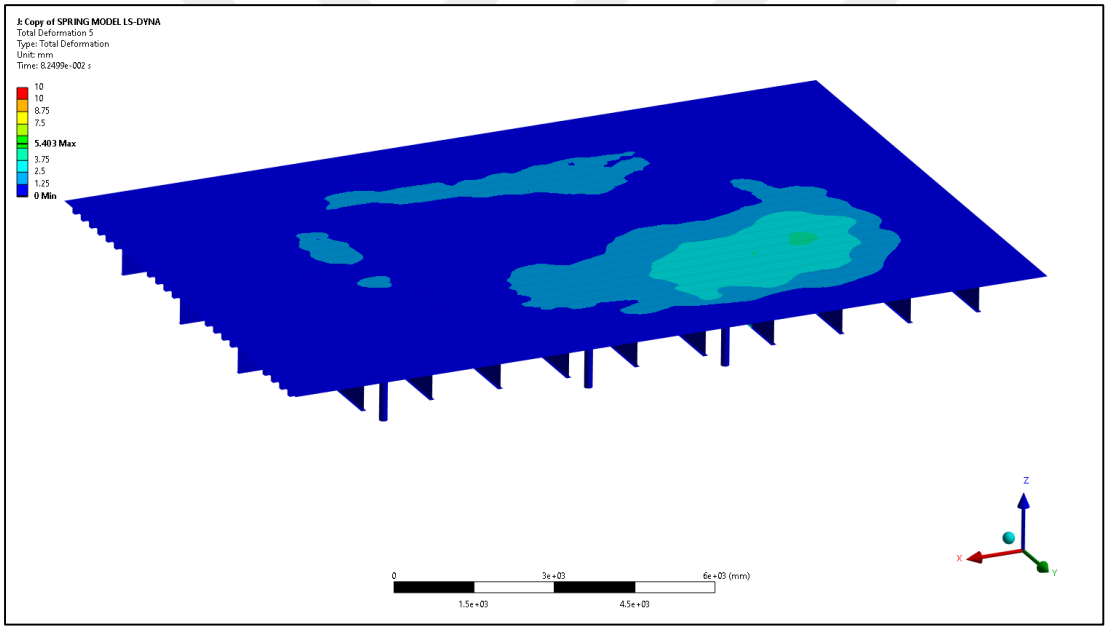

Figure E.6: Deformation (velocity = 2.7 m/s) at time 0.0825.

APPENDIX F

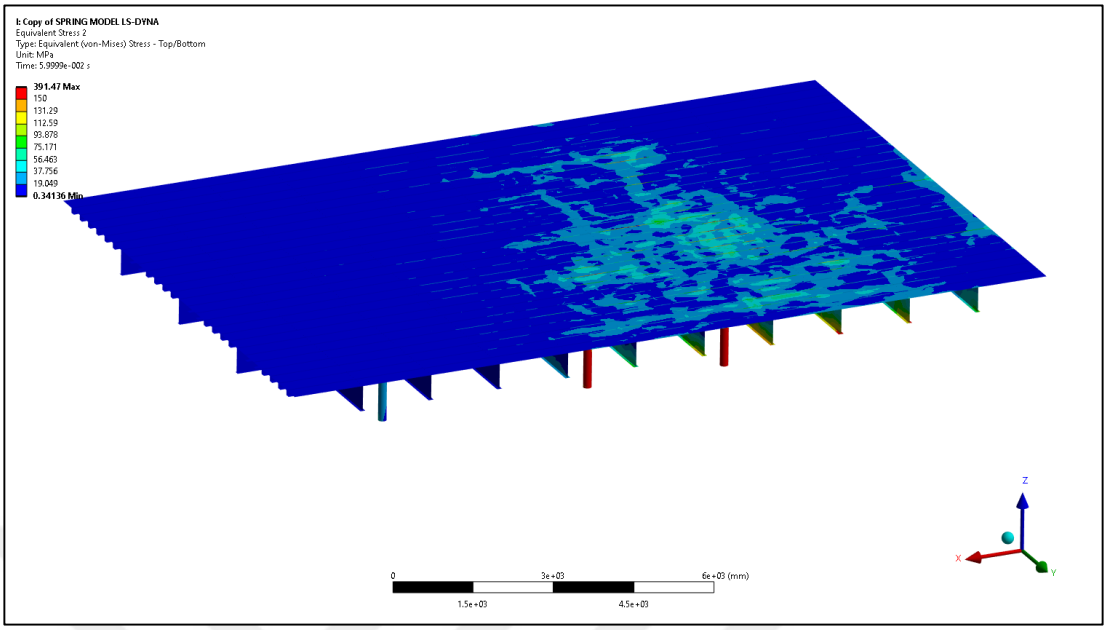

Figure F.1 : Von misses stress (velocity = 3.54 m/s) at time 0.06.

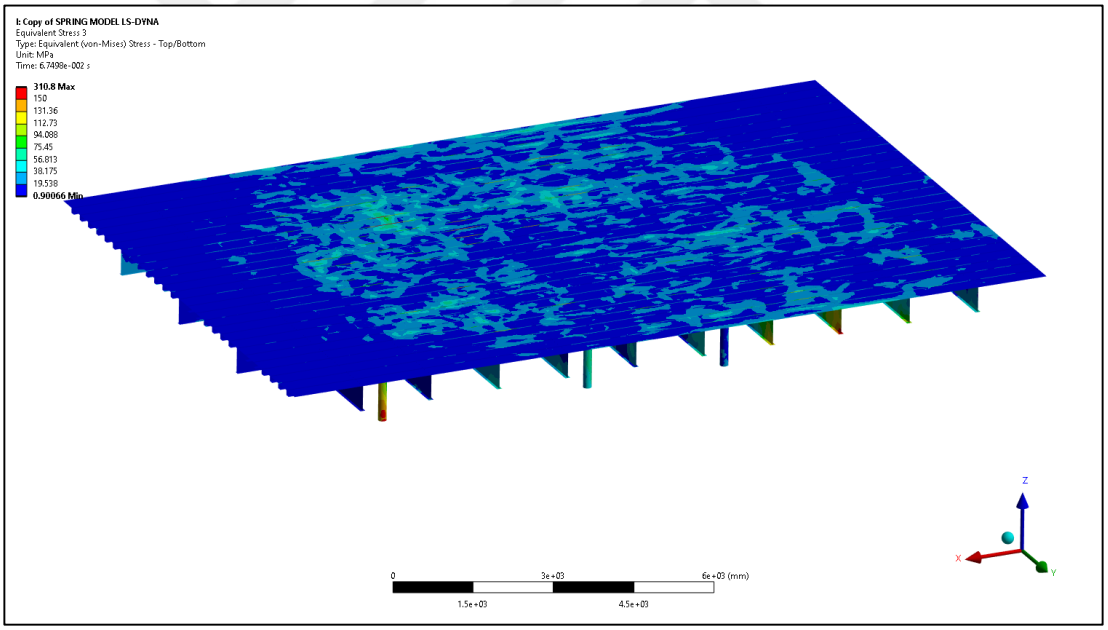

Figure F.2 : Von misses stress (velocity = 3.54 m/s) at time 0.0675.

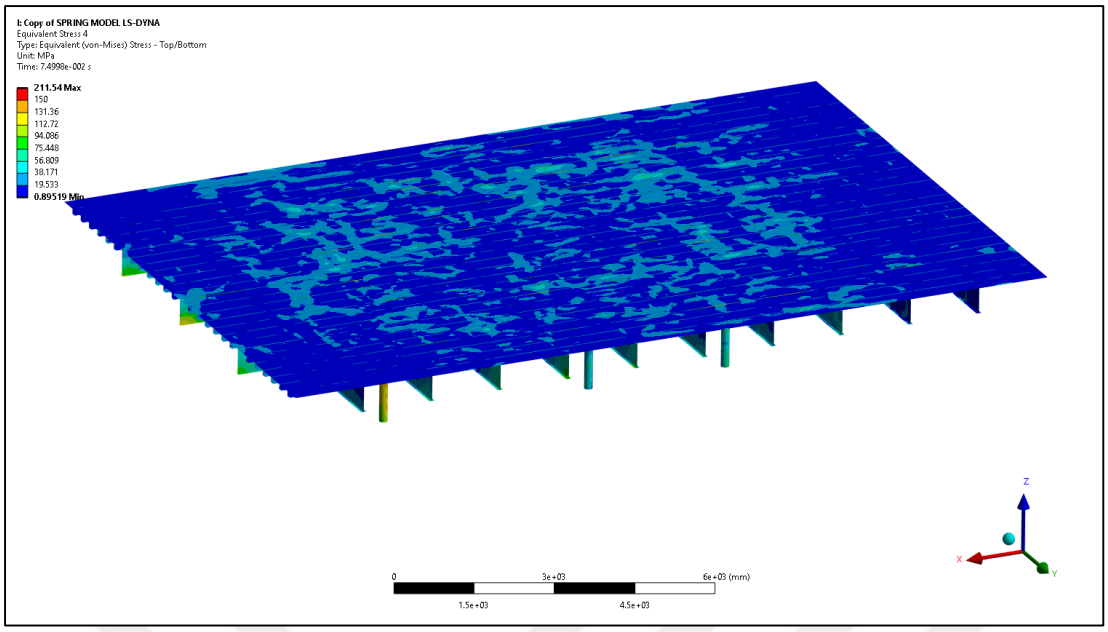

Figure F.3 : Von misses stress (velocity = 3.54 m/s) at time 0.075

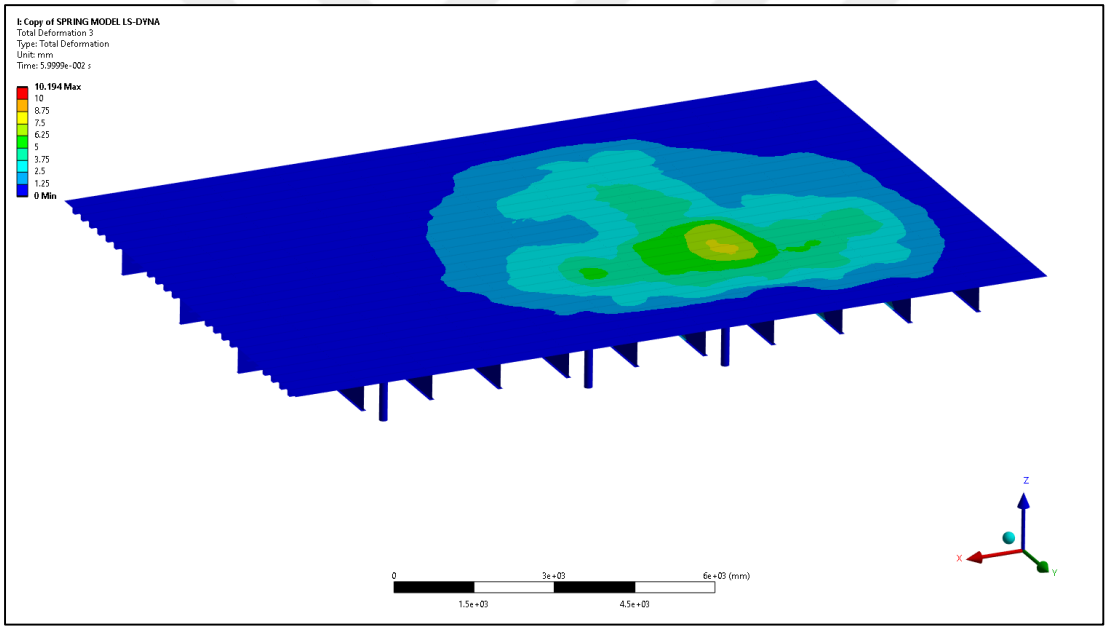

Figure F.4 : Deformation (velocity = 3.54 m/s) at time 0.06.

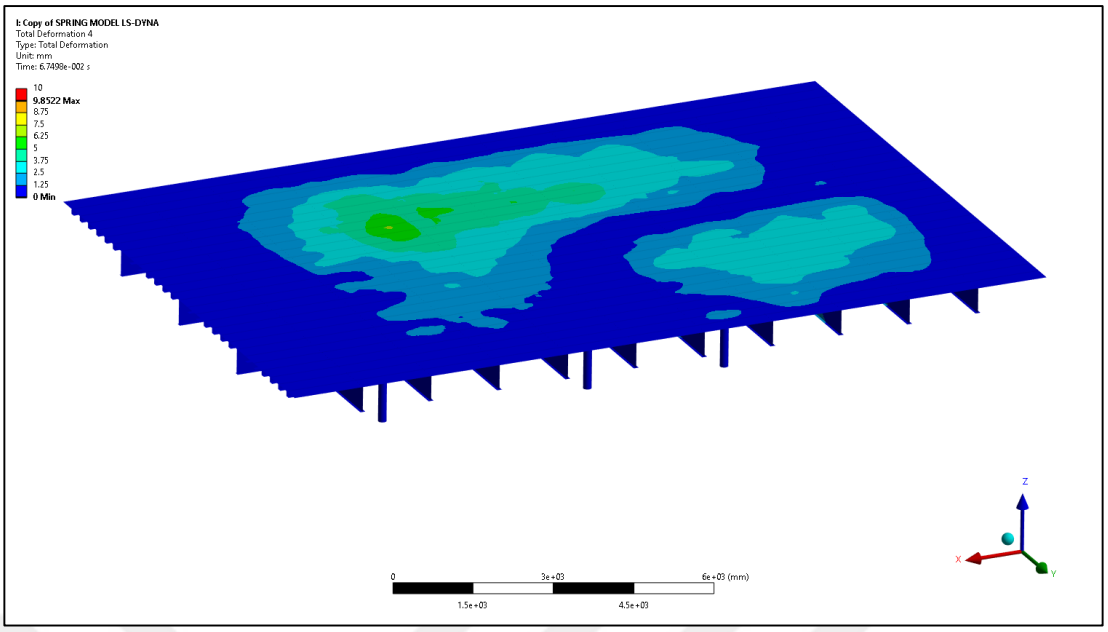

Figure F.5 : Deformation (velocity = 3.54 m/s) at time 0.0675.

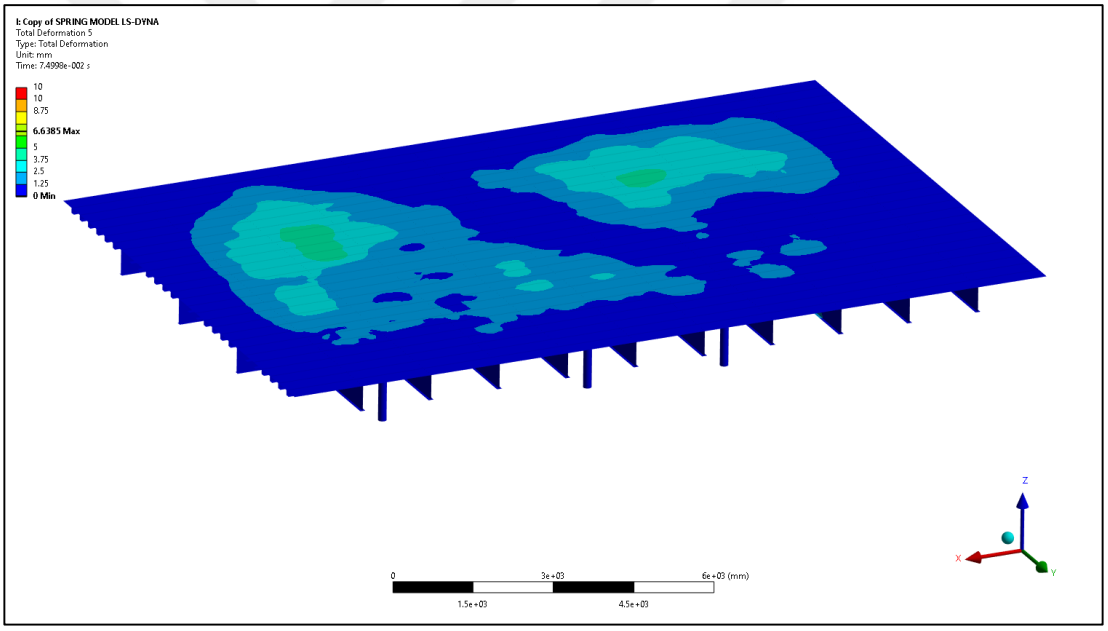

Figure F.6 : Deformation (velocity = 3.54 m/s) at time 0.075.

CURRICULUM VITAE

Name Surname **:** Mustafa Enes PEKDEMIR

EDUCATION **:**

- **B.Sc.** **:** 2021, Istanbul Technical University, Faculty of Naval Architecture and Ocean Engineering, Department of Shipbuilding and Ocean Engineering

PUBLICATIONS, PRESENTATIONS AND PATENTS ON THE THESIS:

- **Pekdemir M. E.** 2024: Analysis and Functionality of Collision Dampers for Aircraft Carrier Decks during Landings. 3rd International Graduate Research Symposium - IGRS'24, May 8-10, Istanbul, Turkey.